ESTIMATION AND MITIGATION OF MICROVIBRATIONS IN SPACECRAFT APPLICATIONS

M. Tech. Thesis

By

VARADE TEJAS DEELIP

DEPARTMENT OF MECHANICAL ENGINEERING

INDIAN INSTITUTE OF TECHNOLOGY INDORE

JUNE 2025

ESTIMATION AND MITIGATION OF MICROVIBRATIONS IN SPACECRAFT APPLICATIONS

A THESIS

Submitted in partial fulfillment of the
requirements for the award of the degree
of
Bachelor and Master of Technology (Dual Degree)

by

VARADE TEJAS DEELIP

DEPARTMENT OF MECHANICAL ENGINEERING
INDIAN INSTITUTE OF TECHNOLOGY INDORE

JUNE 2025

INDIAN INSTITUTE OF TECHNOLOGY INDORE

CANDIDATE'S DECLARATION

I hereby certify that the work which is being presented in the thesis entitled **Estimation and Mitigation of Micro-vibrations in Spacecraft Applications** in the partial fulfillment of the requirements for the award of the degree of **BACHELOR AND MASTER OF TECHNOLOGY (DUAL DEGREE)** and submitted in the **DEPARTMENT OF MECHANICAL ENGINEERING, Indian Institute of Technology Indore**, is an authentic record of my own work carried out during the time period from JULY 2023 to MAY 2025 under the supervision of **Dr. Krishna Mohan Kumar, Assistant Professor, Department of Mechanical Engineering, Indian Institute of Technology Indore** and **Dr. Nazeer Ahmad, Scientist, Structures Group, U R Rao Satellite Centre, ISRO.**

The matter presented in this thesis has not been submitted by me for the award of any other degree of this or any other institute.

08/06/2025

(Varade Tejas Deelip)

This is to certify that the above statement made by the candidate is correct to the best of my/our knowledge.

K. M. Kumar

(Dr. Krishna Mohan Kumar)

Ku. Varade Tejas Deelip has successfully given his/her M. Tech. Oral Examination held on **May 23, 2025.**

K. M. Kumar

Signature(s) of Supervisor(s) of M. Tech. thesis

Date: June 10, 2025

Convener, DPGC

Date:19-06-2025

ACKNOWLEDGEMENTS

Above all, I would like to thank 'Ganpati Bappa' the primary source of my knowledge and wisdom, for the life experiences, accomplishments, and failures that have shaped me into the person I am today. My sincere gratitude goes to my teachers, grandparents, parents and little brother for their love, affection, and believe in me.

The entire B. Tech + M. Tech. program has been a valuable experience for me, not only in terms of acquiring skills in the field of Mechanical Engineering, but also in terms of learning a lot more about scientific research methods, applications of engineering technology, role of art in my life, positive attitude towards life, and interpersonal relationships.

I thank my supervisor, **Dr. K. M. Kumar,** for encouraging me to harness the best out of me. I thank him for providing me an opportunity to work in the Theoretical and Applied Acoustics Lab (TAAL) at IIT Indore. He provided valuable suggestions to carry out the research work in a very systematic way. I thank, **Dr. Nazeer Ahmad, ISITE (URSC - ISRO),** for helping me with the essentials of the theoretical understanding of the literature and the subsequent mathematical formulation. And, all of it has given me a purpose to work hard with enthusiasm. To me, all of you have been outstanding teachers, mentors, and role models.

I want to thank **Mr. Gaurav Sharma** (Ph.D. scholar, TAAL Lab) and **Mr. Asif Nisar** (MS. Res. scholar, TAAL Lab) for helping me throughout my whole M. Tech. journey at IIT Indore. I also want to thank **Mr. Ajeet Kumar** (my room-mate) for being my buddy during my whole B. Tech + M. Tech. journey at IIT Indore.

My sincere gratitude to each and every person of this campus of IIT Indore, who helped me in the last five years, to shape a significant part of what I am today.

Thanks a lot, everyone...!

Varade Tejas Deelip

Dedicated to my teachers, grandparents, parents, and little brother, for their love, care, and blessings...!

Abstract

The motion of any spacecraft is divided into two stages – the launch and the in-orbit motion. Consequently, the loads acting on the spacecraft are also of different nature in both these motions. Both these loads propagate through the spacecraft structure, which is primarily made of honeycomb sandwich panels. These sandwich panels are made of outer face sheet and inner honeycomb core. Both these components are made of aluminium of different grades. The loads acting on the spacecraft propagate through this structure and are critical for the subsystems mounted on these structures.

The launch loads are characterized by high amplitude (reaching up to 10 g's) and low frequency. These loads are further amplified by the low inherent damping characteristics of the sandwich panels. The in-orbit loads are extremely low amplitude and low frequency vibrations, known as micro-vibrations. These micro-vibrations are critically responsible for the pointing accuracy of the satellites. These have been discussed in detail in the upcoming chapter.

Several researches have been carried out to study the nature of these micro-vibrations and their isolation techniques. These have been discussed in the chapter on literature review. The most widely used technique for micro-vibration isolation is the use of Gough Stewart Platform (henceforth abbreviated as GSP), for the six degrees of freedom vibration isolation between the source and the body, or the body and the vibration sensitive equipment. The most important parameter that governs the isolation characteristics of the GSP are the leg stiffness and the leg damping characteristics.

This work focuses on studying the response of a GSP to Negative Stiffness (NS) characteristics and consequently Quasi Zero Stiffness (QZS) characteristics in the legs of the GSP. We first reproduce the analytical results of the most basic negative stiffness mechanism – the Oblique Springs Mechanism. Further, the behaviour of the GSP is studied when oblique springs mechanism is introduced in the legs of the GSP. The kinematic and dynamic formulation for equations of motion of the GSP have been done. These equations then help to get the analytical results.

Further we introduce three different types of NS mechanisms, two utilizing torsion springs for generating NS characteristics, and one with helical compression springs for NS characteristics. The static analysis for these configurations is done, and the force-displacement and stiffness-displacement characteristics are studied. The theoretical conditions for the QZS condition are being derived.

The scope of this work is limited to the analytical formulation of the motion of a GSP and the force and stiffness analysis of the newly introduced NS mechanisms. Further, experimental study and verification using software can be done, to verify the results obtained from analytical formulation. Also, some corrective measures can be undertaken to correct the deviations of the actual characteristics from the analytical results.

TABLE OF CONTENTS

LIST OF FIGURES xi
ACRONYMS xiii
Chapter 1 – Introduction 1
1.1 - Introduction to Micro-Vibrations 1
1.2 - Ill Effects of Micro Vibrations 1
1.3 - Applications of Micro Vibrations 2
1.4 - Micro Vibrations in Spacecrafts 2
1.4.1 - Sources of Micro-Vibrations in Spacecrafts 3
1.4.2 - Attitude Control and Spacecraft Flywheel Rotor Systems (SFRS) 4
1.5 - Motivation – Why are micro-vibrations in spacecraft a concern? 5
1.6 - Existing Isolation Systems 6
1.7 - Organization of the Thesis 6
Chapter 2 – Literature Review and Problem Formulation 7
2.1 – Introduction 7
2.2 – The theory of Single Axis Vibration Isolation 7
2.3 Previous literature 9
2.3.1 – A novel vibration isolation system for reaction wheel on space telescopes 9
2.3.2 – Dynamically isotropic Gough–Stewart platform for micro-vibration isolation in spacecraft 10
Chapter 3 – Negative Stiffness and Quasi Zero Stiffness 12
3.1 – Introduction 12
3.2 – Stiffness Characteristics of Springs 12
3.2.1 – Helical Compression Springs 12
3.2.2 – Torsion Springs. 14
3.3 - Concept of Negative Stiffness and Quasi Zero Stiffness 16
3.4 – The Oblique Springs Configuration for Negative Stiffness in a system 17
3.4.1 – Analytical Formulation for Force and Stiffness 17
3.4.2 – Approximation of Oblique Springs Formulation to Duffing's Non-Linear Oscillator 20
3.4.3 – Comparison of Exact and Approximate Force and Stiffness for Oblique Springs 22
3.4.4 – Why is Negative Stiffness (NS) important? 23
3.4.5 – Solution of the approximate Duffing's Equation for Oblique Springs. 24
3.5 – Conclusion 28

Chapter 4 – New Possible Configurations for Quasi Zero Stiffness 29
4.1 – Introduction 29
4.2 – Torsion Spring Configuration 1 29
4.2.1 – Analytical Formulation for Force and Stiffness 29
4.2.2 – Stiffness plot for Torsion Spring Configuration 1, for different values of control parameters. 35
4.3 – Torsion Spring Configuration 2 37
4.3.1 – Analytical Formulation for Force and Stiffness 37
4.3.2 – Stiffness plot for Torsion Spring Configuration 2, for different values of control parameters. 42
4.4 – Helical Compression Spring Configuration 43
4.4.1 – Analytical Formulation for Force and Stiffness 43
4.4.2 – Stiffness plot for Negative Helical Spring Configuration, for different values of control parameter. 47
4.5 – Conclusion 48
Chapter 5 – Analytical formulation of Gough Stewart Platform 49
5.1 – Introduction 49
5.2 – The Geometry of Gough Stewart Platform 50
5.3 – Co-ordinate System Assignment 51
5.4 – Position and Orientation of the Base and the Platform. 53
5.4.1 – Position and Orientation of the Base. 53
5.4.2 – Position and Orientation of the Platform. 54
5.5 – Kinematics of the Base and the Platform. 55
5.5.1 – Kinematics of the Base. 55
5.5.1 – Kinematics of the Platform. 56
5.6 – Kinematics of the Leg. 57
5.6.1 – Expressions for the Leg Length and its time derivatives. 57
5.6.2 – Leg Coordinate Frame. 60
5.6.3 – Kinematics of the Universal Joint between the Base and the Legs. 61
5.7 – Dynamics of the Base, the Platform, and the Leg. 63
5.7.1 – Dynamics of the Base. 64
5.7.2 – Dynamics of the Platform. 66
5.7.3 – Dynamics of the Leg. 69
5.7.4 – Expressions for the Reaction Forces and the Moments. 72
5.8 – Differential Equation of Motion to be solved to get platform position and orientation 76
5.9 – Conclusion 77

Chapter 6 – Conclusion and Scope for Future Work. 78
6.1 – Conclusions 78
6.2 – Scope for Future Work. 79
Appendix A 80
A.1 – Derivation of Eqn. [4.2] 80
A.2 – Derivation of Eqn. [4.4] 81
A.3 – Derivation of Eqn. [4.15] 83
A.4 – Derivation of Eqn. [4.23] 86
References 88

LIST OF FIGURES

Figure 1. 1 a – Satellite pointing error (blue line) together with requirement (red dot), b – Resulting effects on image quality, c – Comparative result with corrective measures and reduced imager motion 2
Figure 1. 2 - Sources of Micro-Vibrations in Spacecrafts 3
Figure 1. 3 - Disturbance Sources of Micro-Vibrations in SFRS 5

Figure 2. 1 - Schematic of a Single Axis Isolator 7
Figure 2. 2 - Frequency response curves of the single axis isolator 8
Figure 2. 3 - Proposed Single Strut with Negative Stiffness Characteristics 9
Figure 2. 4 - Comparison curves of disturbance attenuation when the damping coefficient is 200 Ns/m 9
Figure 2. 5 - Comparison curves of disturbance attenuation when the damping coefficient is 130 Ns/m 10
Figure 2. 6 - (a) Transmissibility curve for a non-isotropic design, (b) Modified Gough-Stewart platform (MGSP) 11
Figure 2. 7 - Experimental result for translation modes (i.e. X, Y, and Z modes) 11

Figure 3. 1– Helical Compression Spring under compressive force 13
Figure 3. 2– Deflection in Torsion Spring under external force 14
Figure 3. 3 – Oblique Springs Configuration 17
Figure 3. 4 – Normalized Force vs Normalized Displacement 22
Figure 3. 5 – Normalized Stiffness vs Normalized Displacement 22
Figure 3. 6 – Oblique Springs Configuration subjected to harmonic excitation of mass 25
Figure 3. 7 – Displacement Amplitude vs Frequency response for harmonic force excitation of the mass 25
Figure 3. 8 – Oblique Springs Configuration subjected to harmonic excitation of base 27
Figure 3. 9 – Displacement Transmissibility vs Frequency response for harmonic base excitation of the mass 27

Figure 4. 1– Torsion Spring Configuration 1, Free State (FS), Intermediate State (IS), and Pre-stressed State (PCS at equilibrium position) of the torsion spring 30
Figure 4. 2 – Intermediate State (displaced state), and Pre-stressed State (equilibrium position) of the torsion spring configuration 1 31
Figure 4. 3 – Normalized Stiffness vs Normalized Displacement for varying l 35
Figure 4. 4 – Normalized Stiffness vs Normalized Displacement for varying α 35
Figure 4. 5 – Normalized Stiffness vs Normalized Displacement for varying R 36
Figure 4. 6 – Normalized Stiffness vs Normalized Displacement for varying μ 36
Figure 4. 7 – Torsion Spring Configuration 2, Free State (FS), Intermediate State (IS), and Pre-stressed State (PCS at equilibrium position) of the torsion spring 37
Figure 4. 8 – Intermediate State (displaced state), and Pre-stressed State (equilibrium position) of the torsion spring configuration 2 38
Figure 4. 9 – Normalized Stiffness vs Normalized Displacement for varying A/R 42
Figure 4. 10 – Helical Compression Spring Configuration, Initial State and Displaced State 44
Figure 4. 11 – Normalized Stiffness vs Normalized Displacement for varying B 47

Figure 5. 1 – The components of a GSP and the joints that are present in its legs 50
Figure 5. 2 – Frames of reference in a GSP 52
Figure 5. 3 – Frames of reference and vector diagram for kinematic study 53
Figure 5. 4 – Frame of reference attached to the universal joint 60
Figure 5. 5 – Free body diagram of the base, the leg and the platform 63
Figure 5. 6 – Forces and moments on the base, in world frame 64
Figure 5. 7 – Forces and moments on the platform, in world frame 67
Figure 5. 8 – Forces and moments on the leg, in world frame 69

ACRONYMS

NS – Negative Stiffness

PS – Positive Stiffness

QZS – Quasi Zero Stiffness

GSP – Gough Stewart Platform

MGSP – Modified Gough Stewart Platform

ACS – Attitude Control Systems

SFRS – Spacecraft Flywheel Rotor Systems

RWA – Reaction Wheel Assemblies

CMG – Control Moment Gyroscopes

Chapter 1 – Introduction

1.1 - Introduction to Micro-Vibrations

Vibration is a mechanical phenomenon characterized by the oscillatory motion of a body or particle about its stable equilibrium position, typically resulting from dynamic imbalances, external excitations, or internal structural responses. Micro-vibrations refer to extremely low-amplitude vibrations, generally in the range of a few micro-g's (μg), where 1 μg equals 9.81×10^{-6} m/s². These minute oscillations can occur over a broad frequency spectrum, typically from a few hertz (Hz) up to 1 kilohertz (kHz). Although subtle, micro-vibrations can significantly impact the performance and precision of high-sensitivity instruments, especially in aerospace, optics, and microelectromechanical systems (MEMS) applications.

1.2 - Ill Effects of Micro Vibrations

Micro-vibrations, though low in amplitude, can have significant adverse effects on sensitive systems and human perception. In optical systems, such as telescopes or imaging satellites, these vibrations can lead to deviations in the line-of-sight, resulting in image blurring, reduced resolution, and degraded data quality. Precision instruments like electron microscopes, mass spectrometers, nuclear magnetic resonance (NMR) systems, and magnetic resonance imaging (MRI) scanners are particularly susceptible to micro-vibrations. Even minute oscillations can disrupt measurements, cause signal noise, or lead to misalignments, ultimately compromising the accuracy and reliability of results in laboratory settings. Moreover, individuals with hyperacusis—a heightened sensitivity to sound—may find certain low-frequency vibrations distressing, as their brain may amplify or misinterpret these mechanical stimuli, leading to discomfort, anxiety, or pain. In such cases, micro-vibrations not only interfere with technical operations but also negatively affect human well-being. Therefore, effective isolation and damping of vibrations are critical in environments requiring high precision and sensory comfort.

1.3 - Applications of Micro Vibrations

Micro-vibrations have diverse applications across medical and industrial fields due to their controlled and precise nature. In healthcare, micro-vibration therapy is used to manage disuse syndrome by promoting muscle relaxation, reducing muscle stiffness, and increasing skin blood flow, thereby enhancing patient recovery. In advanced manufacturing, particularly semiconductor fabrication, micro-vibration measurement systems play a critical role in monitoring and isolating vibrations to protect ultra-sensitive equipment, improve process accuracy, and ensure personnel safety. Additionally, syringe micro-vibrating devices have shown promise in medical procedures by improving the diffusion of injected anesthesia into tissues, resulting in more effective and less painful administration.

1.4 - Micro Vibrations in Spacecrafts

Satellites are constructed from very lightweight materials and micro-vibrations can be easily transmitted through the flexible structure towards sensitive payloads or on-board instruments potentially causing severe performance degradation. In observation missions, micro-vibrations reduce image quality by introducing jitter motion during the exposure interval of the optical instruments. For Example – The line-of-sight jitter on the detector plane shown in Fig. 4a introduces the significant distortions visible in Fig. 4b. Image distortions can be corrected on the ground by dedicated algorithms

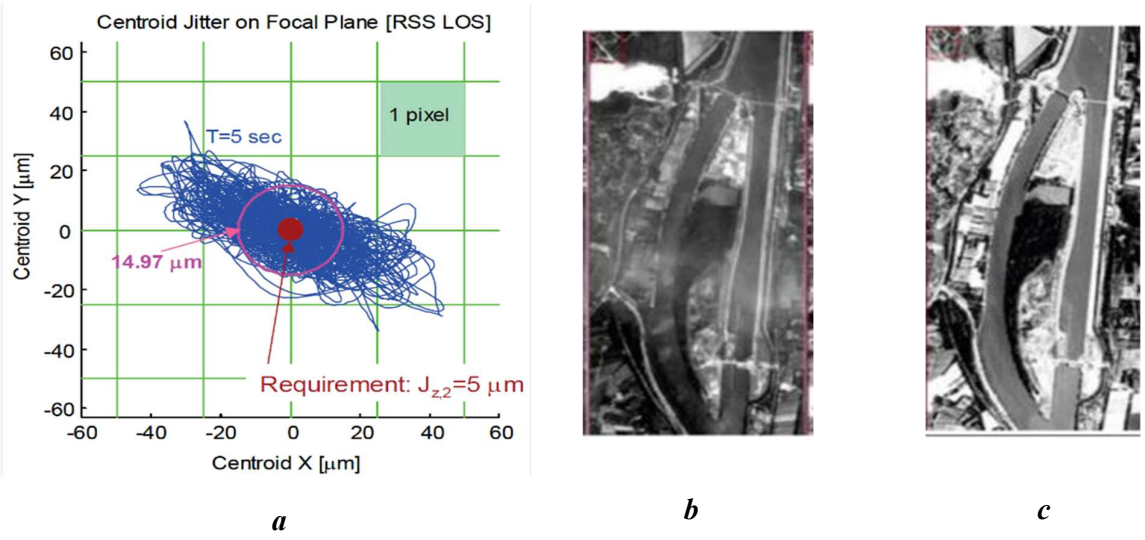

a *b* *c*

Figure 1. 1 a – Satellite pointing error (blue line) together with requirement (red dot), b – Resulting effects on image quality, c – Comparative result with corrective measures and reduced imager motion

1.4.1 - Sources of Micro-Vibrations in Spacecrafts

When classified on the basis of origin, micro-vibrations are a result of both external and internal disturbances, as shown in the figure below. However, internal disturbances are far more important.

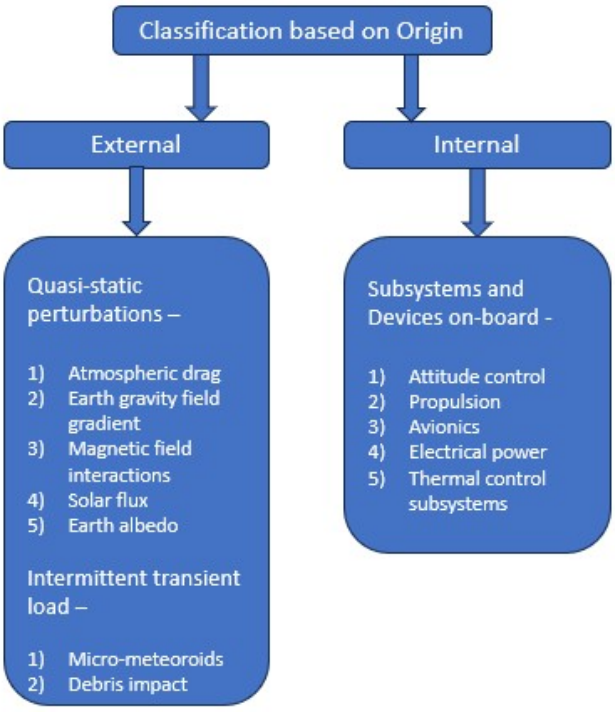

Figure 1. 2 - Sources of Micro-Vibrations in Spacecrafts

Depending on their temporal behaviour, they can be further classified as –

a) **Single disturbance events –**
   - Intermittent impulsive disturbances with small dynamic amplitudes
   - Frequent causes – sudden stress release, micro cracking in laminates, buckling of foils, etc.

b) **Continuous disturbances –**
   - Also known as vibratory loads
   - Either narrowband harmonic disturbances or broadband perturbations
   - Causes – infrared sensors, solar array drive mechanisms, cryocoolers, electric motors, data storage devices, rotating equipment such as Momentum/Reaction Wheel Assemblies and Gyroscopes.

Of all possible sources, the ones generated by Reaction Wheel Assemblies (RWA) or Control Moment Gyroscopes (CMG) are the most significant. These RWA or CMG are used for the Attitude and Pointing Control of the spacecraft.

1.4.2 - Attitude Control and Spacecraft Flywheel Rotor Systems (SFRS)

1.4.2.1 - Attitude Control –

The control of a spacecraft's angular orientation and rotational motion, whether with respect to the celestial reference frame or a target body such as Earth or the Moon, is referred to as attitude control. The Attitude Control System (ACS) is responsible for maintaining and adjusting this orientation and typically consists of three primary subsystems: attitude sensors, which provide real-time measurements of the spacecraft's orientation; a control algorithm or controller, which processes sensor data and determines the required corrective actions; and actuators, which execute the necessary torques or forces—such as reaction wheels, control moment gyroscopes, or thrusters—to achieve the desired attitude.

1.4.2.2 - Spacecraft Flywheel Rotor Systems (SFRS) –

A spacecraft flywheel rotor system is a type of momentum exchange device used in attitude control to manage the orientation of the spacecraft without expending propellant. It consists of a high-speed spinning rotor mounted on a motor, where changes in the wheel's angular momentum produce a reactive torque on the spacecraft due to the conservation of angular momentum. By accelerating or decelerating the flywheel, precise control of the spacecraft's attitude can be achieved along a specific axis.

1.4.2.3 - Types of SFRS –

- **Fixed Shaft Type** – Reaction Wheel Assemblies (RWA), Momentum Wheel Assemblies (MWA)
- **Non-fixed Shaft Type** – Control Moment Gyroscope (CMG)

The **Flywheel** and the **Bearing Systems** are the core components of the SFRS.

The bearing systems have two categories – **Mechanical bearings** and **Magnetic bearings**. Presently most of the SFRS in service are supported by mechanical rolling bearings.

1.4.2.4 - Disturbance Sources of Micro-Vibrations in SFRS

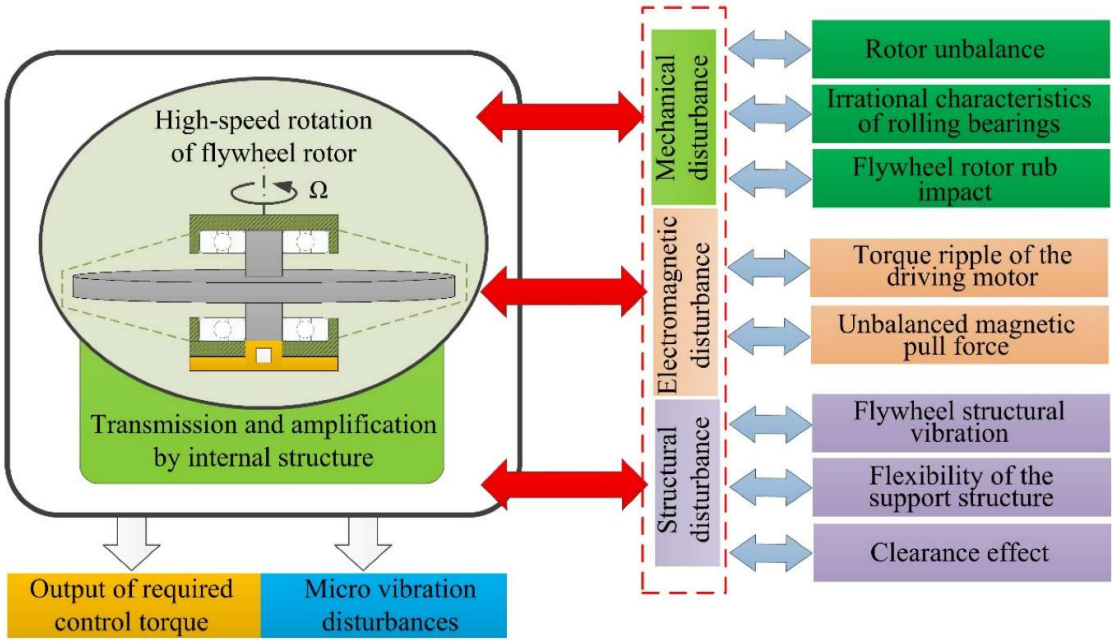

Figure 1. 3 - Disturbance Sources of Micro-Vibrations in SFRS

The above diagram summarises the different disturbance sources of micro-vibrations, that are present in the spacecraft.

1.5 - Motivation – Why are micro-vibrations in spacecraft a concern?

- The pointing stability of the Hubble Space Telescope (HST) of NASA is required to be less than 0.007 arcsec within 24 hr.
- The Space Interference Mission (SIM) and Advanced Technology Large Space Telescope (ATLAST) require pointing stability to reach 0.0016 arcsec, and the vibration interference to the platform is required to be below 10^{-6} g level.
- For a laser beam with a diameter of 100 mm emitted by a laser communication satellite, a jitter of 0.001 radians at a distance of 500 km will reduce the beam intensity received by the receiver by 100 times.
- The James Webb Space Telescope (JWST) requires that the line of sight motion should be 4 milli arc seconds.

1.6 - Existing Isolation Systems

The following micro-vibration isolation systems are currently used in the existing spacecrafts.

1) HST – Viscous Fluid Dampers, to attenuate axial disturbances
2) Defence Satellite Communication Systems III Spacecraft – Four damped stainless steel spring isolator
3) Chandra X-Ray Observatory – Hexapod isolator to achieve multi dimensional vibration isolation.

1.7 - Organization of the Thesis

Chapter 2 – Literature Review

Chapter 3 – Concept of Negative Stiffness and Quasi Zero Stiffness

Chapter 4 – New Possible Configurations for Negative Stiffness

Chapter 5 – Analytical Formulation of Gough Stewart Platform

Chapter 6 – Conclusions and Scope for Future Work

Chapter 2 – Literature Review and Problem Formulation

2.1 – Introduction

This chapter highlights previous pivotal investigations into the area of vibration isolation, particularly, micro-vibration isolation for spacecrafts. Through the literature review it is known that several researchers have worked on this problem statement and have proposed solutions that have been on board critical space missions. However, since the space applications are dynamic in nature, and owing to several constraints in these difficult missions, different missions require different ways of tackling this problem. Hence, this field of research is still evolving.

The use of dynamic stiffness elements, or High Static but Low Dynamic Stiffness (HSLDS) configurations have proven to be an effective way to achieve high level of micro-vibration isolation. Hence, there is scope in exploring newer and more effective HSLDS configurations for varied space applications. These HSLDS configurations are a result of the use of Negative Stiffness (NS) elements in vibration isolation systems.

2.2 – The theory of Single Axis Vibration Isolation

A single-axis isolator is shown in Fig. [2.1], where $\boldsymbol{M}$ is the mass of the sensitive equipment, and $\boldsymbol{K}$ and $\boldsymbol{c'}$ are the stiffness and the damping of the isolator, respectively. The transfer function of the passive vibration isolator can be written as

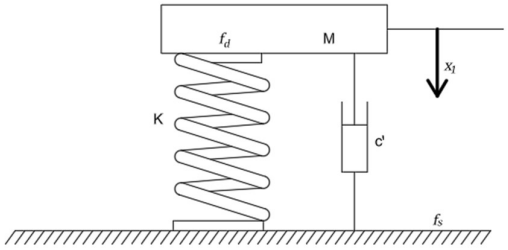

Figure 2. 1 - Schematic of a Single Axis Isolator

$$\boldsymbol{G(s) = \frac{c's + K}{Ms^2 + c's + K}} \qquad \boldsymbol{(2.1)}$$

The undamped natural frequency of the transfer function is $\boldsymbol{\omega_n}$, and the damping ratio is $\boldsymbol{\zeta}$. Substituting $\boldsymbol{s = j\omega}$, into Eqn. [2.1] and letting the frequency ratio $\boldsymbol{g = {\omega}/{\omega_n}}$, we get Eqn. [2.2], to represent the vibration isolation effect.

$$\boldsymbol{\mu_F = \frac{|f_s|}{|f_d|} = \sqrt{\frac{1 + 4\,\zeta^2 g^2}{(1 - g^2)^2 + 4\,\zeta^2 g^2}}} \qquad \boldsymbol{(2.2)}$$

In Fig. [2.2], it is evident that if the damping ratio $\boldsymbol{\zeta'}$ increases, the resonance amplitude decreases. Unfortunately, the high-frequency attenuation decreases as well. Therefore, the design of the isolator involves a tradeoff between the resonance amplitude and the high frequency attenuation. The ideal isolator should include frequency dependent damping, with high damping below the critical frequency $\sqrt{\boldsymbol{2}}\boldsymbol{\omega_n}$ to reduce the amplification peak and low damping above $\sqrt{\boldsymbol{2}}\boldsymbol{\omega_n}$ to improve the decay rate.

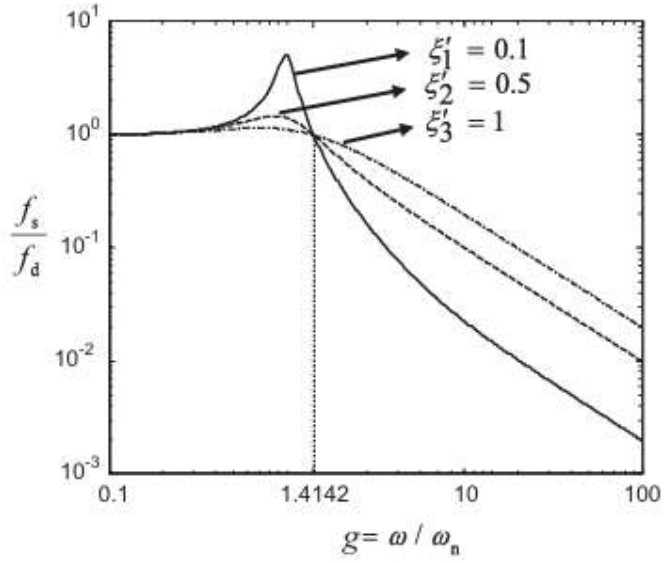

Figure 2. 2 - Frequency response curves of the single axis isolator

2.3 Previous literature

2.3.1 – A novel vibration isolation system for reaction wheel on space telescopes

Zhang, Y., Guo, Z., He, H., Zhang, J., Liu, M., & Zhou, Z. (2014). A novel vibration isolation system for reaction wheel on space telescopes. *Acta Astronautica*, *102*, 1-13. []

- This study aims to validate the feasibility and effectiveness of this new vibration isolation system having TMDs and NSS from a theoretical perspective.
- First, the integrated satellite dynamic model is constructed, including the RWs and the vibration isolation systems.
- Next, its frequency domain characteristics are described, and the application of the vibration isolation system for RWs is presented.
- Finally, the effective attenuation of RW disturbances is illustrated via the new vibration isolation system, and its safety performance is verified with numerical simulations.

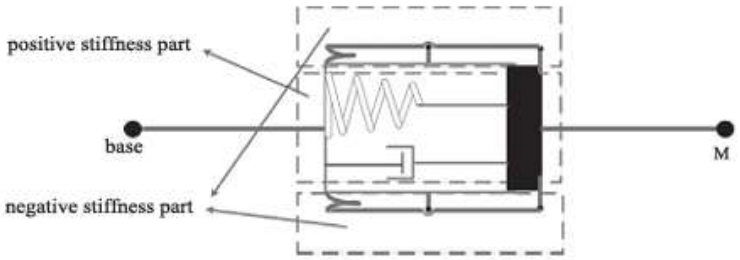

Figure 2. 3 - Proposed Single Strut with Negative Stiffness Characteristics

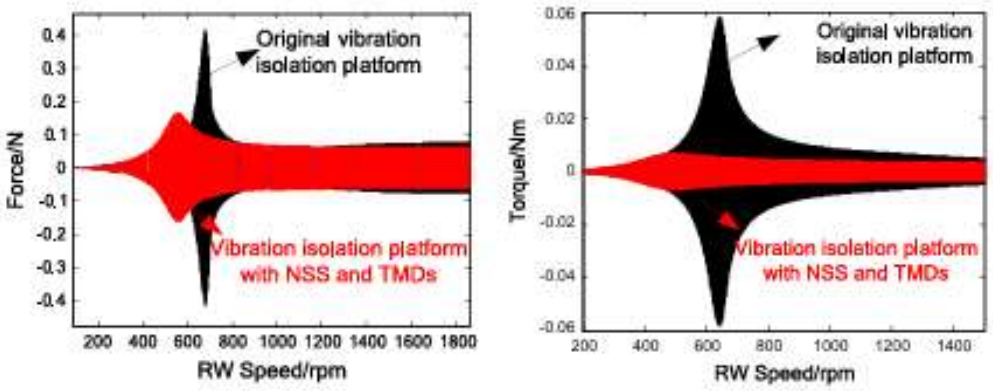

Figure 2. 4 - Comparison curves of disturbance attenuation when the damping coefficient is 200 Ns/m

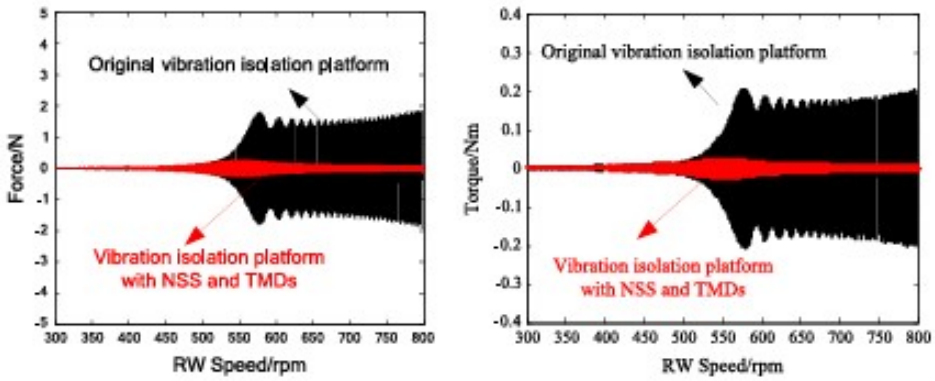

Figure 2. 5 - Comparison curves of disturbance attenuation when the damping coefficient is 130 Ns/m

2.3.2 – Dynamically isotropic Gough–Stewart platform for micro-vibration isolation in spacecraft

Singh, Y. P., Ahmad, N., & Ghosal, A. (2024). Dynamically isotropic Gough–Stewart platform for micro-vibration isolation in spacecrafts. *Mechanism and Machine Theory*, *201*, 105735.

- This paper deals with the modeling, simulation, and experimental validation of a Modified Gough–Stewart Platform (MGSP) i.e. 2 radii Gough–Stewart Platform for vibration isolation.
- Here the first six natural frequencies corresponding to the first six degrees of freedom are nearly the same, enabling effective attenuation of the first six modes.
- The approach accommodates various payload configurations, including variable center of mass and mass/inertia properties.
- The validation of the design is demonstrated using the finite element software ANSYS, and the model is further refined to incorporate flexural joints and structural damping.
- A prototype of the MGSP featuring flexural joints was tested, and it yielded experimental outcomes in close agreement with the finite element analysis results.

- The first six natural frequencies were close to the expected 29 Hz and vibration isolation of about 22 dB/octave.
- The close agreement among analytical, finite element, and experimental outcomes underscores the efficacy of our design approach and the suitability of an MGSP for micro-vibration isolation applications in spacecraft.

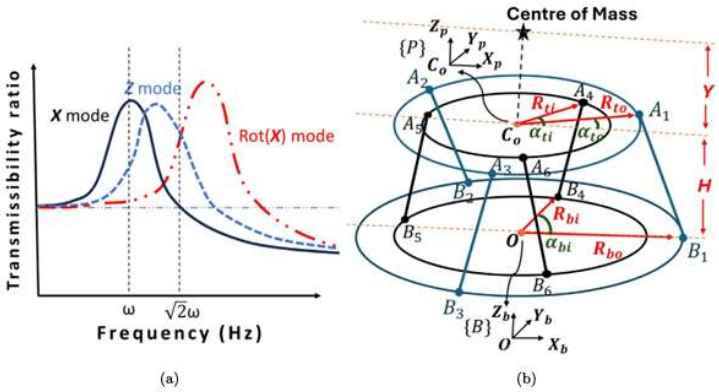

Figure 2. 6 - (a) Transmissibility curve for a non-isotropic design, (b) Modified Gough-Stewart platform (MGSP)

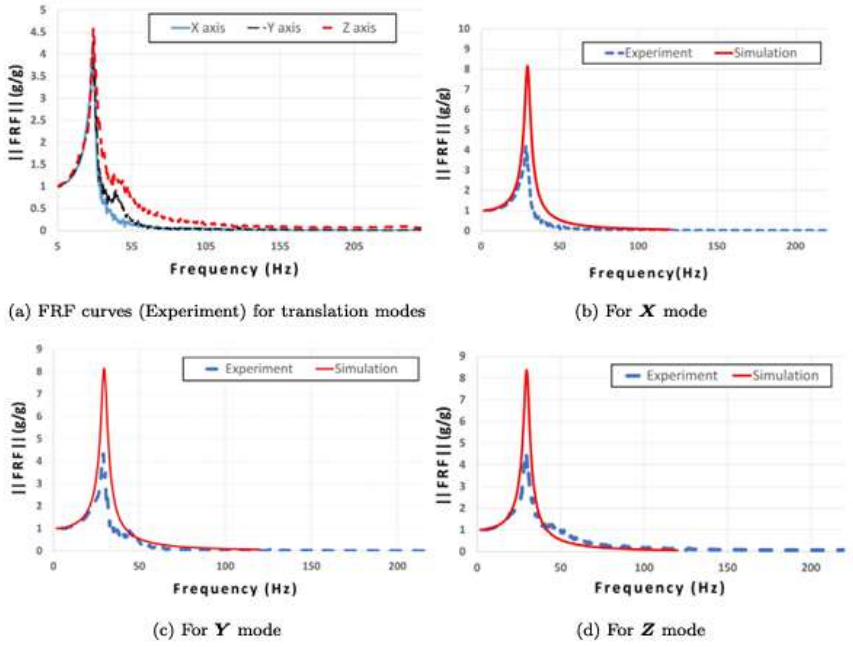

Figure 2. 7 - Experimental result for translation modes (i.e. X, Y, and Z modes)

Chapter 3 – Negative Stiffness and Quasi Zero Stiffness

3.1 – Introduction

Mechanical Stiffness refers to the material's or a structure's ability to resist the external force acting on it, or resist the deformation caused by the external force. A stiffer material or structure undergoes lower deformation or deflection (in case of bending loads). Material stiffness refers to the resistance to deformation offered by a material in any form. Material stiffness is a tensor quantity and is different for deformations in different directions. The modulus of elasticity is a direct measure of the material stiffness in the elastic limit, where the stress is proportional to strain. Structural stiffness however refers to the ability to resist deformation, of a structure made from a particular material. The structural stiffness can change if the material changes, and, also if the geometry of the structure changes. For example, a straight steel rod has different bending stiffness as compared to a curved steel rod.

Since, stiffness is a measure of the material's or structure's ability to resist external forces, it plays an important role in determining the vibration isolation characteristics of a structure. In mechanical structures or machinery, springs are the most widely used stiffness elements to counter the effect of unwanted external disturbances. Hence, it is necessary to understand the stiffness characteristics of springs.

In the coming section, we will discuss the stiffness characteristics of helical compression and torsion springs.

3.2 – Stiffness Characteristics of Springs

3.2.1 – Helical Compression Springs.

Fig [3.1], shows a helical compression spring being subjected to a compressive force. The force-deflection relation for the spring is obtained using Castigliano's theorem, as follows –

$$y = \frac{8FD^3N}{d^4G} \qquad (3.1)$$

The stiffness or spring rate of the spring is given by

$$\boldsymbol{k = \frac{\partial F}{\partial y} = \frac{d^4 G}{8 D^3 N}} \qquad \boldsymbol{(3.2)}$$

Where –

$y = deflection\ from\ the\ mean\ position$

$F = External\ force\ applied$

$d = wire\ diameter$

$G = Modulus\ of\ Rigidity\ of\ Material$

$D = Nominal\ Diameter\ of\ Spring$

$N = Number\ of\ active\ turns$

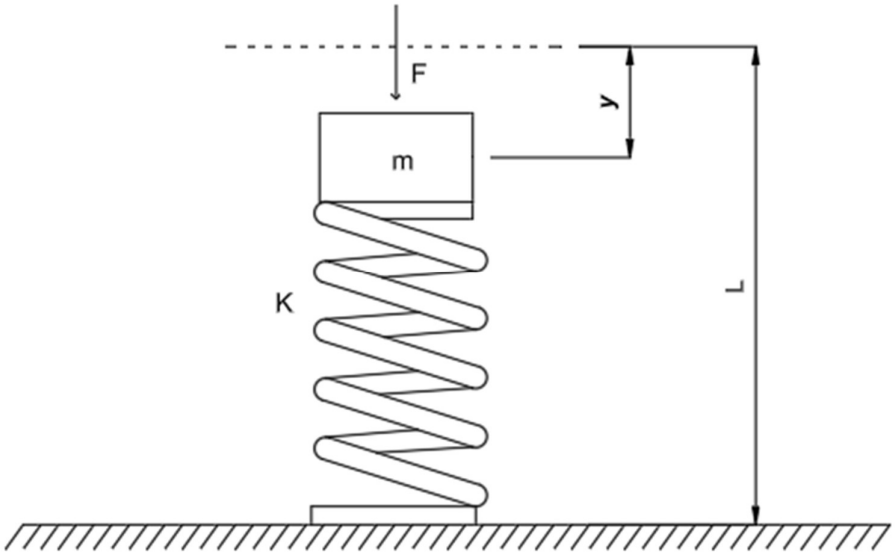

Figure 3. 1– Helical Compression Spring under compressive force

From Eqn. [3.1], we can see that the force-deflection relation for the helical compression spring is linear in nature. And the expression for the spring stiffness is only a function of material and geometrical properties of the spring. It does not depend upon the displacement of the point of application of force, from the equilibrium position. Thus, the helical compression spring has linear stiffness characteristics.

3.2.2 – Torsion Springs.

Fig [3.2], shows a torsion spring being subjected to an external force on its leg, that causes a moment about the center O of the spring. The moment-angular deflection relation for the spring is obtained using Castigliano's theorem, as follows –

$$\boldsymbol{\theta_t = \frac{64MDN_a}{d^4E}} \qquad (\mathbf{3.3})$$

The stiffness or spring rate of the spring is given by

$$\boldsymbol{k_t = \frac{\partial M}{\partial \theta_t} = \frac{d^4E}{64DN_a}} \qquad (\mathbf{3.4})$$

Where –

$\theta_t = angular\ deflection\ from\ the\ mean\ position$

$M = Moment\ due\ to\ external\ force\ applied$

$d = wire\ diameter$

$E = Modulus\ of\ Elasticity\ of\ Material$

$D = Nominal\ Diameter\ of\ Spring$

$N_a = Number\ of\ active\ turns$

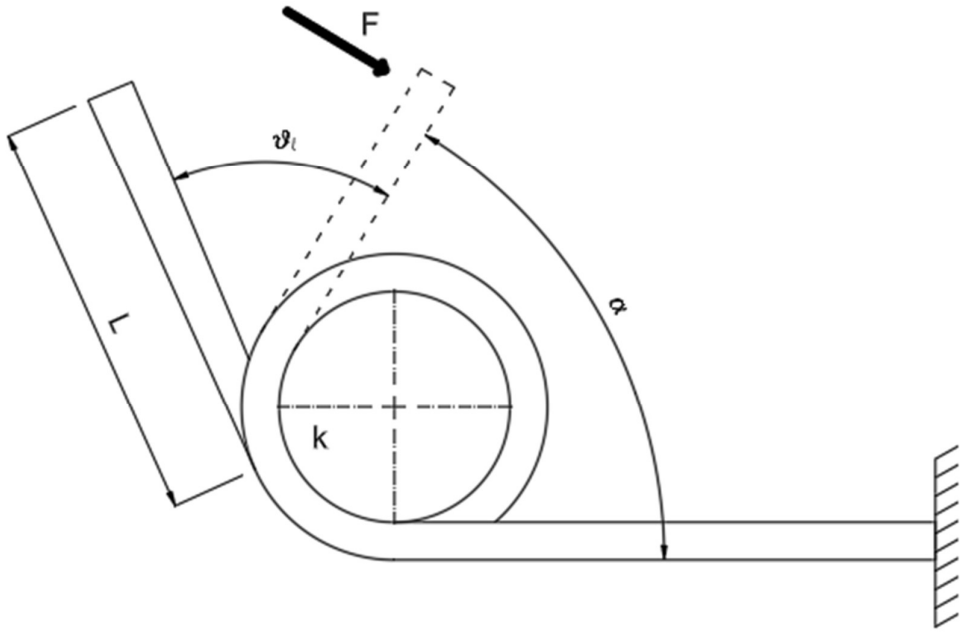

Figure 3. 2– Deflection in Torsion Spring under external force

From Eqn. [3.3], we can see that the moment-angular deflection relation for the torsion spring is linear in nature. And the expression for the spring stiffness is only a function of material and geometrical properties of the spring. It does not depend upon the angular displacement of the leg, from the equilibrium position. Thus, the torsion spring has linear stiffness characteristics.

In chapter 2, we discussed the single spring mass damper system for vibration isolation, in section [], which uses helical compression spring as stiffness element. This is the most basic isolation system that can be used to isolate the disturbances in a single degree of freedom. It works in two ways, one is to isolate the base from the internal disturbances in the payload, and the second is to isolate sensitive payloads from disturbances coming from the base. This isolation system uses only a single positive stiffness element, with constant stiffness.

Now, for any system to undergo vibrations, the two important properties it should have, are stiffness and inertia. The property of inertia comes from the mass present in the system. We have also seen in chapter 2 that to have a vibration isolation over a wide range of frequency, it is desired to have a lower natural frequency in the system. Also, in micro-vibration isolation for spacecraft applications the range of frequencies of loads is quite low. Hence, to avoid catastrophic failures at resonant frequencies, the natural frequency of the system should be low. In order the have lower natural frequency, the system must have lower stiffness values. However, lower values of stiffness can affect the load carrying capacity of the system. Thus, the conclusion is that a good vibration isolation system must have high static stiffness to carry the desired payloads, and, also lower dynamic stiffness to lower the natural frequency of the system. This desire provides us the motivation to study and use isolation systems with variable stiffness elements, which can provide very low values of stiffness and consequently natural frequency at equilibrium position. A potential way to achieve variable structural stiffness in a system is to use negative stiffness configuration.

3.3 - Concept of Negative Stiffness and Quasi Zero Stiffness

In certain mechanisms, there may exist a stiffness element, which is configured in such a way; that the force applied by this element on the mass, in response to the deflection of the mass from its equilibrium position, is opposite to the restoring force, or in the direction of the deflection. This stiffness element tries to reduce the restoring force acting on the mass, and subsequently the stiffness of the entire system. The stiffness offered by such an element in the system is termed as Negative Stiffness (NS). The use of negative stiffness elements in a system is an effective way to achieve lower dynamic stiffness.

The Negative Stiffness (NS) offered by such an element tries to counter the actual Positive Stiffness (PS) present in the system, thereby reducing the system stiffness. In such a case, it may so happen that the positive and negative stiffness cancel out each other, to theoretically give a net zero stiffness in the system at a certain point, or sufficiently close to zero over a range of deflection. This phenomenon is known as the condition of Quasi Zero Stiffness (QZS). The mathematical condition of QZS is a function of the stiffness and geometrical parameters of the system. If this mathematical condition is met in practical scenarios, the system can have absolute zero stiffness at a certain point, or sufficiently close to zero over a range of deflection. If the stiffness and geometrical parameters of the system have mathematical values such that there is a certain error in the mathematical condition, the system will still have variable stiffness characteristics, but may not have absolute QZS characteristics.

The most basic and widely studied configuration for negative stiffness is the Oblique Springs Mechanism. In the following section we reproduce certain results of this configuration as a base for our further study of negative stiffness configurations.

3.4 – The Oblique Springs Configuration for Negative Stiffness in a system

3.4.1 – Analytical Formulation for Force and Stiffness

Fig [3.3], shows a schematic diagram of the oblique spring configuration. It consists of a central helical spring that takes up the deadweight of the payload mass. Two other springs are also connected to the mass. At their natural length, the two other springs are in oblique direction (hence the term oblique springs used). However, at the equilibrium position, the oblique springs are horizontal with precompression. Due, to this precompression the oblique springs apply force on the mass in horizontal direction, with no vertical component at equilibrium position. Thus, at the equilibrium position, the net forces acting on the system are zero.

When, the mass is subjected to an upward vertical displacement of $\boldsymbol{x}$, the central spring offers a restoring force in downward direction. However, the oblique springs release some amount of their precompression, and a net upward vertical force acts on the mass due to these springs. This upward force reduces the restoring force acting on the mass.

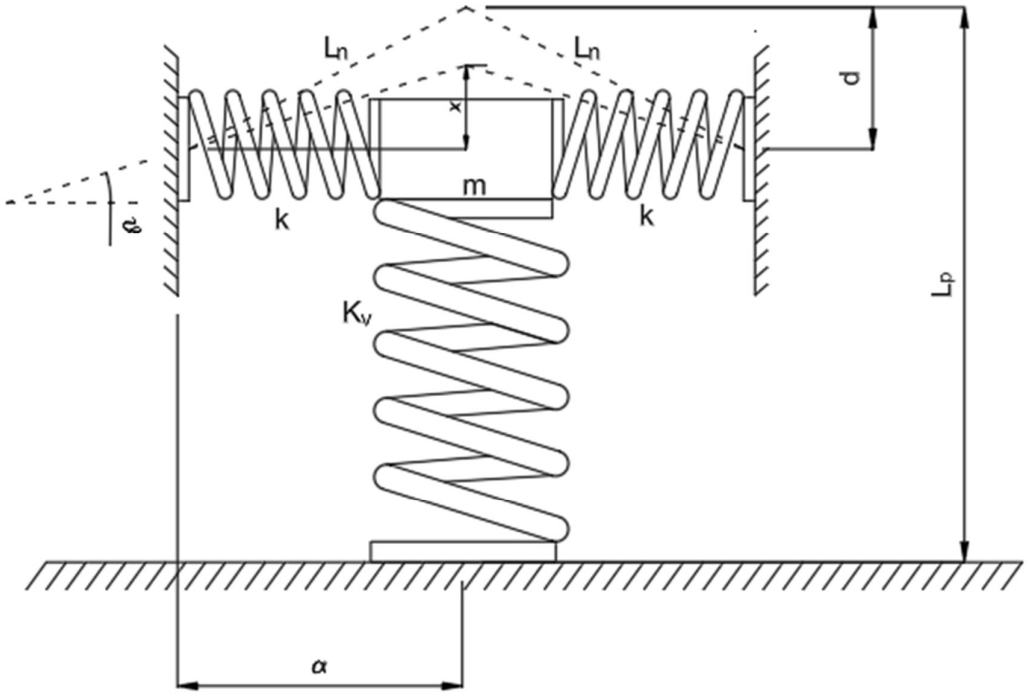

Figure 3. 3 – Oblique Springs Configuration

From Fig [3.3], the expressions for the forces acting on the mass are –

$$F_p = K_v x \tag{3.5}$$

$$F_n = k\left(L_n - \sqrt{\alpha^2 + x^2}\right) \tag{3.6}$$

Where, F_p *and* F_n, are forces due to the central and the oblique springs respectively.

The net vertical force acting on the mass will be

$$F = F_p - 2F_n \sin\theta$$

$$F = K_v x - 2k\left(L_n - \sqrt{\alpha^2 + x^2}\right) . \frac{x}{\sqrt{\alpha^2 + x^2}}$$

$$F = K_v x - 2kx\left[\frac{L_n}{\sqrt{\alpha^2 + x^2}} - 1\right] \tag{3.7}$$

This expression for force can be normalized, by normalizing the displacement x by α, and F by $K_v\alpha$. Thus, the expression for the normalized force will become –

$$f = \bar{x} - \frac{2K}{K_v}\bar{x}\left[\frac{\frac{L_n}{\alpha}}{\sqrt{1 + \bar{x}^2}} - 1\right] \tag{3.8}$$

Where, f is the normalized force and $\bar{x}$ is the normalized displacement.

The normalised stiffness of the system can be obtained by differentiating the expression for f w.r.t $\bar{x}$. Thus, the expression for the normalised stiffness will be –

$$\overline{K_o} = \frac{\partial f}{\partial \bar{x}} = 1 - \frac{2K}{K_v}\left[\frac{\frac{L_n}{\alpha}}{(1 + \bar{x}^2)^{1.5}} - 1\right] \tag{3.9}$$

From Eqn. [3.8], we see that the expression for the net restoring force acting on the system is not a linear function of the displacement. And from Eqn. [3.9], we see that the stiffness of the system is not constant, but is now a function of the displacement of the mass from the mean

position. Thus, the oblique springs configuration provides us a variable stiffness mechanism that can keep the dynamic stiffness of the system low as required.

The force applied by the oblique springs on the mass is in the direction of the displacement, thus providing a negative stiffness in the system. For the system to exhibit quasi zero stiffness (QZS) characteristics, the system must have zero stiffness at the equilibrium position. Solving the above expression for $\overline{K_o}$, yields the following condition.

For QZS characteristics –

$$\overline{K_o} = 0 \qquad at \qquad \bar{x} = 0$$

$$Therefore, \qquad 1 - \frac{2K}{K_v}\left[\frac{\frac{L_n}{\alpha}}{(1 + \bar{x}^2)^{1.5}} - 1\right] = 0 \qquad at \quad \bar{x} = 0$$

yields the condition

$$\frac{L_n}{\alpha} = 1 + \frac{K_v}{2K} \qquad \begin{cases} Condition\ for \\ QZS\ at\ Equilibrium\ position \end{cases} \qquad (3.10)$$

Thus, the Eqn. [3.10], gives us the mathematical condition between the geometrical and stiffness parameters, which will result into QZS characteristics into the system, at equilibrium position. Using Eqn. [3.10], in Eqn. [3.9], we get the expression for the stiffness of the system as

$$\overline{K_o} = \left(\frac{2K}{K_v} + 1\right)\left[1 - \frac{1}{(1 + \bar{x}^2)^{1.5}}\right] \qquad (3.11)$$

From Eqn. [3.11], we see that the stiffness of a system having oblique springs configuration is a function of displacement of the mass, and is hence dynamic in nature. Also, the stiffness is a function of only one unknown parameter K/K_v. An appropriate value of this parameter will help us to get desired stiffness characteristics in the system. However, the disadvantage of only

one unknown parameter is that we have less control parameters in the system for stiffness control.

3.4.2 – Approximation of Oblique Springs Formulation to Duffing's Non-Linear Oscillator

The term $\left(\frac{1}{\sqrt{1+\bar{x}^2}}\right)$ in the expression for normalized force can be approximated using binomial expansion as $(\mathbf{1-0.5\,\bar{x}^2})$. With this approximation, the expression for the normalised force will then become

$$\boldsymbol{f = \bar{x}\left[1-\frac{2KL_n}{K_v\alpha}+\frac{2K}{K_v}\right]+\frac{KL_n}{K_v\alpha}\bar{x}^3} \qquad (\mathbf{3.12})$$

Which is of the form of $\boldsymbol{f = \alpha x + \mu x^3}$ **,** which represents the force in a standard duffing's nonlinear oscillator. Approximating the oblique springs configuration to duffing's nonlinear oscillator will help us in studying the response of the system analytically, since, the duffing's equation can be solved analytically using the harmonic balance method.

Differentiating Eqn. [3.12], we get the expression for the approximate normalized stiffness of the system as

$$\boldsymbol{\overline{K_o} = 1 - \frac{2K}{K_v}\left[\frac{L_n}{\alpha} - \frac{3L_n}{2\alpha}\bar{x}^2 - 1\right]} \qquad (\mathbf{3.13})$$

For the system to exhibit quasi zero stiffness (QZS) characteristics, the system must have zero stiffness at the equilibrium position. Solving the above approximate expression for $\boldsymbol{\overline{K_o}}$, yields the following condition.

For QZS characteristics –

$$\boldsymbol{\overline{K_o} = 0 \quad at \quad \bar{x} = 0}$$

$$\textit{Therefore,} \qquad \boldsymbol{1 - \frac{2K}{K_v}\left[\frac{L_n}{\alpha} - \frac{3L_n}{2\alpha}\bar{x}^2 - 1\right] = 0 \quad at \quad \bar{x} = 0}$$

yields the condition

$$\frac{L_n}{\alpha} = 1 + \frac{K_v}{2K} \qquad \begin{cases} \textbf{Condition for} \\ \textbf{QZS at Equilibrium position} \end{cases} \quad (3.14)$$

Thus, the approximate expression for stiffness also yields the same mathematical condition for QZS characteristics in the system. And, hence similar comments can be made for the condition of QZS as made above.

An important point to note here is that, this approximation is being used to get the response of the system from the result of duffing's oscillator. However, this approximation is valid for only small values of $\bar{x}$. At sufficiently large values of $\bar{x}$, the exact and approximate expressions for force and stiffness exhibit large errors, and hence the duffing's solution may not express the true response of the system.

Using Eqn. [3.14], i.e. the condition for QZS at equilibrium position, in Eqn. [3.13], we get the expression for the approximate stiffness of the system as

$$\overline{K}_o = \frac{3}{2}\left[\frac{2K}{K_v} + 1\right]\bar{x}^2 \qquad (3.15)$$

Again, the stiffness is a function of only one unknown parameter K/K_v. The expression for approximate stiffness of the system is nonlinear and a quadratic function of $\bar{x}$.

3.4.3 – Comparison of Exact and Approximate Force and Stiffness for Oblique Springs

Fig [3.4] shows the plot of expression for exact and approximate force as a function of $\bar{x}$ and Fig [3.5] shows the plot of expression for exact and approximate stiffness as a function of $\bar{x}$.

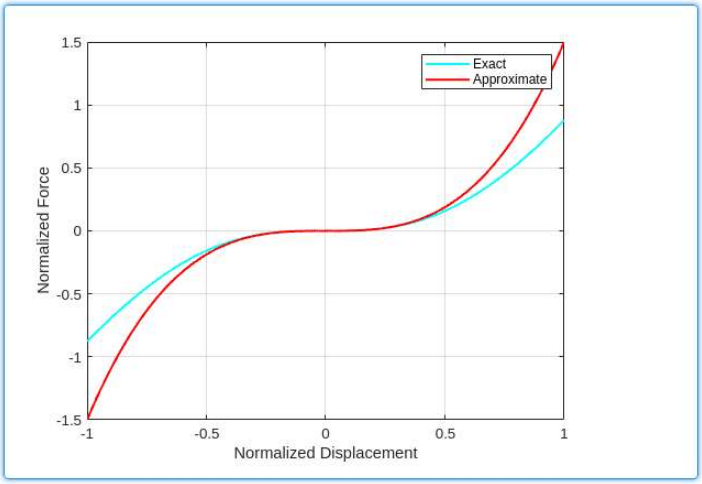

Figure 3. 4 – Normalized Force vs Normalized Displacement

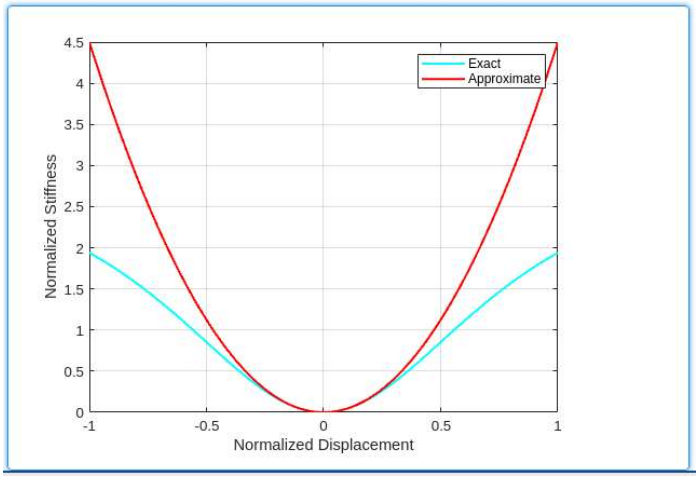

Figure 3. 5 – Normalized Stiffness vs Normalized Displacement

From Fig [3.4], we see that the exact and approximate forces have small amount of error up to certain range of the normalized displacement. This range can be increased or decreased depending on the values of the unknown control parameters, and, also if we take higher order polynomial approximation (binomial expansion), in the force expression. Also, at higher values of $\bar{x}$, the numerical values of approximate force are higher as compared to the exact values. This is expected since, the expression for approximate force has cubic polynomial increase

(Ref. Eqn. [3.15]), whereas the expression for exact force has linear increase at higher values of $\bar{x}$. Thus, we infer that the system behaves linearly at higher values of $\bar{x}$.

From Fig [3.5], we see that the exact and approximate stiffness have small amount of error up to certain range of the normalized displacement. This range can be increased or decreased depending on the values of the unknown control parameters, and, also if we take higher order polynomial approximation (binomial expansion), in the force expression. As expected, the plot for stiffness is symmetric w.r.t the normalized displacement. At higher values of $\bar{x}$**,** the numerical values of approximate stiffness are higher as compared to the exact values. This is expected, since at higher values of $\bar{x}$**,** the oblique springs release all their precompression after a certain value of $\bar{x}$**.** After this point the oblique springs also contribute to the stiffness of the central spring, thereby making the stiffness of the system constant. This behaviour is seen in Fig [3.9], at higher values of $\bar{x}$. However, the expression for approximate force has quadratic polynomial increase. This explains why at higher values of $\bar{x}$ the approximate stiffness is significantly higher as compared to exact stiffness.

However, since we deal with vibrations of amplitudes in **µg's,** in spacecraft applications, and the normalization parameter α is of the order of **mm**. This approximation can be used in practical conditions since, the range of operation of $\bar{x}$ is quite less in these applications.

3.4.4 – Why is Negative Stiffness (NS) important?

a) From the Fig [3.4], of the normalized force and Fig [3.5], of the normalized stiffness, it is seen that the force and stiffness values are very close to zero, in the vicinity of the equilibrium position.

b) This means the system offers very low restoring forces in this region and thus prevents the mass from further vibrations.

c) It is inferred that the combined stiffness elements (PS and NS), provide a softer stiffness compared to the PS element.

d) Consequently, the natural frequency of the system is low, which is desired for low frequency vibration isolation.

3.4.5 – Solution of the approximate Duffing's Equation for Oblique Springs.

After studying the force and stiffness behaviour of the oblique springs configuration, it is important to study the response of the system to external excitations. The particular area of interest is the transmissibility of the system, when the system is subjected to external excitations.

The equation of motion of the mass in oblique springs configuration can be solved numerically to get the response. However, the approximation for the force and stiffness converts the equation of motion into standard duffing's oscillator equation, which can be solved using the harmonic balance method.

3.4.5.1 – Harmonic Excitation of the Mass.

Fig [3.6], shows a mass with oblique springs configuration, subjected to harmonic excitation $\boldsymbol{F = f\ \sin \omega t}$. The differential equation of motion of the mass under harmonic force excitation will be –

$$\ddot{x} + \delta\dot{x} + \beta x + \mu x^3 = f sin(\omega t) \qquad (3.16)$$

Where $\boldsymbol{\delta}$, $\boldsymbol{\beta}$ and $\boldsymbol{\mu}$ are the system parameters, in terms of the stiffness and geometrical parameters, for the oblique springs configuration. The above equation represents a standard duffing's oscillator.

Solving the above equation using Harmonic Balance Method, we a get the following polynomial equation for the displacement amplitude of the mass under harmonic excitation.

$$36\mu^2 R^6 + 24\mu(\beta - \omega^2)R^4 + 4[(\beta - \omega^2)^2 + (\delta\omega)^2]R^2 - f^2 = 0 \qquad (3.17)$$

The above equation is a cubic polynomial in $\boldsymbol{R^2}$**,** where $\boldsymbol{R}$ is the amplitude of the displacement of the mass. The above polynomial equation is solved for appropriate values $\boldsymbol{\delta}$, $\boldsymbol{\beta}$ and $\boldsymbol{\mu}$**,** to get the frequency response of the system i.e. the variation of $\boldsymbol{R}$ w.r.t $\boldsymbol{\omega}$**.**

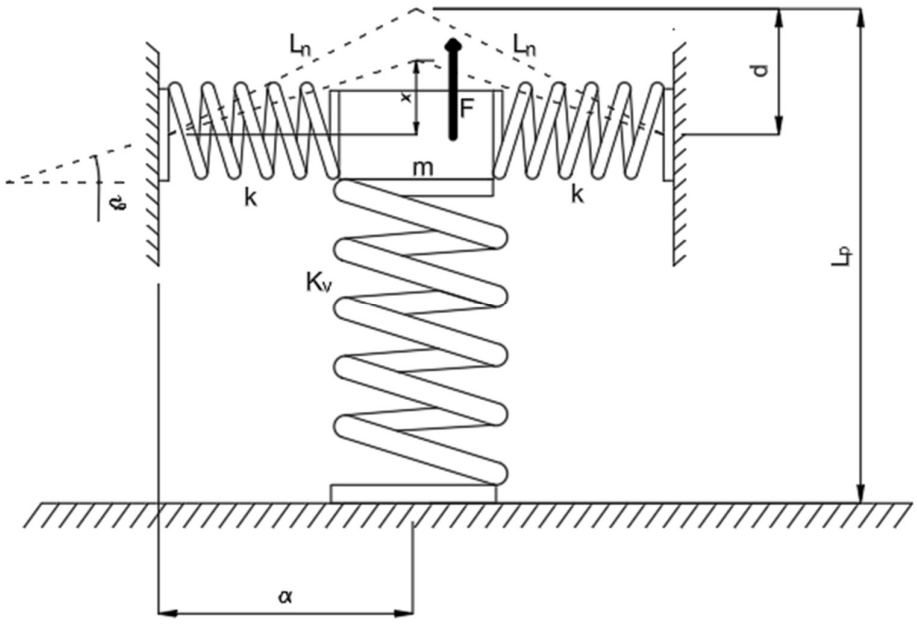

Figure 3. 6 – Oblique Springs Configuration subjected to harmonic excitation of mass

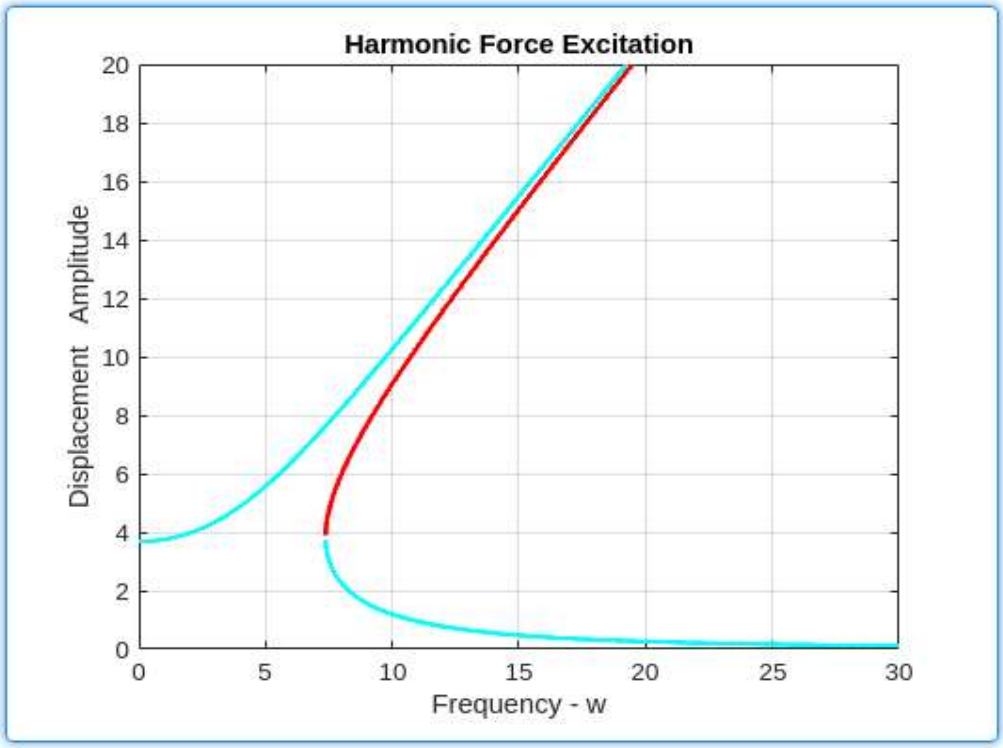

Figure 3. 7 – Displacement Amplitude vs Frequency response for harmonic force excitation of the mass

Fig [3.7], shows the frequency response of the system for certain values of $\boldsymbol{\delta}$, $\boldsymbol{\beta}$ and $\boldsymbol{\mu}$ over a range of $\boldsymbol{\omega}$. The blue plot shows the region of stability whereas the red plot shows the region of instability. An important observation in this plot is the jump phenomenon. Initially as the $\boldsymbol{\omega}$ increases from zero, the response of the system follows the blue curve up to the point from where the curve comes back, i.e. the top of the red curve. The red curve is unstable meaning if the mass goes into the red region, its unstable and suddenly jumps off to the lower blue curve, which is again a stable region. In practical conditions as soon as the mass reaches the top of the red curve, it suddenly jumps off to the lower blue curve and then the response of the system follows the lower blue curve. This is known as the jump phenomenon.

3.4.5.2 – Base Excitation or Support Motion.

Fig [3.8], shows a mass with oblique springs configuration, subjected to base excitation $\boldsymbol{y = Y\ \sin \omega t}$. The differential equation of motion of the mass under base excitation will be –

$$\ddot{x} + \delta\dot{x} + \gamma x + \mu x^3 = Y[\delta\omega cos(\omega t) + \beta \sin(\omega t)] \qquad (3.18)$$

Where $\boldsymbol{\delta}$, $\boldsymbol{\gamma}$ and $\boldsymbol{\mu}$ are the system parameters, in terms of the stiffness and geometrical parameters, for the oblique springs configuration. The above equation represents a standard duffing's oscillator.

Solving the above equation using Harmonic Balance Method, we a get the following polynomial equation for the displacement amplitude of the mass under base excitation.

$$36\mu^2R^6 + 24\mu(\gamma - \omega^2)R^4 + 4[(\gamma - \omega^2)^2 + (\delta\omega)^2]R^2 - Y^2[(\delta\omega)^2 + \beta^2] = 0 \qquad (3.19)$$

The above equation is a cubic polynomial in $\boldsymbol{R^2}$**,** where $\boldsymbol{R}$ is the amplitude of the displacement of the mass. The above polynomial equation is solved for appropriate values $\boldsymbol{\delta}$, $\boldsymbol{\gamma}$ and $\boldsymbol{\mu}$**,** to get the frequency response of the system i.e. the variation of $\boldsymbol{TR}$ w.r.t $\boldsymbol{\omega}$**.**

Where, $\boldsymbol{TR}$ is the displacement transmissibility which is given by –

$$TR = \frac{2R}{Y}$$

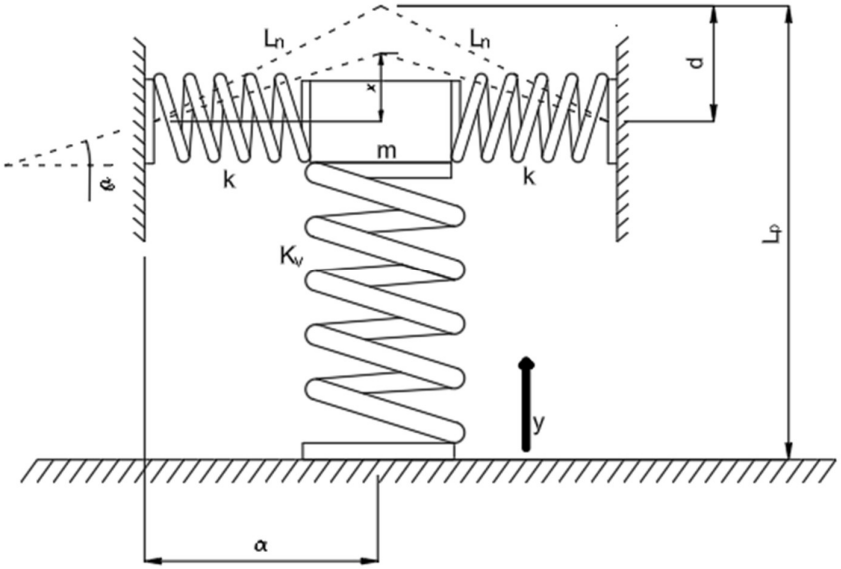

Figure 3. 8 – Oblique Springs Configuration subjected to harmonic excitation of base

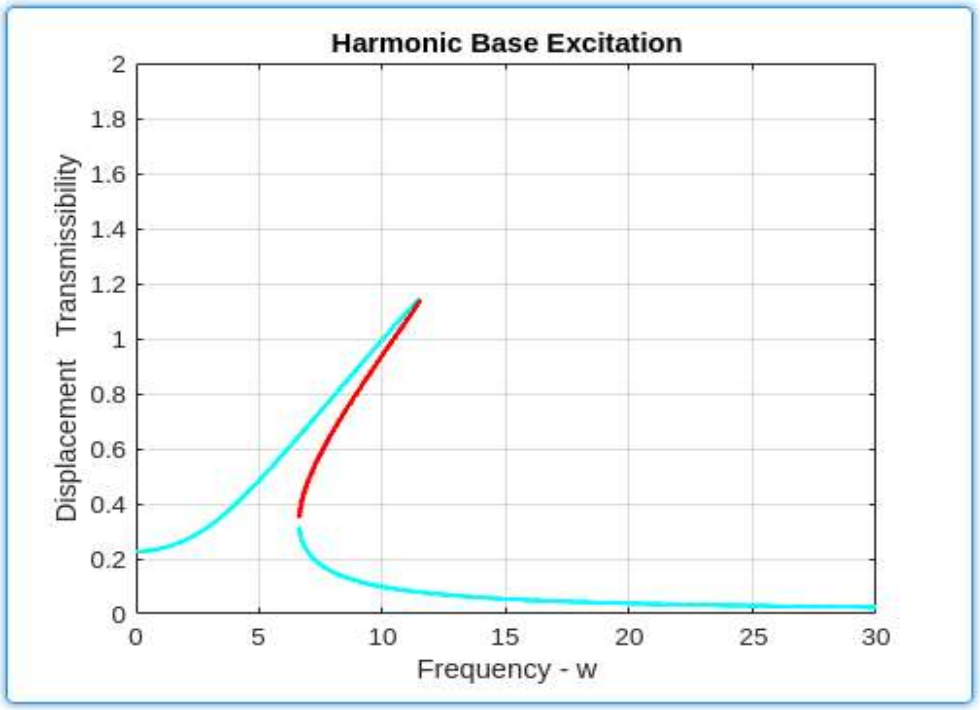

Figure 3. 9 – Displacement Transmissibility vs Frequency response for harmonic base excitation of the mass

Fig [3.9], shows the plot of transmissibility of the system for certain values of $\boldsymbol{\delta}$, $\boldsymbol{\beta}$ and $\boldsymbol{\mu}$ over a range of $\boldsymbol{\omega}$. The blue plot shows the region of stability whereas the red plot shows the region of instability. The plot is similar to the plot discussed in section 3.4.4.1 and shows a similar jump phenomenon.

3.5 – Conclusion.

1) Structural stiffness is an important parameter that governs the dynamic behaviour of the system.

2) For isolation over a wide frequency range, it is desired to have low stiffness in the system.

3) Negative Stiffness mechanisms can give us a system with low dynamic stiffness, without compromising the static stiffness of the system.

4) The oblique springs mechanism is a simple and effective mechanism to get NS in the system. However, it has only one unknown control parameter to control the behaviour of the system.

5) The response of the system can be studied for small values of the normalized displacement, by approximating the oblique springs mechanism to standard duffing's oscillator.

6) The response obtained from the duffing's approximation shows that the system exhibits the jump phenomenon at certain frequency. This sudden change in the mass displacement can cause system failure, and need to be handled appropriately.

Chapter 4 – New Possible Configurations for Quasi Zero Stiffness

4.1 – Introduction

In chapter 3, we saw the role of stiffness in vibration isolation in a system and, also, the importance of NS and QZS to improve the vibration isolation characteristics over a wide frequency range. We discussed the static analysis and frequency response of the Oblique Springs configuration.

In this chapter we will look at new possible configurations that can help achieve negative stiffness characteristics in a system. In all the configurations the main positive stiffness element, which is also responsible for the static stiffness of the system is a helical compression spring which has linear characteristics. Different structural elements can be used to generate the required negative stiffness characteristics. Examples being a cantilever beam, a fixed curved beam, torsion springs etc.

Here we present three different configurations. Two of which use torsion springs in different configuration, and one which uses vertical helical compression spring, to generate the desired negative stiffness characteristics in the system. The static force and stiffness analysis is done for all configurations and expressions for the nonlinear stiffness of the system are obtained. The variation of the stiffness is studied for varying unknown control parameters of the system.

Refer to section 3.2 of chapter 3, for the stiffness characteristics of helical compression springs and torsion springs.

4.2 – Torsion Spring Configuration 1

4.2.1 – Analytical Formulation for Force and Stiffness

Fig [4.1], shows a schematic diagram of the Torsion Spring Configuration 1. It consists of a central helical spring that takes up the deadweight of the payload mass. Three torsion springs are also connected to the mass, which are at $120°$ from each other when viewed from the top. However, only one is shown in the diagram. The other two have similar contribution in the expressions and the appropriate multiplication factor of 3 is considered. At the equilibrium position, the torsion springs have initial outer angular deflection, as shown in Fig [4.2]. The

horizontal motion of the torsion spring is restricted by the outer sleeve and the circular cam profile (hereafter referred to as cam profile 1), present on the vertical rod attached to the central spring. Due to this restriction the spring cannot release its deflection and remains stressed. Due to this pre stress the three torsion springs apply forces of equal magnitude in the horizontal plane on the cam profile 1, via the circular profile of the torsion spring (hereafter referred to as cam profile 2). These force vectors cancel out each other in the horizontal plane with no vertical component, and hence, there is no net force applied by the torsion springs on the central rod (consequently the mass), at the equilibrium position. Thus, at the equilibrium position, the net forces acting on the system are zero.

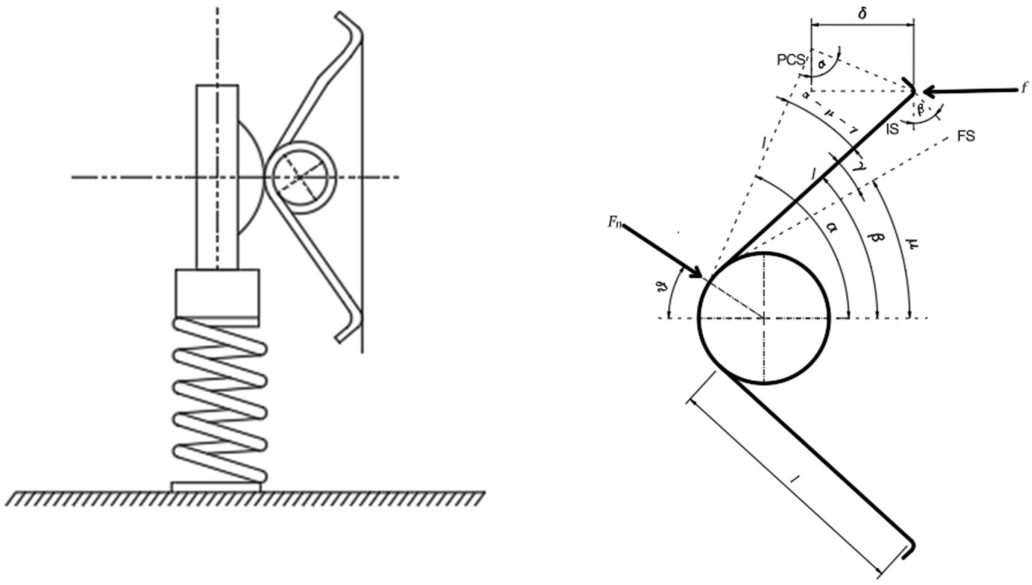

Figure 4. 1– Torsion Spring Configuration 1, Free State (FS), Intermediate State (IS), and Pre-stressed State (PCS at equilibrium position) of the torsion spring

When, the mass is subjected to an upward vertical displacement of $\boldsymbol{x}$, the central spring offers a restoring force in downward direction. However, the torsion springs release some amount of their pre stress, due to the horizontal movement of the cam profile 2. Here it is assumed that the cam profile 2 is constrained to move in horizontal direction only. Thus, due this vertical movement of cam profile 1 and the resulting horizontal movement of cam profile 2, the line of action between the two cam profiles change, and a net upward vertical force acts on the mass due to these torsion springs. This upward force reduces the restoring force acting on the mass.

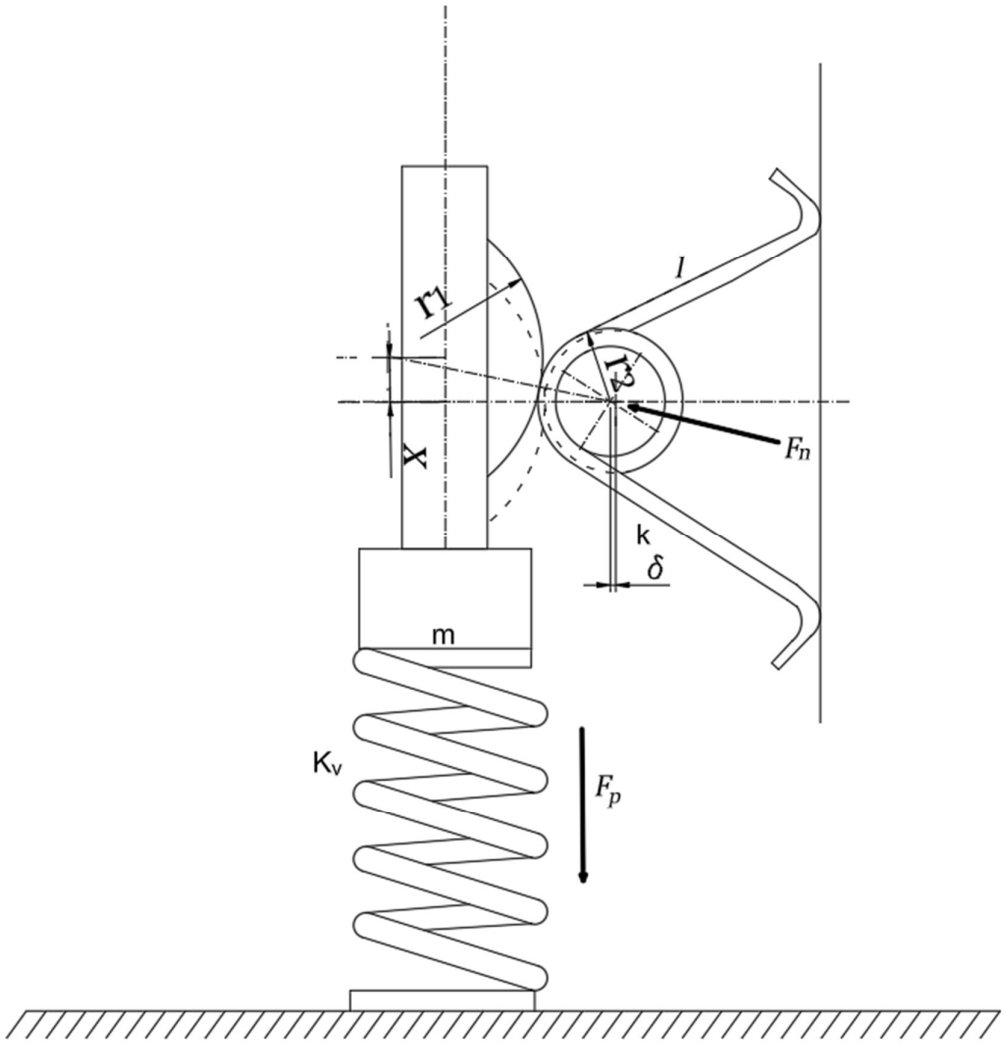

Figure 4. 2 – Intermediate State (displaced state), and Pre-stressed State (equilibrium position) of the torsion spring configuration 1

From Fig [4.3], the expressions for the forces acting on the mass are –

$$\boldsymbol{F_p = K_v x} \qquad (\mathbf{4.1})$$

$$\boldsymbol{F_n = \frac{2k\gamma}{\cos\theta.\sin(\mu+\gamma).l}} \qquad \begin{cases} \boldsymbol{Refer\ Appendix\ (A.1)} \\ \boldsymbol{for\ the\ derivation} \end{cases} \qquad (\mathbf{4.2})$$

Where, F_p *and* F_n, are forces due to the central and the torsion springs respectively.

The net vertical force acting on the mass will be

$$F = F_p - 3F_n \sin\theta$$

$$F = K_v x - 3 \cdot \frac{2\,k\,\gamma}{l\,\sin(\mu + \gamma)} \cdot \frac{x}{\sqrt{R^2 - x^2}} \qquad (4.3)$$

Substituting the expression for γ ,

$$\gamma = \alpha - \mu - \left\{\frac{R - \sqrt{R^2 - x^2}}{l\,\sin\alpha}\right\} \qquad \begin{Bmatrix} Refer\ Appendix\ (A.2) \\ for\ the\ derivation \end{Bmatrix} \qquad (4.4)$$

We get the expression for the net vertical force acting on the mass as

$$F = K_v x - 3 \cdot \frac{2k}{l} \cdot \frac{\alpha - \mu - \left[\frac{R - \sqrt{R^2 - x^2}}{l\,\sin\alpha}\right]}{\sin\left[\alpha - \left(\frac{R - \sqrt{R^2 - x^2}}{l\,sin\,\alpha}\right)\right]} \cdot \frac{x}{\sqrt{R^2 - x^2}} \qquad (4.5)$$

This expression for force can be normalized, by normalizing the displacement x by R, and F by $K_v R$. Thus, the expression for the normalized force will become –

$$f = \bar{x} - 3 \cdot \frac{2k}{lK_v R} \cdot \frac{\alpha - \mu - \frac{R}{l\,\sin\alpha}\left[1 - \sqrt{1 - \bar{x}^2}\right]}{\sin\left[\alpha - \left(\frac{R}{l\,\sin\alpha}\left[1 - \sqrt{1 - \bar{x}^2}\right]\right)\right]} \cdot \frac{\bar{x}}{\sqrt{1 - \bar{x}^2}} \qquad (4.6)$$

Where, f is the normalized force and $\bar{x}$ is the normalized displacement.

The normalised stiffness of the system can be obtained by differentiating the expression for f w.r.t $\bar{x}$. Thus, the expression for the normalised stiffness will be –

$$\overline{K_o} = 1 - \frac{6k}{K_v l R} \cdot \frac{\partial \Pi}{\partial \bar{x}} \qquad (4.7)$$

Where,

$$\boldsymbol{\Pi = \frac{\Lambda - \mu}{\sin \Lambda} \cdot \frac{\bar{x}}{\sqrt{1 - \bar{x}^2}}} \qquad (\mathbf{4.8})$$

$$\boldsymbol{\Lambda = \alpha - \frac{R}{l . \sin \alpha} \left(1 - \sqrt{1 - \bar{x}^2}\right)} \qquad (\mathbf{4.9})$$

From Eqn. [4.6], we see that the expression for the net restoring force acting on the system is not a linear function of the displacement. And from Eqn. [4.7, 4.8, 4.9], we see that the stiffness of the system is not constant, but is now a function of the displacement of the mass from the mean position.

For the system to exhibit quasi zero stiffness (QZS) characteristics, the system must have zero stiffness at the equilibrium position. Solving the above expression for $\overline{K_o}$, yields the following condition.

For QZS characteristics –

$$\boldsymbol{\overline{K_o} = 0 \qquad at \qquad \bar{x} = 0}$$

$$\textit{Therefore,} \qquad \boldsymbol{1 - \frac{6k}{K_v l R} \cdot \frac{\partial \Pi}{\partial \bar{x}} = 0 \qquad at \quad \bar{x} = 0}$$

$$\boldsymbol{\Lambda(\bar{x} = 0) = \alpha}$$

$$\boldsymbol{\frac{\partial \Lambda}{\partial \bar{x}} (\bar{x} = 0) = 0}$$

$$\boldsymbol{\frac{\partial \Pi}{\partial \bar{x}} (\bar{x} = 0) = \frac{\alpha - \mu}{\sin \alpha}}$$

Using the above results, in the preceding equation, yields the mathematical condition for QZS in this system as

$$\boldsymbol{\frac{6k}{K_v l R} = \frac{\sin \alpha}{\alpha - \mu}} \qquad \begin{cases} \textit{Condition for} \\ \textit{QZS at Equilibrium position} \end{cases} \qquad (\mathbf{4.10})$$

Thus, the Eqn. [4.10], gives us the mathematical condition between the geometrical and stiffness parameters, which will result into QZS characteristics into the system, at equilibrium position. Using Eqn. [4.10], in Eqn. [4.7], we get the expression for the stiffness of the system as

$$\overline{K_o} = 1 - \frac{\partial \Pi}{\partial \bar{x}} \cdot \left[\frac{\sin \alpha}{\alpha - \mu}\right] \tag{4.11}$$

$$\Pi = \frac{\Lambda - \mu}{\sin \Lambda} \cdot \frac{\bar{x}}{\sqrt{1 - \bar{x}^2}} \tag{4.12}$$

$$\Lambda = \alpha - \frac{R}{l . \sin \alpha}\left(1 - \sqrt{1 - \bar{x}^2}\right) \tag{4.13}$$

From Eqn. [4.11, 4.12, 4.13], we see that the stiffness of a system having torsion spring configuration 1, is a function of displacement of the mass, and is hence dynamic in nature. Also, the stiffness is a function of four unknown parameters viz. R, l, α, μ. Appropriate values of these parameters will help us to get desired stiffness characteristics in the system. The advantage of four unknown parameters is that we have higher number of control parameters in the system for stiffness control. Changing one or more than one parameter will change the behavior of the system and desired stiffness characteristics can be obtained. However, higher number of unknown parameters makes the analytical equation more complex. Also, a slight deviation in even one parameter from the value required for QZS condition, can cause considerable changes in the system's behavior. In practical conditions, not all parameters can always have the exact numerical values as required for QZS condition.

4.2.2 – Stiffness plot for Torsion Spring Configuration 1, for different values of control parameters.

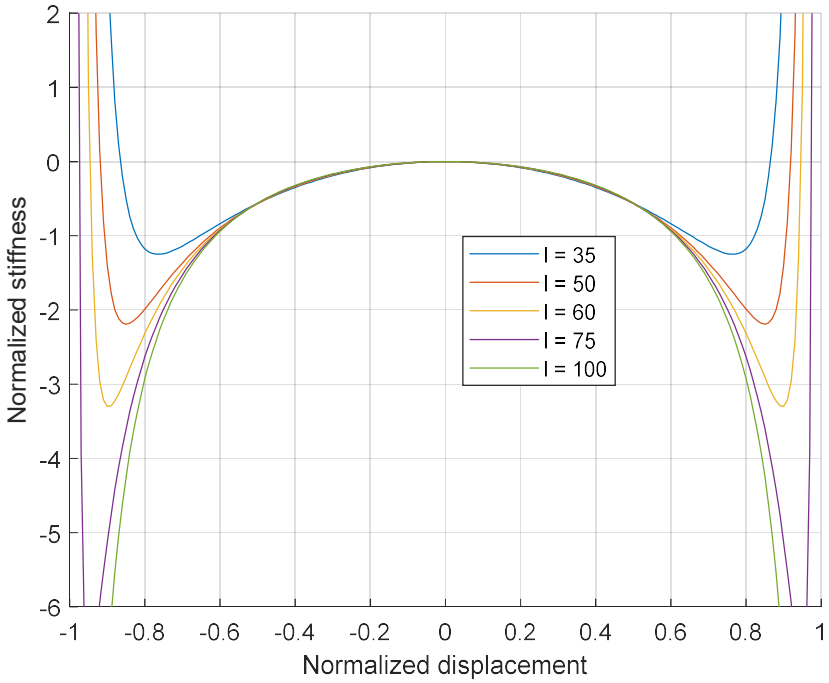

Figure 4. 3 – Normalized Stiffness vs Normalized Displacement for varying l

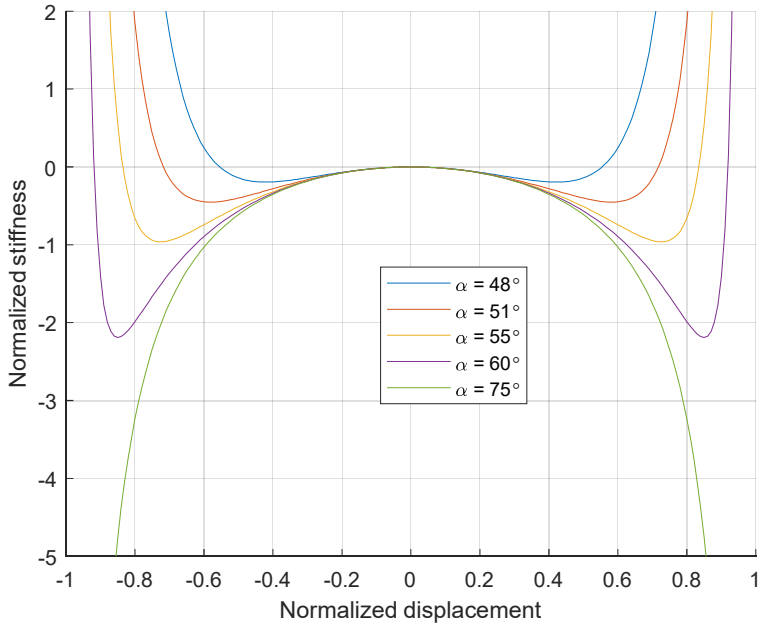

Figure 4. 4 – Normalized Stiffness vs Normalized Displacement for varying α

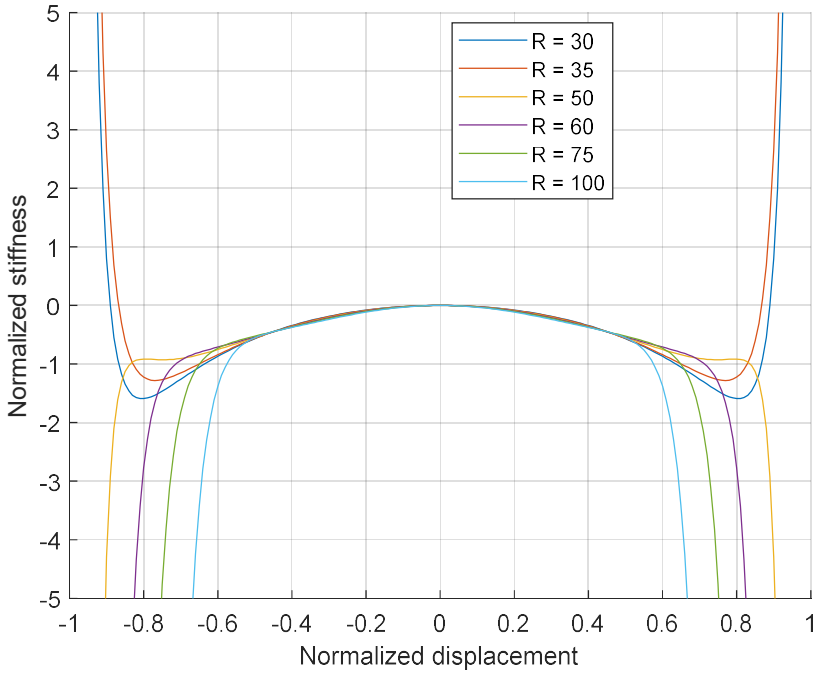

Figure 4. 5 – Normalized Stiffness vs Normalized Displacement for varying R

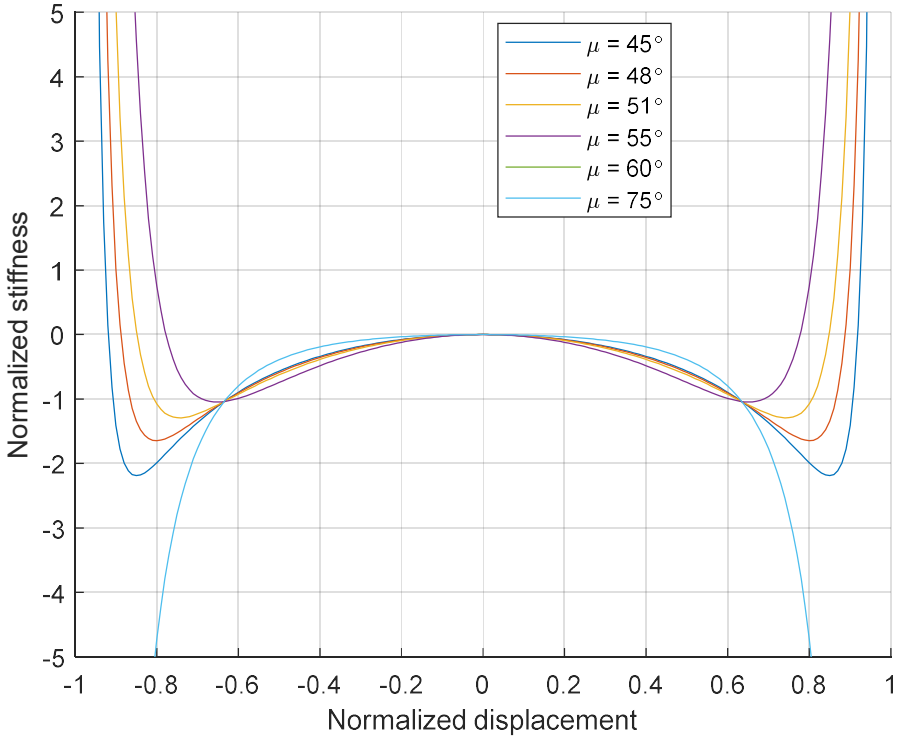

Figure 4. 6 – Normalized Stiffness vs Normalized Displacement for varying μ

4.3 – Torsion Spring Configuration 2

4.3.1 – Analytical Formulation for Force and Stiffness

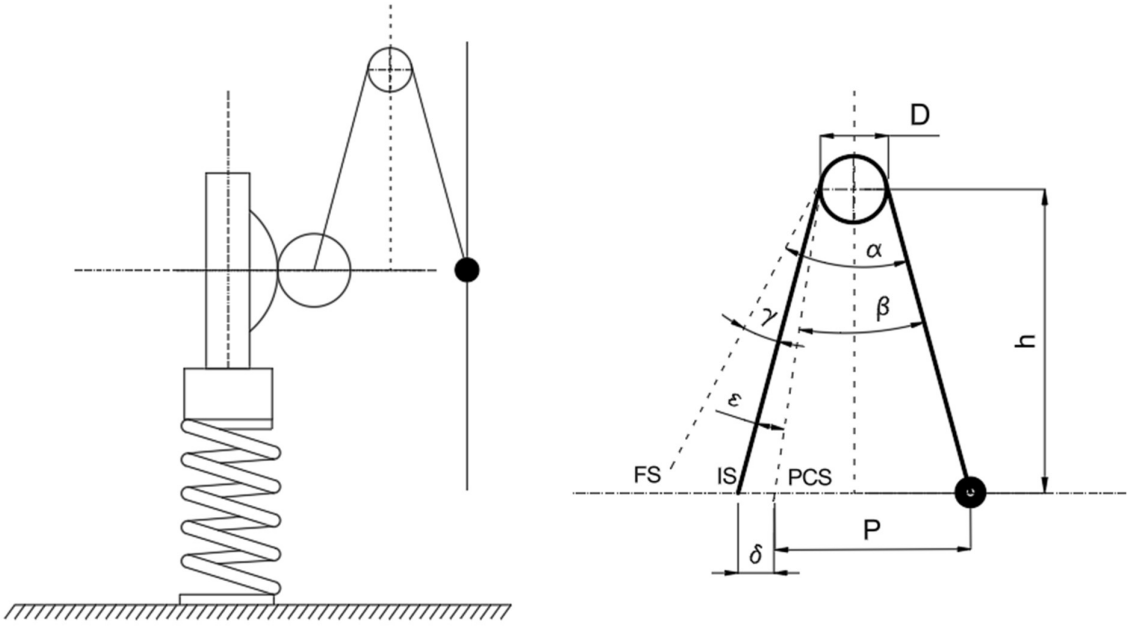

Figure 4. 7 – Torsion Spring Configuration 2, Free State (FS), Intermediate State (IS), and Pre-stressed State (PCS at equilibrium position) of the torsion spring

Fig [4.7], shows a schematic diagram of the Torsion Spring Configuration 1. It consists of a central helical spring that takes up the deadweight of the payload mass. Three torsion springs are also connected to the mass as shown, which are at 120° from each other when viewed from the top. However, only one is shown in the diagram. The other two have similar contribution in the expressions and the appropriate multiplication factor of 3 is considered. At the equilibrium position, the torsion springs have initial inner angular deflection, as shown in Fig [4.7] The motion of the torsion spring is restricted by the outer sleeve and the circular cam profile (hereafter referred to as cam profile 1), present on the vertical rod attached to the central spring. Due to this restriction the spring cannot release its deflection and remains stressed. Due to this pre stress the three torsion springs apply forces of equal magnitude in the horizontal plane on the cam profile 1, via the circular mechanical element (hereafter referred to as cam profile 2), present on one of the legs of the torsion spring. These force vectors cancel out each other in the horizontal plane with no vertical component, and hence, there is no net force

applied by the torsion springs on the central rod (consequently the mass), at the equilibrium position. Thus, at the equilibrium position, the net forces acting on the system are zero.

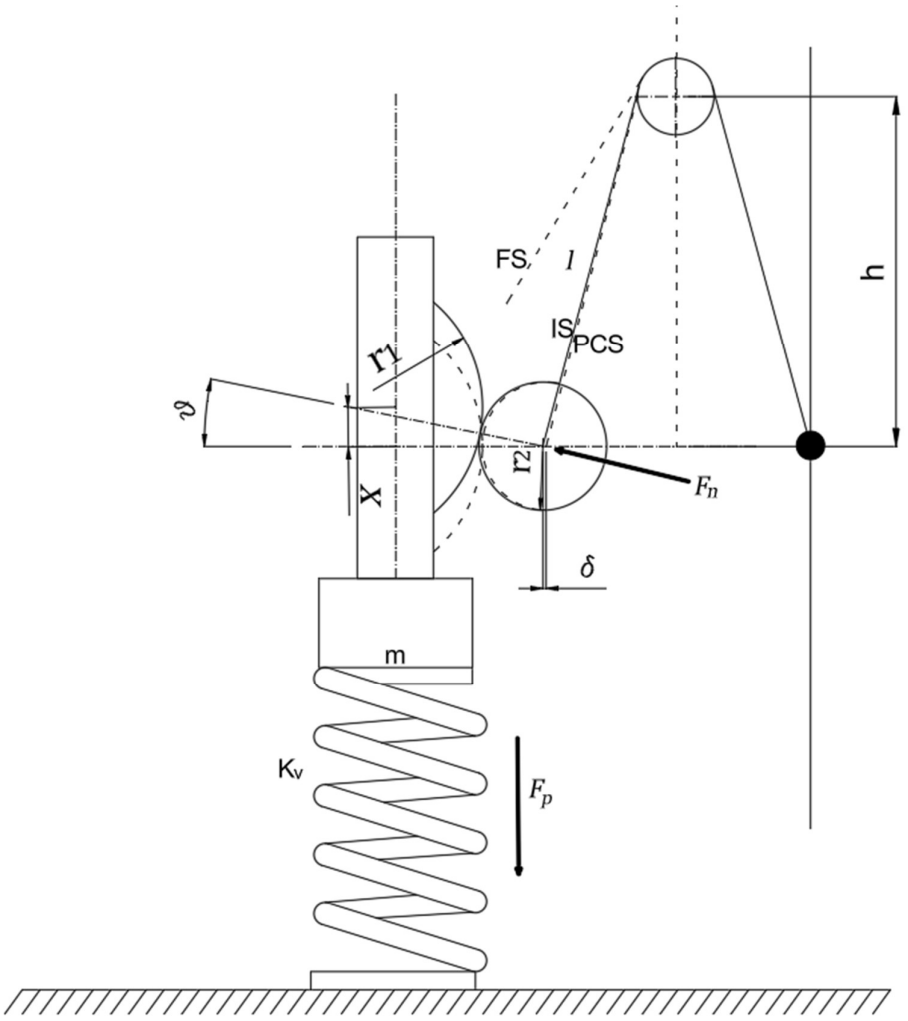

Figure 4. 8 – Intermediate State (displaced state), and Pre-stressed State (equilibrium position) of the torsion spring configuration 2

When, the mass is subjected to an upward vertical displacement of $\boldsymbol{x}$, the central spring offers a restoring force in downward direction. However, the torsion springs release some amount of their pre stress, due to the horizontal movement of the cam profile 2. Here it is assumed that the cam profile 2 is constrained to move in horizontal direction only. Thus, due this vertical movement of cam profile 1 and the resulting horizontal movement of cam profile 2, the line of action between the two cam profiles change, and a net upward vertical force acts on the mass due to these torsion springs. This upward force reduces the restoring force acting on the mass.

From Fig [4.8], the expressions for the forces acting on the mass are –

$$F_p = K_v x \tag{4.14}$$

$$F_n = k\frac{\left\{\alpha - \left(2\sin^{-1}B + \frac{(r_1 + r_2)}{l}\left[1 - \sqrt{1 - \bar{x}^2}\right]\right)\right\}}{l.\left(C.\sqrt{1 - B^2}\right)\left(\sqrt{1 - \bar{x}^2}\right)} \quad \begin{cases} Refer\ Appendix\ (A.3) \\ for\ the\ derivation \end{cases} \tag{4.15}$$

Where, F_p *and* F_n, are forces due to the central and the torsion springs respectively.

The net vertical force acting on the mass will be

$$F = F_p - 3F_n \sin\theta$$

$$F = K_v x - 3k\frac{\left\{\alpha - \left(2\sin^{-1}B + \frac{(r_1 + r_2)}{l}\left[1 - \sqrt{1 - \bar{x}^2}\right]\right)\right\}}{l.\left(C.\sqrt{1 - B^2}\right)\left(\sqrt{1 - \bar{x}^2}\right)}.\frac{x}{(r_1 + r_2)} \tag{4.16}$$

This expression for force is normalized, by normalizing the displacement x by $(r_1 + r_2)$, and F by $K_v(r_1 + r_2)$. Thus, the expression for the normalized force will become –

$$f = \bar{x} - 3Q.\bar{x}.\frac{\left\{1 - \left(2\frac{\sin^{-1}B}{\alpha} + A.\left[1 - \sqrt{1 - \bar{x}^2}\right]\right)\right\}}{\left(C.\sqrt{1 - B^2}\right)\left(\sqrt{1 - \bar{x}^2}\right)} \tag{4.17}$$

Where, Q, A, B, C are non-dimensional parameters as follows.

$$Q = \frac{k\alpha}{K_v l(r_1 + r_2)}, \quad A = \frac{(r_1 + r_2)}{l\alpha}, \quad B = \frac{P - D}{2l}, \quad C = 1 - \frac{l}{3\pi N_a D}$$

The normalised stiffness of the system can be obtained by differentiating the expression for f w.r.t $\bar{x}$. Thus, the expression for the normalised stiffness will be –

$$\overline{K_o} = 1 - \frac{\partial \Lambda}{\partial \bar{x}} \tag{4.18}$$

Where, the term $\boldsymbol{\Lambda}$ is given by,

$$\Lambda = 3Q.\bar{x}\,.\,\frac{\left\{1 - \left(2\frac{\sin^{-1}B}{\alpha} + A.\left[1 - \sqrt{1 - \bar{x}^2}\right]\right)\right\}}{\left(C\,.\,\sqrt{1 - B^2}\right)\left(\sqrt{1 - \bar{x}^2}\right)} \tag{4.19}$$

From Eqn. [4.17], we see that the expression for the net restoring force acting on the system is not a linear function of the displacement. And from Eqn. [4.18, 4.19], we see that the stiffness of the system is not constant, but is now a function of the displacement of the mass from the mean position.

For the system to exhibit quasi zero stiffness (QZS) characteristics, the system must have zero stiffness at the equilibrium position. Solving the above expression for $\overline{K_o}$, yields the following condition.

For QZS characteristics –

$$\overline{K_o} = 0 \qquad at \qquad \bar{x} = 0$$

$$Therefore, \qquad 1 - \frac{\partial \Lambda}{\partial \bar{x}} = 0 \qquad at \quad \bar{x} = 0$$

$$\frac{\partial \Lambda}{\partial \bar{x}}\,(\bar{x} = 0) = \frac{3Q}{C\sqrt{1 - B^2}}\,.\left\{1 - 2\frac{\sin^{-1}B}{\alpha}\right\}$$

Using the above result, in the preceding equation, yields the mathematical condition for QZS in this system as

$$\frac{Q}{C} = \frac{\sqrt{1 - B^2}}{3\left(1 - 2\frac{sin^{-1}B}{\alpha}\right)} \qquad \begin{cases} Condition\ for \\ QZS\ at\ Equilibrium\ position \end{cases} \tag{4.20}$$

Thus, the Eqn. [4.20], gives us the mathematical condition between the geometrical and stiffness parameters, which will result into QZS characteristics into the system, at equilibrium

position. Using Eqn. [4.20], in Eqn. [4.18, 4.19], we get the expression for the stiffness of the system as

$$\overline{K_o} = 1 - 1 . \left[\frac{1 - \frac{A}{R}}{(1 - \bar{x}^2)^{3/2}} + \frac{A}{R} \right] \qquad (4.21)$$

Where, after certain simplifications in the expression for $\overline{K_o}$, we get the non-dimensional parameters A and R as

$$A = \frac{(r_1 + r_2)}{l\alpha}$$

$$R = 1 - 2\frac{\sin^{-1} B}{\alpha}$$

Although, the final expression for $\overline{K_o}$, has two unknown non-dimensional parameters, these two parameters appear in a ratio as A/R. This ultimately makes only one unknown parameter in the expression for $\overline{K_o}$. Thus, in this configuration of torsion spring, we have only one control parameter, to control the stiffness behavior of the system. Appropriate value of this parameter will help us to get desired stiffness characteristics in the system.

An interesting thing about this configuration is that when the value of the parameter A/R equals one, or when $A = R$, the value of $\overline{K_o}$ is zero, for all values of $\bar{x}$.

$$\overline{K_o} = 0 \quad \forall \bar{x} \quad if \quad R = A$$

Thus, theoretically the stiffness of the system becomes zero if $R = A$. This means that there will be no dynamic stiffness in the system for any amount of displacement of the mass from its mean position. However, in practical scenarios, it may be very difficult to satisfy this condition due to restrictions on the numerical values of the geometrical and stiffness parameters of the system, which govern the values of A and R. The disadvantage of only one unknown parameter is that we have less control parameters in the system for stiffness control.

4.3.2 – Stiffness plot for Torsion Spring Configuration 2, for different values of control parameters.

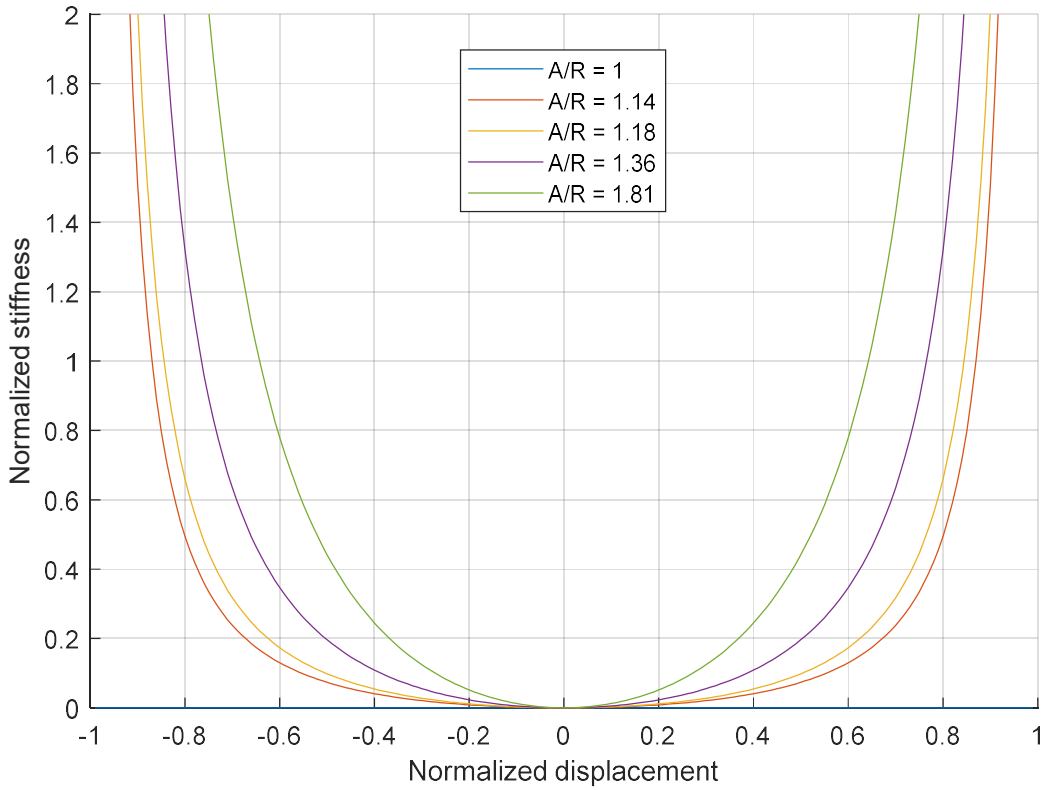

Figure 4. 9 – Normalized Stiffness vs Normalized Displacement for varying A/R

4.4 – Helical Compression Spring Configuration

4.4.1 – Analytical Formulation for Force and Stiffness

Fig [4.10], shows a schematic diagram of the Helical Compression Spring Configuration. It consists of a central helical spring that takes up the deadweight of the payload mass. Six pre-compressed helical springs are also connected to the mass as shown, which are at 60° from each other when viewed from the top. However, only one is shown in the diagram. The other five have similar contribution in the expressions and the appropriate multiplication factor of 6 is considered. At the equilibrium position, the pre-compressed helical springs (hereafter referred to as Negative Helical Springs) have initial pre-compression, as shown in Fig [4.10]. The negative helical spring is connected to piston which is inside a hydraulic fluid filled cylinder, which has a bypass tube at right angles with it. A similar piston is connected to the end of the tube. The other end of this piston has a circular element (hereafter referred to as cam profile 2). This cam profile 2 is in point connection (higher pair), with another circular element (hereafter referred to as cam profile 1), attached to the rod of the central spring. The hydraulic fluid cylinder arrangement helps us to transfer the vertical force exerted by the negative helical spring, in a horizontal direction. During this force transfer, it is assumed that there is negligible change in the fluid velocity between points 1 and 2. Also, that the difference in height of points between 1 and 2 is negligible, hence the change in static pressure due to fluid column is neglected. Therefore, the pressure at both the points 1 and 2 is same.

Due to the pre compression, the negative helical springs apply forces of equal magnitude in the vertical direction on the piston 2. It tries to push the fluid, but the fluid's motion is restricted by the perfectly horizontal contact between the two cam profiles. These horizontal contact force vectors between the cam profiles cancel out each other in the horizontal plane with no vertical component, and hence, there is no net force applied by the negative helical springs on the central rod (consequently the mass), at the equilibrium position. Thus, at the equilibrium position, the net forces acting on the system are zero.

When, the mass is subjected to an upward vertical displacement of $\boldsymbol{x}$, the central spring offers a restoring force in downward direction. However, the negative helical springs release some amount of their pre compression, due to the horizontal movement of the cam profile 2, since the cam profile 2 is constrained to move in horizontal direction only. Here it is assumed that the cam profile 2 is constrained to move in horizontal direction only. Thus, due this vertical

movement of cam profile 1 and the resulting horizontal movement of cam profile 2, the line of action between the two cam profiles change, and a net upward vertical force acts on the mass due to these negative helical springs. This upward force reduces the restoring force acting on the mass.

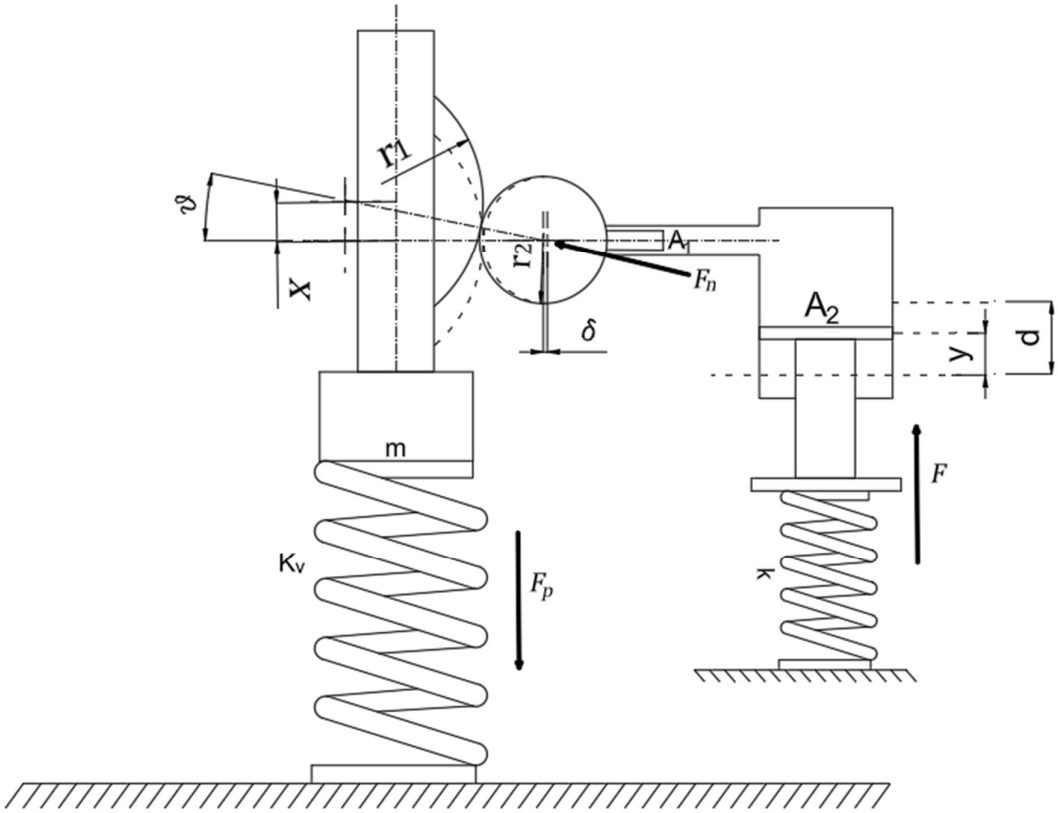

Figure 4. 10 – Helical Compression Spring Configuration, Initial State and Displaced State

From Fig [4.10], the expressions for the forces acting on the mass are –

$$\boldsymbol{F_p = K_v x} \qquad (\mathbf{4.22})$$

$$F_n = \frac{\frac{A_1}{A_2}k\left\{d - \frac{A_1}{A_2}\left[(r_1 + r_2) - \sqrt{(r_1 + r_2)^2 - x^2}\right]\right\}}{\frac{\sqrt{(r_1 + r_2)^2 - x^2}}{(r_1 + r_2)}} \quad \begin{cases} \textbf{Refer Appendix (A.4)} \\ \textbf{for the derivation} \end{cases} \quad (4.23)$$

Where, F_p **and** F_n, are forces due to the central and the torsion springs respectively.

The net vertical force acting on the mass will be

$$F = F_p - 6F_n \sin\theta$$

$$F = K_v x - 6k \frac{\frac{A_1}{A_2}k\left\{d - \frac{A_1}{A_2}\left[(r_1 + r_2) - \sqrt{(r_1 + r_2)^2 - x^2}\right]\right\}}{\frac{\sqrt{(r_1 + r_2)^2 - x^2}}{(r_1 + r_2)}} \cdot \frac{x}{(r_1 + r_2)} \quad (4.24)$$

This expression for force is normalized, by normalizing the displacement x by $(r_1 + r_2)$, and F by $K_v(r_1 + r_2)$. Thus, the expression for the normalized force will become –

$$f = \bar{x} - \frac{6A_1k}{A_2K_v} \cdot \bar{x} \cdot \frac{\left\{\bar{d} - \frac{A_1}{A_2}\left[1 - \sqrt{1 - \bar{x}^2}\right]\right\}}{\left(\sqrt{1 - \bar{x}^2}\right)} \quad (4.25)$$

The normalised stiffness of the system can be obtained by differentiating the expression for f w.r.t $\bar{x}$. Thus, the expression for the normalised stiffness will be –

$$\overline{K_o} = 1 - \frac{\partial \Lambda}{\partial \bar{x}} \quad (4.26)$$

Where, the term Λ is given by,

$$\Lambda = \frac{6A_1k}{A_2K_v} \cdot \bar{x} \cdot \frac{\left\{\bar{d} - \frac{A_1}{A_2}\left[1 - \sqrt{1 - \bar{x}^2}\right]\right\}}{\left(\sqrt{1 - \bar{x}^2}\right)} \quad (4.27)$$

From Eqn. [4.25], we see that the expression for the net restoring force acting on the system is not a linear function of the displacement. And from Eqn. [4.26, 4.27], we see that the stiffness

of the system is not constant, but is now a function of the displacement of the mass from the mean position.

For the system to exhibit quasi zero stiffness (QZS) characteristics, the system must have zero stiffness at the equilibrium position. Solving the above expression for $\overline{K_o}$, yields the following condition.

For QZS characteristics –

$$\overline{K_o} = 0 \qquad at \qquad \bar{x} = 0$$

$$Therefore, \qquad 1 - \frac{\partial \Lambda}{\partial \bar{x}} = 0 \qquad at \quad \bar{x} = 0$$

$$\frac{\partial \Lambda}{\partial \bar{x}} (\bar{x} = 0) \; = \; \frac{6A_1 k}{A_2 K_v} \bar{d}$$

Using the above result, in the preceding equation, yields the mathematical condition for QZS in this system as

$$\frac{6A_1 k}{A_2 K_v} = \frac{1}{\bar{d}} \qquad \begin{cases} Condition\ for \\ QZS\ at\ Equilibrium\ position \end{cases} \qquad (4.28)$$

Thus, the Eqn. [4.28], gives us the mathematical condition between the geometrical and stiffness parameters, which will result into QZS characteristics into the system, at equilibrium position. Using Eqn. [4.28], in Eqn. [4.26, 4.27], we get the expression for the stiffness of the system as

$$\overline{K_o} = 1 - \frac{1}{(1 - \bar{x}^2)^{3/2}} - B + \frac{B}{\sqrt{1 - \bar{x}^2}} + \frac{B\bar{x}^2}{(1 - \bar{x}^2)^{3/2}} \qquad (4.29)$$

Where, after certain simplifications in the expression for $\overline{K_o}$, we get the non-dimensional parameter B as

$$B = \frac{A_1}{A_2 d}$$

This makes only one unknown parameter in the expression for $\overline{K_o}$. Thus, in this configuration of negative helical spring, we have only one control parameter, to control the stiffness behavior of the system. Appropriate value of this parameter will help us to get desired stiffness characteristics in the system.

An interesting thing about this configuration is that when the value of the parameter $\boldsymbol{B}$ equals one, or when $\boldsymbol{B = 1}$, the value of $\overline{K_o}$ is zero, for all values of $\bar{x}$.

$$\overline{K_o} = 0 \quad \forall\, \bar{x} \quad if \quad B = 1$$

Thus, theoretically the stiffness of the system becomes zero if $\boldsymbol{B = 1}$. This means that there will be no dynamic stiffness in the system for any amount of displacement of the mass from its mean position. However, in practical scenarios, it may be very difficult to satisfy this condition due to restrictions on the numerical values of the geometrical and stiffness parameters of the system, which govern the values of $\boldsymbol{B}$.The disadvantage of only one unknown parameter is that we have less control parameters in the system for stiffness control.

4.4.2 – Stiffness plot for Negative Helical Spring Configuration, for different values of control parameter.

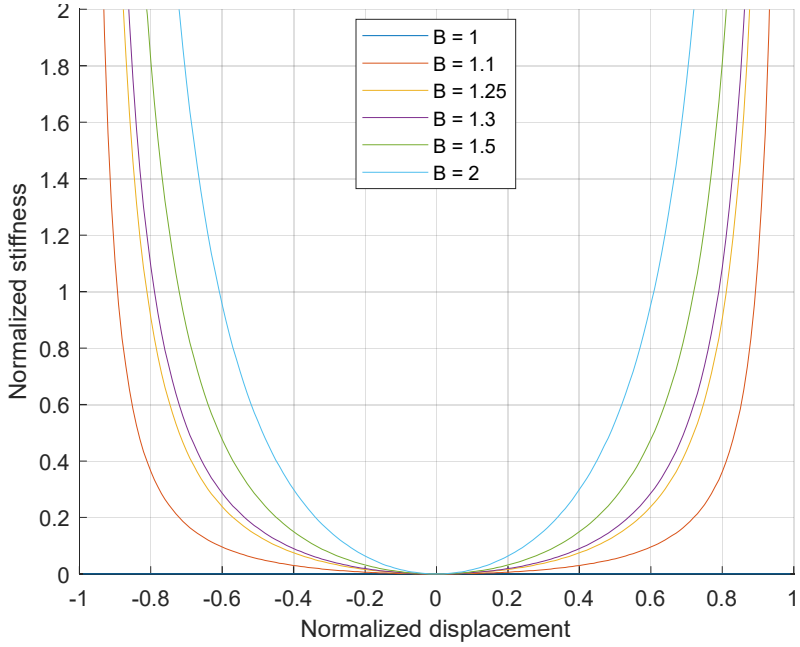

Figure 4. 11 – Normalized Stiffness vs Normalized Displacement for varying B

4.5 – Conclusion.

1) Three different configurations for generating negative stiffness in a simple spring mass system are discussed and their force and stiffness formulation is done.
2) Torsion springs are used in two different configurations as the negative stiffness element.
3) Torsion spring Configuration 1 has four control parameters, which provide higher level of control over the stiffness behaviour. However, higher number of control parameters may lead to higher deviation from QZS condition.
4) Torsion spring Configuration 2 and Negative Helical Spring Configuration has only one control parameter. It is theoretically possible to get zero dynamic stiffness in the system under certain mathematical condition on this control parameter.

Chapter 5 – Analytical formulation of Gough Stewart Platform

5.1 – Introduction

In chapter 3 and chapter 4, we have thoroughly discussed how certain configurations of mechanical stiffness elements, help us achieve negative stiffness in a structure. Consequently, it provides the condition of high static stiffness but low dynamic stiffness, which helps in reducing the natural frequency of a vibration isolation system and, also, to increase the frequency range over which isolation is required. However, these configurations discussed excitations in only one degree of freedom. The micro-vibrations in spacecrafts are of multi-degree of freedom nature. Hence, a complete 6 degrees of freedom vibration isolation system is required in these applications.

Gough Stewart Platforms (hereafter referred to as GSP) are the most widely used vibration isolation systems for six degrees of freedom vibration isolation due to its high stiffness, precision, and load-bearing capabilities. Each of the six legs can extend or contract independently, allowing the platform to move in all six degrees of freedom: three translational (X, Y, Z) and three rotational (pitch, roll, yaw). The GSP can be used for both active and passive vibration isolation.

In active vibration isolation applications, the Gough-Stewart platform acts as an active or semi-active system to counteract unwanted motion. Sensors detect vibrations in real-time, and control algorithms adjust the length of the struts accordingly to compensate for the disturbances. This dynamic response effectively isolates the payload—such as sensitive scientific instruments, optical equipment, or spacecraft components—from environmental or mechanical vibrations.

The platform's closed-loop kinematic structure offers advantages like high responsiveness and stability. Its compact and symmetrical design also supports uniform distribution of forces, enhancing performance. Overall, the Gough-Stewart platform provides a robust solution for precision vibration isolation in critical high-tech and aerospace applications.

5.2 – The Geometry of Gough Stewart Platform

Fig [5.1], shows the schematic diagram of a 6-6 GSP. It consists of mainly 3 components. A fixed base, a movable platform and 6 identical legs connecting the base and the platform. The legs or limbs are usually connected to the base and the platform in a circle of constant radius. However, in Modified Gough Stewart Platform (MGSP), three legs are connected on an inner radius and three on outer radius. The advantage of MGSP is higher number of control parameters. This kinematic structure allows the moving platform of the GSP to have a six degrees of freedom motion, three translations in $\boldsymbol{x, y, z}$ axes and three rotations $\boldsymbol{\phi, \theta, \psi}$.

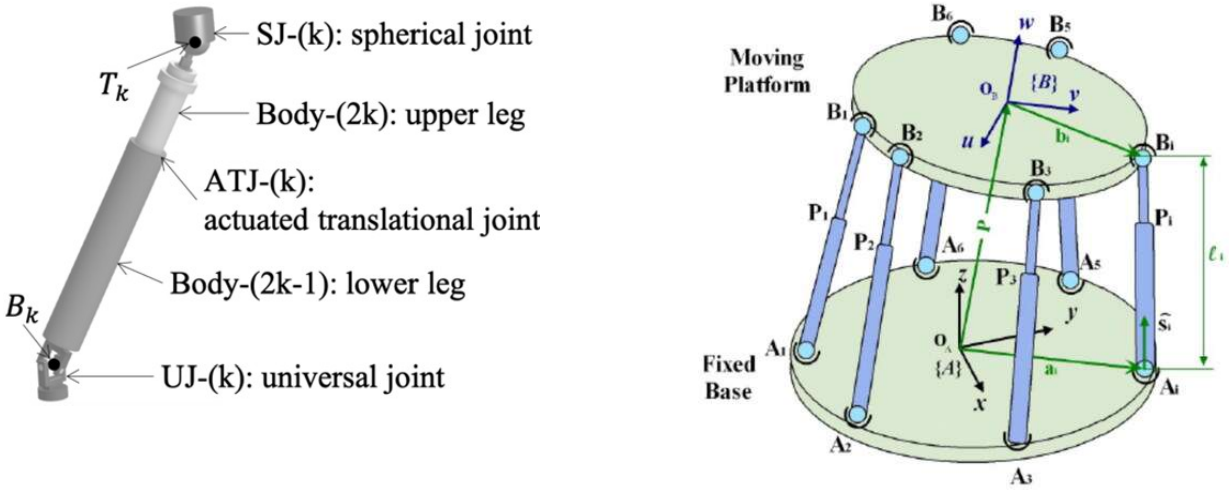

Figure 5. 1 – The components of a GSP and the joints that are present in its legs

Fig [5.1], shows the joints which are present between the base and legs and the platform and legs. The base is connected with the legs via universal joints or spherical joints. Also, the moving platform is connected with the legs via universal joints or spherical joints. The legs consist of two components viz part 1 and part 2. The parts 1 and 2 are connected via prismatic joints. The possible combinations of joints are universal-prismatic-spherical (UPS joint), spherical-prismatic-universal (SPU joint), or spherical-prismatic-spherical (SPS joint). The legs cannot have universal joints at both of its ends, otherwise it will restrict the motion of the moving platform in certain degrees of freedom. In GSP, the prismatic joint is the active joint, whereas the spherical and universal joints are passive joints.

In applications where GSP's are used parallel robots for position and orientation control, the parts 1 and 2 of the legs are connected via a linear actuator. This actuator which is externally powered, helps achieve the desired position and orientation of the moving platform w.r.t the base, by changing the lengths of the legs. As a result of the extension or contraction of the legs, each of the legs have different lengths and consequently the platform achieves the desired position and orientation.

In vibration isolation applications, the base is subjected to harmonic excitations and the sensitive payloads are mounted on the moving platforms. The parts 1 and 2 of the legs are connected via stiffness and damping elements. These elements are responsible for the transfer of vibrations from the base to the platform. When the base is subjected to harmonic excitations in six degrees of freedom, the platform will also have harmonic response in all six degrees of freedom. The goal is to achieve minimum transmissibility possible. In micro-vibration isolation for spacecraft applications, the GSP can be used between the source and the spacecraft bus, for source isolation; or between the payload and the spacecraft bus, for payload isolation.

In the coming sections we will discuss the kinematic and dynamic formulation of the base, the platform, and the legs.

5.3 – Co-ordinate System Assignment

Fig [5.2], shows the schematic diagram of a 6-6 GSP with a base (bottom hexagon), a platform (top hexagon) and six legs (represented by solid lines between the base and the platform). The circles on the vertices of the hexagons represent the joints between the components. Here it is assumed that the base and legs are connected via a universal joint and the platform and the legs are connected via a spherical joint.

The top platform is assigned a coordinate frame with its origin $\boldsymbol{o}$ at its geometrical center. It is represented by lower case letters ($\boldsymbol{x},\ \boldsymbol{y},\ \boldsymbol{z}$). The $\boldsymbol{x}$ and $\boldsymbol{y}$ axes lie in the plane of the platform, as seen in the top view Fig [5.2], whereas the $\boldsymbol{z}$ axis is perpendicular to the plane of the platform.

The base is also assigned a coordinate frame, similar to the platform frame, with its origin $\boldsymbol{O}$ at its geometrical center. It is represented by upper case letters ($\boldsymbol{X},\ \boldsymbol{Y},\ \boldsymbol{Z}$). All other details regarding the frame remain same as that of the platform frame.

Since, in vibration isolation applications, the base is subjected to excitations. Hence, the frame attached to the base is not a fixed frame but a non-inertial frame of reference. To write the equations of motion using newton's laws, it is important to define a fixed inertial frame of reference known as the world frame. We define a world coordinate system represented by upper case primed letters ($\boldsymbol{X'}$, $\boldsymbol{Y'}$, $\boldsymbol{Z'}$). The origin of this frame $\boldsymbol{O'}$ lies at the initial location of the COM of the base, and the axes are aligned with the axes of the base frame. The motion of the base and the platform frames are defined w.r.t this world frame.

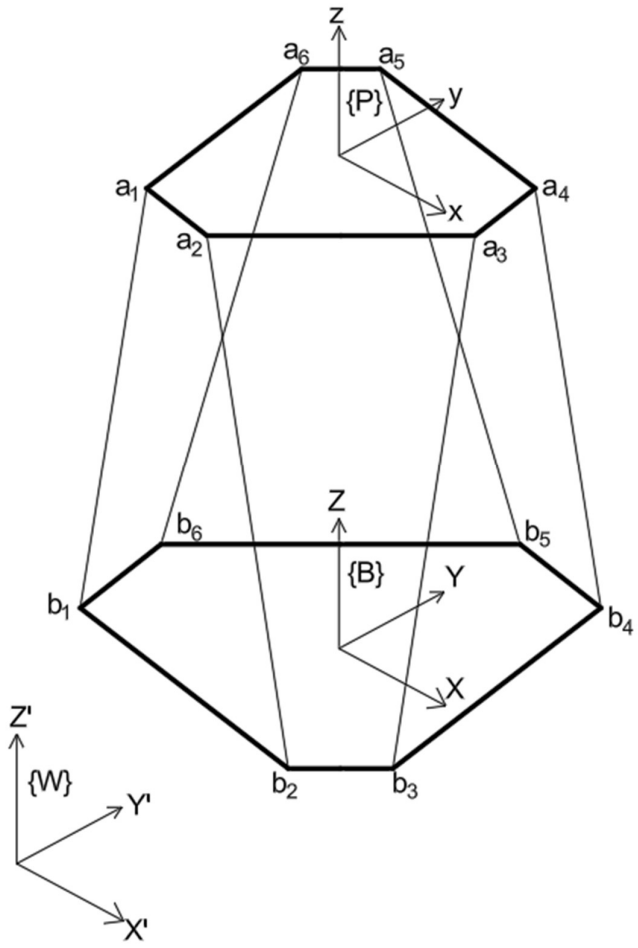

Figure 5. 2 – Frames of reference in a GSP

The terms {$\boldsymbol{W}$} represents world frame, {$\boldsymbol{B}$} represents base frame, and {$\boldsymbol{P}$} represents platform frame.

For the kinematic and dynamic formulation of the legs, a leg frame connected to each leg also needs to be defined. This frame is defined in the section 5.6.2.

5.4 – Position and Orientation of the Base and the Platform.

5.4.1 – Position and Orientation of the Base.

Fig [5.3], shows the coordinate frames of the GSP and the associated vectors.

$$\bar{O} = \textbf{position vector of } O \textbf{ w.r.t } O'$$

$$\bar{O} = (X'_B,\ Y'_B,\ Z'_B)^T$$

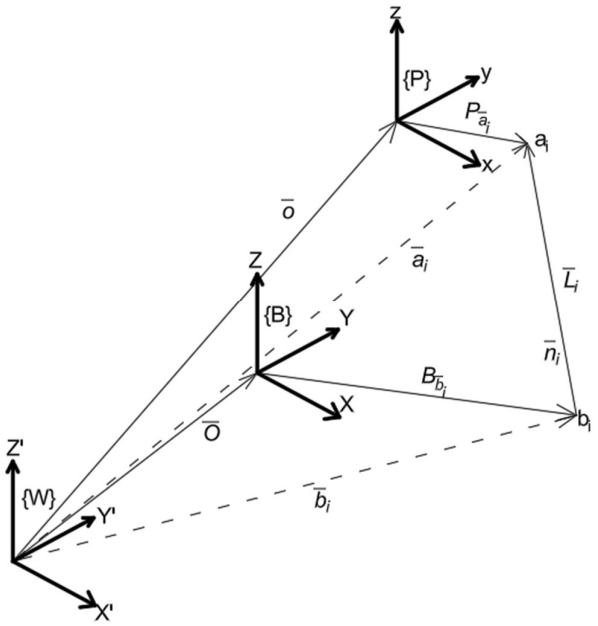

Figure 5. 3 – Frames of reference and vector diagram for kinematic study

The orientation of the $\{B\}$ w.r.t $\{W\}$, is defined using the three xyz euler angles $\phi'_B,\ \theta'_B,\ \psi'_B$.

The position and orientation of $\{B\}$ w.r.t $\{W\}$, is given by the vector

$$\bar{B} = \textbf{position and orientation of } \{B\} \textbf{ w.r.t } \{W\}$$

$$\bar{B} = (X'_B,\ Y'_B,\ Z'_B,\ \phi'_B,\ \theta'_B,\ \psi'_B)^T$$

The rotation matrix from $\{\boldsymbol{B}\}$ frame to $\{\boldsymbol{W}\}$ frame, is represented by $\boldsymbol{W_{R_B}}$, and is given for the $\boldsymbol{xyz}$ euler angles $\boldsymbol{\phi'_B,\ \theta'_B,\ \psi'_B}$ as –

$$\boldsymbol{W_{R_B}} = \begin{bmatrix} \boldsymbol{c\theta'_B \,.\, c\psi'_B} & \boldsymbol{-c\theta'_B \,.\, s\psi'_B} & \boldsymbol{s\theta'_B} \\ \boldsymbol{s\phi'_B \,.\, s\theta'_B \,.\, c\psi'_B \ +\ c\phi'_B \,.\, s\psi'_B} & \boldsymbol{-s\phi'_B \,.\, s\theta'_B \,.\, s\psi'_B \ +\ c\phi'_B \,.\, c\psi'_B} & \boldsymbol{-s\phi'_B \,.\, c\theta'_B} \\ \boldsymbol{-c\phi'_B \,.\, s\theta'_B \,.\, c\psi'_B \ +\ s\phi'_B \,.\, s\psi'_B} & \boldsymbol{c\phi'_B \,.\, s\theta'_B \,.\, s\psi'_B \ +\ s\phi'_B \,.\, c\psi'_B} & \boldsymbol{c\phi'_B \,.\, c\theta'_B} \end{bmatrix}$$

The terms $\boldsymbol{b_i}$; $(\boldsymbol{i = 1\ to\ 6})$ represent the joints between the base and the legs.

$$\boldsymbol{\overline{b_i} \ =\ position\ vector\ of\ \ b_i\ w.r.t\ \{W\}}$$

$$\boldsymbol{\overline{B_{b_i}} \ =\ position\ vector\ of\ \ b_i\ w.r.t\ \{B\}}$$

$$\boldsymbol{\overline{B_{b_i}} \ =\ \left(X_{b_i}\,,\ Y_{b_i}\,,\ Z_{b_i} \right)^T}$$

5.4.2 – Position and Orientation of the Platform.

Fig [5.3], shows the coordinate frames of the GSP and the associated vectors.

$$\boldsymbol{\overline{o} \ =\ position\ vector\ of\ \ o\ w.r.t\ O'}$$

$$\boldsymbol{\overline{o} \ =\ (X'_P,\ Y'_P,\ Z'_P)^T}$$

The orientation of the $\{\boldsymbol{P}\}$ w.r.t $\{\boldsymbol{W}\}$, is defined using the three $\boldsymbol{xyz}$ euler angles $\boldsymbol{\phi'_P,\ \theta'_P,\ \psi'_P}$.

The position and orientation of $\{\boldsymbol{P}\}$ w.r.t $\{\boldsymbol{W}\}$, is given by the vector

$$\boldsymbol{\overline{P} \ =\ position\ and\ orientation\ of\ \{P\}\ w.r.t\ \{W\}}$$

$$\boldsymbol{\overline{P} \ =\ (X'_P,\ Y'_P,\ Z'_P,\ \phi'_P,\ \theta'_P,\ \psi'_P)^T}$$

The rotation matrix from $\{\boldsymbol{P}\}$ frame to $\{\boldsymbol{W}\}$ frame, is represented by $\boldsymbol{W_{R_P}}$, and is given for the $\boldsymbol{xyz}$ euler angles $\boldsymbol{\phi'_P,\ \theta'_P,\ \psi'_P}$ as –

$$W_{R_P} = \begin{bmatrix} c\theta'_P \,.\, c\psi'_P & -c\theta'_P \,.\, s\psi'_P & s\theta'_P \\ s\phi'_P \,.\, s\theta'_P \,.\, c\psi'_P \;+\; c\phi'_P \,.\, s\psi'_P & -s\phi'_P \,.\, s\theta'_P \,.\, s\psi'_P \;+\; c\phi'_P \,.\, c\psi'_P & -s\phi'_P \,.\, c\theta'_P \\ -c\phi'_P \,.\, s\theta'_P \,.\, c\psi'_P \;+\; s\phi'_P \,.\, s\psi'_P & c\phi'_P \,.\, s\theta'_P \,.\, s\psi'_P \;+\; s\phi'_P \,.\, c\psi'_P & c\phi'_P \,.\, c\theta'_P \end{bmatrix}$$

The terms a_i ; $(i = 1\ to\ 6)$ represent the joints between the platform and the legs.

$$\overline{a_i} \;=\; position\ vector\ of\ \ a_i\ \ w.r.t\ \{W\}$$

$$\overline{P_{a_i}} \;=\; position\ vector\ of\ \ a_i\ \ w.r.t\ \{P\}$$

$$\overline{P_{a_i}} = \left(x_{a_i}\,,\, y_{a_i}\,,\, z_{a_i} \right)^T$$

5.5 – Kinematics of the Base and the Platform.

5.5.1 – Kinematics of the Base.

The position and orientation of $\{B\}$ w.r.t $\{W\}$, is given by the vector

$$\overline{B} \;=\; position\ and\ orientation\ of\ \{B\}\ w.r.t\ \{W\}$$

$$\overline{B} \;=\; \left(X'_B,\ Y'_B,\ Z'_B,\ \phi'_B,\ \theta'_B,\ \psi'_B \right)^T$$

The skew symmetric angular velocity tensor of the base, in world frame, or $\{B\}$ w.r.t $\{W\}$, will be given by

$$\omega_B^{ss} = \dot{W_{R_B}} \,.\, W_{R_B}{}^T \qquad (5.1)$$

Where, $\dot{W_{R_B}}$ represents the time derivative of the rotation matrix from $\{B\}$ frame to $\{W\}$ frame. The matrix ω_B^{ss} is 3×3 skew symmetric matrix, having the form –

$$\omega_B^{ss} = \begin{bmatrix} 0 & -\omega_{B_{Z'}} & \omega_{B_{Y'}} \\ \omega_{B_{Z'}} & 0 & -\omega_{B_{X'}} \\ -\omega_{B_{Y'}} & \omega_{B_{X'}} & 0 \end{bmatrix}$$

Therefore, the angular velocity vector of the base in world frame, or $\{\boldsymbol{B}\}$ w.r.t $\{\boldsymbol{W}\}$, will be given by

$$\overline{\boldsymbol{\omega_B}} = \begin{bmatrix} -\boldsymbol{\omega}_{\boldsymbol{B}}^{\boldsymbol{ss}}\,(\mathbf{2},\mathbf{3}) \\ \boldsymbol{\omega}_{\boldsymbol{B}}^{\boldsymbol{ss}}\,(\mathbf{1},\mathbf{3}) \\ -\boldsymbol{\omega}_{\boldsymbol{B}}^{\boldsymbol{ss}}\,(\mathbf{1},\mathbf{2}) \end{bmatrix} \qquad (\mathbf{5.2})$$

The angular acceleration vector of the the base in world frame, or $\{\boldsymbol{B}\}$ w.r.t $\{\boldsymbol{W}\}$, will then be given by

$$\overline{\boldsymbol{\alpha_B}} = \dot{\boldsymbol{\omega}}_{\boldsymbol{B}} \qquad (\mathbf{5.3})$$

Where, $\dot{\boldsymbol{\omega}}_{\boldsymbol{B}}$ represents the time derivative of $\overline{\boldsymbol{\omega_B}}$.

5.5.1 – Kinematics of the Platform.

The position and orientation of $\{\boldsymbol{P}\}$ w.r.t $\{\boldsymbol{W}\}$, is given by the vector

$$\overline{\boldsymbol{P}} = \textbf{position and orientation of } \{\boldsymbol{P}\} \textbf{ w.r.t } \{\boldsymbol{W}\}$$

$$\overline{\boldsymbol{P}} = (\boldsymbol{X'_P},\ \boldsymbol{Y'_P},\ \boldsymbol{Z'_P},\ \boldsymbol{\phi'_P},\ \boldsymbol{\theta'_P},\ \boldsymbol{\psi'_P})^{\boldsymbol{T}}$$

The skew symmetric angular velocity tensor of the platform, in world frame, or $\{\boldsymbol{P}\}$ w.r.t $\{\boldsymbol{W}\}$, will be given by

$$\boldsymbol{\omega}_{\boldsymbol{P}}^{\boldsymbol{ss}} = \dot{\boldsymbol{W}}_{\boldsymbol{R_P}} \cdot \boldsymbol{W}_{\boldsymbol{R_P}}{}^{\boldsymbol{T}} \qquad (\mathbf{5.4})$$

Where, $\dot{\boldsymbol{W}}_{\boldsymbol{R_P}}$ represents the time derivative of the rotation matrix from $\{\boldsymbol{P}\}$ frame to $\{\boldsymbol{W}\}$ frame. The matrix $\boldsymbol{\omega}_{\boldsymbol{P}}^{\boldsymbol{ss}}$ is $\mathbf{3} \times \mathbf{3}$ skew symmetric matrix, having the form –

$$\boldsymbol{\omega}_{\boldsymbol{P}}^{\boldsymbol{ss}} = \begin{bmatrix} 0 & -\boldsymbol{\omega}_{\boldsymbol{P_{Z'}}} & \boldsymbol{\omega}_{\boldsymbol{P_{Y'}}} \\ \boldsymbol{\omega}_{\boldsymbol{P_{Z'}}} & 0 & -\boldsymbol{\omega}_{\boldsymbol{P_{X'}}} \\ -\boldsymbol{\omega}_{\boldsymbol{P_{Y'}}} & \boldsymbol{\omega}_{\boldsymbol{P_{X'}}} & 0 \end{bmatrix}$$

Therefore, the angular velocity vector of the base in world frame, or $\{\boldsymbol{P}\}$ w.r.t $\{\boldsymbol{W}\}$, will be given by

$$\overline{\omega_P} = \begin{bmatrix} -\omega_P^{ss}(2,3) \\ \omega_P^{ss}(1,3) \\ -\omega_P^{ss}(1,2) \end{bmatrix} \quad (5.5)$$

The angular acceleration vector of the the base in world frame, or $\{P\}$ w.r.t $\{W\}$, will then be given by

$$\overline{\alpha_P} = \dot{\omega}_P \quad (5.6)$$

Where, $\dot{\omega}_P$ represents the time derivative of $\overline{\omega_P}$.

5.6 – Kinematics of the Leg.

5.6.1 – Expressions for the Leg Length and its time derivatives.

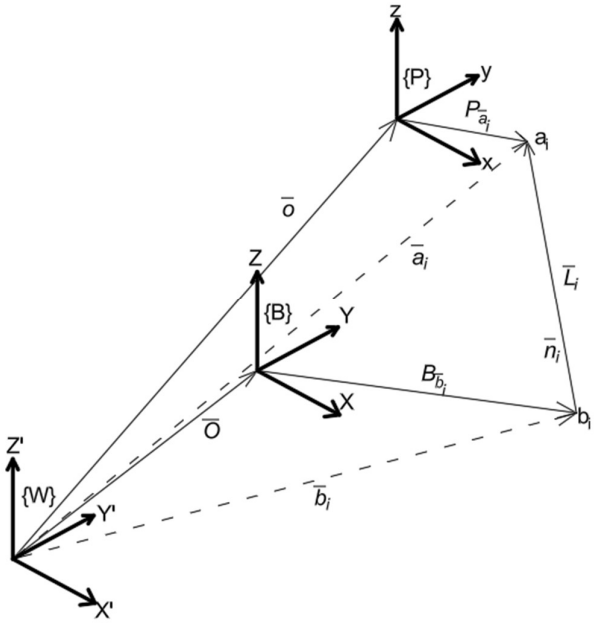

Fig [5.3] – Frames of reference and vector diagram for kinematic study

Refer Fig [5.3]. The position vectors of the points $\boldsymbol{b_i}$; $(\boldsymbol{i = 1\ to\ 6})$ i.e. the joints between the base and legs, in the world frame $\{W\}$ is given by

$$\overline{\boldsymbol{b_i}} = \textbf{position vector of } \boldsymbol{b_i} \textbf{ w.r.t } \{\boldsymbol{W}\}$$

$$\overline{\boldsymbol{b_i}} = \overline{\boldsymbol{O}} + \boldsymbol{W_{R_B}}\overline{\boldsymbol{B_{b_i}}} \tag{5.7}$$

Therefore, the time derivative of $\overline{\boldsymbol{b_i}}$, which represents the rate of change of position vector of $\boldsymbol{b_i}$; $(\boldsymbol{i = 1 \textit{ to } 6})$, will be

$$\dot{\boldsymbol{b}}_i = \dot{\boldsymbol{O}} + \overline{\boldsymbol{\omega_B}} \times \left(\boldsymbol{W_{R_B}}\overline{\boldsymbol{B_{b_i}}}\right) \tag{5.8}$$

$$\dot{\boldsymbol{b}}_i = \dot{\boldsymbol{O}} + \boldsymbol{\omega_B^{ss}}\left(\boldsymbol{W_{R_B}}\overline{\boldsymbol{B_{b_i}}}\right) \tag{5.9}$$

The acceleration of the position vector $\overline{\boldsymbol{b_i}}$ will be –

$$\ddot{\boldsymbol{b}}_i = \ddot{\boldsymbol{O}} + \overline{\boldsymbol{\alpha_B}} \times \left(\boldsymbol{W_{R_B}}\overline{\boldsymbol{B_{b_i}}}\right) + \overline{\boldsymbol{\omega_B}} \times \left[\overline{\boldsymbol{\omega_B}} \times \left(\boldsymbol{W_{R_B}}\overline{\boldsymbol{B_{b_i}}}\right)\right] \tag{5.10}$$

Similar formulation can be done for the joints between the platform and the legs.

The position vectors of the points $\boldsymbol{a_i}$; $(\boldsymbol{i = 1 \textit{ to } 6})$ i.e. the joints between the platform and legs, in the world frame $\{\boldsymbol{W}\}$ is given by

$$\overline{\boldsymbol{a_i}} = \textbf{position vector of } \boldsymbol{a_i} \textbf{ w.r.t } \{\boldsymbol{W}\}$$

$$\overline{\boldsymbol{a_i}} = \overline{\boldsymbol{o}} + \boldsymbol{W_{R_P}}\overline{\boldsymbol{P_{a_i}}} \tag{5.11}$$

Therefore, the time derivative of $\overline{\boldsymbol{a_i}}$, which represents the rate of change of position vector of $\boldsymbol{a_i}$; $(\boldsymbol{i = 1 \textit{ to } 6})$, will be

$$\dot{\boldsymbol{a}}_i = \dot{\boldsymbol{o}} + \overline{\boldsymbol{\omega_P}} \times \left(\boldsymbol{W_{R_P}}\overline{\boldsymbol{P_{a_i}}}\right) \tag{5.12}$$

$$\dot{\boldsymbol{a}}_i = \dot{\boldsymbol{o}} + \boldsymbol{\omega_P^{ss}}\left(\boldsymbol{W_{R_P}}\overline{\boldsymbol{P_{a_i}}}\right) \tag{5.13}$$

The acceleration of the position vector $\overline{\boldsymbol{a_i}}$ will be –

$$\ddot{\boldsymbol{a}}_i = \ddot{\boldsymbol{o}} + \overline{\boldsymbol{\alpha_P}} \times \left(\boldsymbol{W_{R_P}}\overline{\boldsymbol{P_{a_i}}}\right) + \overline{\boldsymbol{\omega_P}} \times \left[\overline{\boldsymbol{\omega_P}} \times \left(\boldsymbol{W_{R_P}}\overline{\boldsymbol{P_{a_i}}}\right)\right] \tag{5.14}$$

Where, $' \times '$ represents the cross product of the vectors.

From Fig [5.3], we see

$$\bar{L}_\iota = \bar{a}_\iota - \bar{b}_\iota \tag{5.15}$$

Where, $\bar{L}_\iota$ is a vector along the axis of the leg, expressed in world frame.

Therefore,

$$l_i \bar{n}_\iota = \bar{a}_\iota - \bar{b}_\iota \tag{5.16}$$

Where, l_i is the length of the leg at any instant and $\bar{n}_\iota$ is the unit vector along the axis of the leg.

The leg length can be found from Eqn. [5.15] by

$$l_i = \sqrt{\bar{L}_\iota \,.\, \bar{L}_\iota} \tag{5.17}$$

Where, $'.'$ represents the dot product of the vectors.

Therefore,

$$\bar{n}_\iota = \frac{\bar{a}_\iota - \bar{b}_\iota}{l_i} \tag{5.18}$$

We can write from Eqn. [5.16]

$$l_i = \left(\bar{a}_\iota - \bar{b}_\iota\right) . \bar{n}_\iota \tag{5.19}$$

Therefore, the time rate of change of leg length is the component of the time rate of change of $\bar{L}_\iota$ along the axis of the leg.

$$\dot{l}_\iota = \dot{L}_\iota \,.\, \bar{n}_\iota$$

$$\dot{l}_\iota = \left(\dot{a}_\iota - \dot{b}_\iota\right) . \bar{n}_\iota \tag{5.20}$$

The term $\dot{l}_\iota$ represents the leg length extension rate, or the velocity of the prismatic joint between the parts 1 and 2 of the leg.

The acceleration of the prismatic joint between the parts 1 and 2 of the leg will be given by.

$$\ddot{l}_\iota = \left(\ddot{a}_\iota - \ddot{b}_\iota\right) . \bar{n}_\iota + \left(\dot{a}_\iota - \dot{b}_\iota\right) . \dot{n}_\iota \tag{5.21}$$

Where, $\dot{n}_\iota$ is the time rate of change of the unit vector $\bar{n}_\iota$. Since, it is a unit vector, its time rate of change will only be because of the angular velocity of the legs. Therefore,

$$\dot{\boldsymbol{n}}_{\boldsymbol{\iota}} = \overline{\boldsymbol{\omega}_{\boldsymbol{\iota}}} \times \overline{\boldsymbol{n}_{\boldsymbol{\iota}}} \tag{5.22}$$

$$\ddot{\boldsymbol{l}}_{\boldsymbol{\iota}} = \left(\ddot{\boldsymbol{a}}_{\boldsymbol{\iota}} - \ddot{\boldsymbol{b}}_{\boldsymbol{\iota}}\right).\overline{\boldsymbol{n}_{\boldsymbol{\iota}}} + \left(\dot{\boldsymbol{a}}_{\boldsymbol{\iota}} - \dot{\boldsymbol{b}}_{\boldsymbol{\iota}}\right).\left(\overline{\boldsymbol{\omega}_{\boldsymbol{\iota}}} \times \overline{\boldsymbol{n}_{\boldsymbol{\iota}}}\right) \tag{5.23}$$

The expression for the angular velocity vector of the legs $\overline{\boldsymbol{\omega}_{\boldsymbol{\iota}}}$ will be derived in the section 5.6.3.

5.6.2 – Leg Coordinate Frame.

Refer Fig [5.4]. A right-handed orthogonal coordinate frame is defined for each of the legs. This $\boldsymbol{i^{th}}$ coordinate frame, $(\boldsymbol{i = 1\ to\ 6})$, is attached to the universal joint between the base and the leg. The origin of the frame is located at the anchor points $\boldsymbol{b_i}$; $(\boldsymbol{i = 1\ to\ 6})$. The three axes of the frame are represented by $\{\boldsymbol{L_i}\} = \left(\boldsymbol{u_i}, \boldsymbol{v_i}, \boldsymbol{c_i}\right)$. Where $\boldsymbol{u_i}$ is aligned along the fixed axis of the universal joint, and $\boldsymbol{v_i}$ is aligned along the second axis (rotating axis) of the universal joint. Here we assume that for each leg, the $\boldsymbol{u_i}$ axis is aligned with the unit vector, along the position vectors of the anchor points $\boldsymbol{b_i}$; $(\boldsymbol{i = 1\ to\ 6})$ measured in $\{\boldsymbol{B}\}$ frame and expressed in $\{\boldsymbol{W}\}$ frame, i.e. $\boldsymbol{W_{R_B}}\overline{\boldsymbol{B_{b_\iota}}}$.

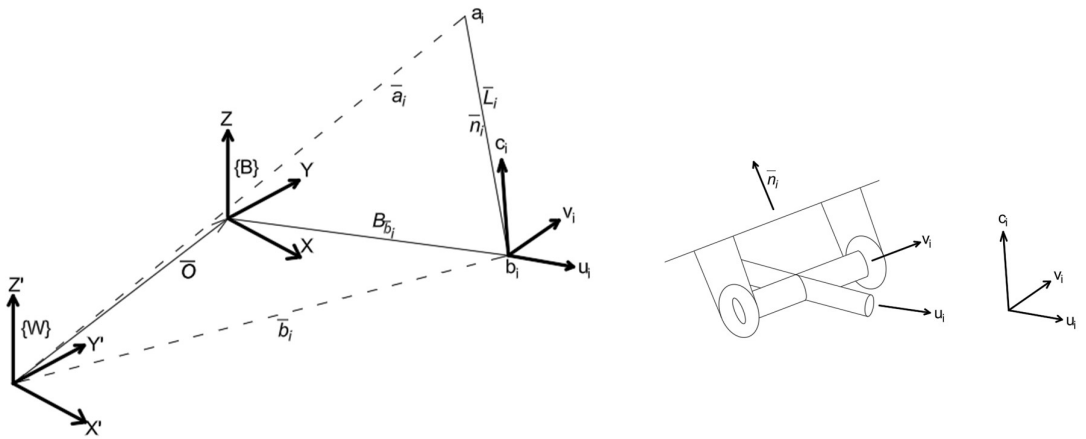

Figure 5. 4 – Frame of reference attached to the universal joint

Therefore,

$$\boldsymbol{u_i} = \frac{\boldsymbol{W_{R_B}}\overline{\boldsymbol{B_{b_i}}}}{\left\|\boldsymbol{W_{R_B}}\overline{\boldsymbol{B_{b_i}}}\right\|} \tag{5.24}$$

Where, $\left\|\boldsymbol{W_{R_B}}\overline{\boldsymbol{B_{b_i}}}\right\|$ is the norm of the vector $\boldsymbol{W_{R_B}}\overline{\boldsymbol{B_{b_i}}}$.

From Fig [5.4], we see that the axis $\boldsymbol{v_i}$ is orthogonal to both the vectors $\boldsymbol{u_i}$ and $\overline{\boldsymbol{n_i}}$. Therefore, the axis $\boldsymbol{v_i}$ is given by

$$\boldsymbol{v_i} = \frac{(\boldsymbol{u_i} \times \overline{\boldsymbol{n_i}})}{\|(\boldsymbol{u_i} \times \overline{\boldsymbol{n_i}})\|} \tag{5.25}$$

The axis $\boldsymbol{c_i}$ is defined an axis orthogonal to both the vectors $\boldsymbol{u_i}$ and $\boldsymbol{v_i}$. Therefore,

$$\boldsymbol{c_i} = \boldsymbol{u_i} \times \boldsymbol{v_i} \tag{5.26}$$

Thus, a coordinate frame attached to each of the six legs, defined by the $\{\boldsymbol{L_i}\} = (\boldsymbol{u_i}, \boldsymbol{v_i}, \boldsymbol{c_i})$ as above is attached to the anchor points $\boldsymbol{b_i}$; $(\boldsymbol{i = 1\ to\ 6})$.

5.6.3 – Kinematics of the Universal Joint between the Base and the Legs.

The kinematic formulation for the universal joint between the base and the legs, will help us find the expressions for the angular velocity vector and the angular acceleration vector of the legs.

Since, we have now defined a frame attached to the universal joint of the leg where the unit vectors along the axes of this frame are expressed in world frame $\{\boldsymbol{W}\}$, we can now define a rotation matrix from the $\{\boldsymbol{L_i}\}$ frame to the $\{\boldsymbol{W}\}$ frame.

$$\boldsymbol{W_{R_{Li}}} = [(\boldsymbol{u_i}) \quad (\boldsymbol{v_i}) \quad (\boldsymbol{c_i})] \tag{5.27}$$

Where, $(\boldsymbol{u_i})$, $(\boldsymbol{v_i})$, $(\boldsymbol{c_i})$ represent the column vectors $\boldsymbol{u_i}$, $\boldsymbol{v_i}$, $\boldsymbol{c_i}$ respectively.

The skew symmetric angular velocity tensor of the $\boldsymbol{i^{th}}$ leg, in world frame, or $\{\boldsymbol{L_i}\}$ w.r.t $\{\boldsymbol{W}\}$, will be given by

$$\omega_{Li}^{ss} = \dot{W}_{R_{Li}} \cdot W_{R_{Li}}{}^{T} \tag{5.28}$$

Where, $\dot{W}_{R_{Li}}$ represents the time derivative of the rotation matrix from $\{L_i\}$ frame to $\{W\}$ frame. The matrix ω_{Li}^{ss} is 3×3 skew symmetric matrix, having the form –

$$\omega_{Li}^{ss} = \begin{bmatrix} 0 & -\omega_{Li_{Z'}} & \omega_{Li_{Y'}} \\ \omega_{Li_{Z'}} & 0 & -\omega_{Li_{X'}} \\ -\omega_{Li_{Y'}} & \omega_{Li_{X'}} & 0 \end{bmatrix} \tag{5.29}$$

Therefore, the angular velocity vector of the i^{th} leg, in world frame, or $\{L_i\}$ w.r.t $\{W\}$, will be given by

$$\overline{\omega_i} = \begin{bmatrix} -\omega_{Li}^{ss}(2,3) \\ \omega_{Li}^{ss}(1,3) \\ -\omega_{Li}^{ss}(1,2) \end{bmatrix} \tag{5.30}$$

The angular acceleration vector of the the i^{th} leg, in world frame, or $\{L_i\}$ w.r.t $\{W\}$, will then be given by

$$\overline{\alpha_i} = \dot{\omega}_i \tag{5.31}$$

Where, $\dot{\omega}_i$ represents the time derivative of $\overline{\omega_i}$.

5.7 – Dynamics of the Base, the Platform, and the Leg.

Fig [5.5], shows the free body diagrams of the base, the leg, and the platform of a GSP. The base is subjected to the gravity force, and the reaction force and moment between the legs and the base. Since, the base is assumed to be moving because of the external excitations, we do not consider any reaction force between the base and the spacecraft bus. The legs are acted upon by the gravity forces of parts 1 and 2, the reaction force and moment between the legs and the base, and the reaction force between the legs and the platform. A reaction moment exists between the base and the legs because of the universal joint. However, since a spherical joint is present between the legs and the platform, there will be no reaction moment at the top end of the leg. The platform is acted upon by the gravity force, and the reaction force between the legs and the platform.

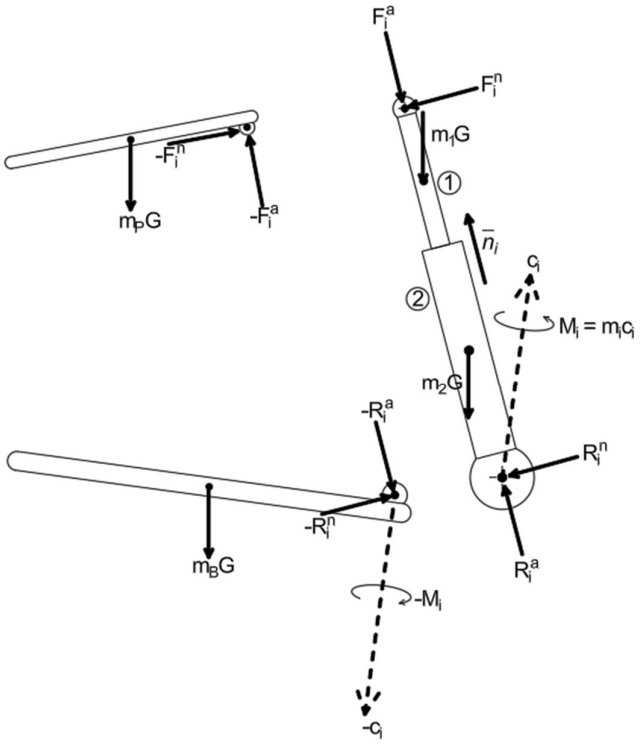

Figure 5. 5 – Free body diagram of the base, the leg and the platform

5.7.1 – Dynamics of the Base.

Fig [5.6], shows the forces and moments acting on the base, and, also the position vectors of the points of application of these forces and moments. The reaction forces and the moment is shown for only one anchor point of the joint. Similar terminology is applicable for each $\boldsymbol{i^{th}}$ joint, $(\boldsymbol{i = 1\ to\ 6})$.

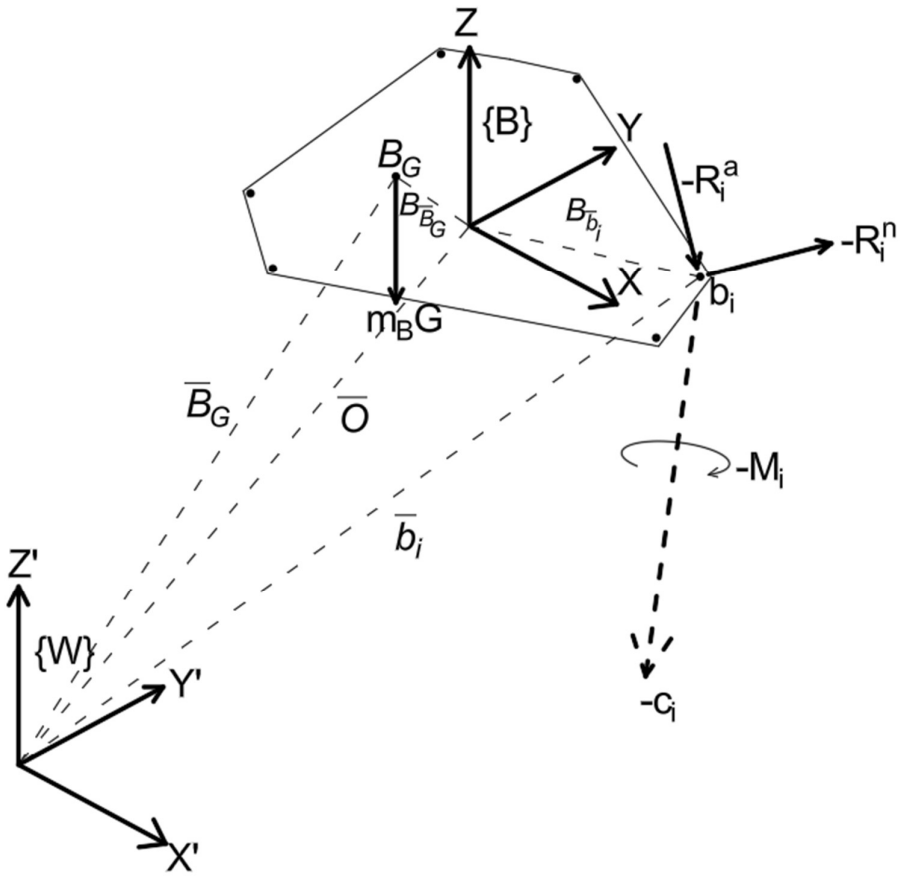

Figure 5. 6 – Forces and moments on the base, in world frame

The position vector of the COM $\boldsymbol{B_G}$ of the base, in the world frame $\{\boldsymbol{W}\}$ is given by

$$\overline{\boldsymbol{B_G}} = \boldsymbol{position\ vector\ of}\ \ \boldsymbol{B_G}\ \boldsymbol{w.r.t}\ \{\boldsymbol{W}\}$$

$$\overline{\boldsymbol{B_G}} = \overline{\boldsymbol{O}} + \boldsymbol{W_{R_B}}\overline{\boldsymbol{B_{B_G}}} \qquad (\mathbf{5.32})$$

Where, $\overline{\boldsymbol{B_{B_G}}}$ is the position vector of $\boldsymbol{B_G}$ in base frame $\{\boldsymbol{B}\}$.

The velocity $\overline{v_{B_G}}$ of the COM of base is given by the time derivative of the position vector $\overline{B_G}$.

$$\overline{v_{B_G}} = \dot{B}_G = \dot{O} + \overline{\omega_B} \times \left(W_{R_B} \overline{B_{B_G}}\right) \quad (5.33)$$

The acceleration $\overline{a_{B_G}}$ of the COM of base is given by the time derivative of the velocity vector $\overline{v_{B_G}}$.

$$\overline{a_{B_G}} = \ddot{B}_G = \ddot{O} + \overline{\alpha_B} \times \left(W_{R_B} \overline{B_{B_G}}\right) + \overline{\omega_B} \times \left[\overline{\omega_B} \times \left(W_{R_B} \overline{B_{B_G}}\right)\right] \quad (5.34)$$

The force balance equation for the base will be –

$$-\sum R_i^a - \sum R_i^n + m_B G = m_B \ddot{B}_G \quad (5.35)$$

The expression for the angular momentum of the base will be

$$\bar{L}_B = \bar{I}_B \overline{\omega_B} + m_B\left(\overline{B_G} \times \overline{v_{B_G}}\right) \quad (5.36)$$

Where, $\bar{I}_B$ is the inertia tensor of the base in the world frame $\{W\}$ and is given by –

$$\bar{I}_B = W_{R_B} B_{\bar{I}_B} {W_{R_B}}^T \quad (5.37)$$

Where, $B_{\bar{I}_B}$ is the inertia tensor of the base in the base frame $\{B\}$.

The expression for the time rate of change of angular momentum of the base will be

$$\dot{L}_B = \bar{I}_B \overline{\alpha_B} + \overline{\omega_B} \times (\bar{I}_B \overline{\omega_B}) + m_B\left(\overline{B_G} \times \overline{a_{B_G}}\right) \quad (5.38)$$

The moment balance equation for the base will be –

$$\overline{B_G} \times m_B G - \sum \bar{b}_i \times R_i^a - \sum \bar{b}_i \times R_i^n - \sum M_i = \dot{L}_B \quad (5.39)$$

$$\bar{B}_G \times m_B G - \sum \bar{b}_i \times R_i^a - \sum \bar{b}_i \times R_i^n - \sum M_i = \bar{I}_B \overline{\alpha_B} + \bar{\omega}_B \times (\bar{I}_B \overline{\omega_B}) + m_B\left(\overline{B_G} \times \overline{a_{B_G}}\right)$$

Therefore,

$$\sum \bar{b}_i \times R_i^a = \bar{B}_G \times m_B G - \bar{I}_B \overline{\alpha_B} - \bar{\omega}_B \times (\bar{I}_B \overline{\omega_B}) - m_B\left(\overline{B_G} \times \overline{a_{B_G}}\right) - \sum \bar{b}_i \times R_i^n - \sum M_i$$

Let,

$$V_B = \bar{B}_G \times m_B G - \bar{I}_B \overline{\alpha_B} - \bar{\omega}_B \times (\bar{I}_B \overline{\omega_B}) - m_B\left(\overline{B_G} \times \overline{a_{B_G}}\right) \qquad (5.40)$$

Therefore,

$$\sum \bar{b}_i \times R_i^a = V_B - \sum \bar{b}_i \times R_i^n - \sum M_i \qquad (5.41)$$

5.7.2 – Dynamics of the Platform.

Fig [5.7], shows the forces acting on the platform, and, also the position vectors of the points of application of these forces. The reaction forces are shown for only one anchor point of the joint. Similar terminology is applicable for each i^{th} joint, $(i = 1 \text{ to } 6)$.

The position vector of the COM P_G of the platform, in the world frame $\{W\}$ is given by

$$\overline{P_G} = \text{position vector of } P_G \text{ w.r.t } \{W\}$$

$$\overline{P_G} = \bar{o} + W_{R_P} \overline{P_{P_G}} \qquad (5.42)$$

Where, $\overline{P_{P_G}}$ is the position vector of P_G in platform frame $\{P\}$.

The velocity $\overline{\boldsymbol{v}_{\boldsymbol{P_G}}}$ of the COM of platform is given by the time derivative of the position vector $\overline{\boldsymbol{P_G}}$.

$$\overline{\boldsymbol{v}_{\boldsymbol{P_G}}} = \dot{\boldsymbol{P}}_{\boldsymbol{G}} = \dot{\boldsymbol{o}} + \overline{\boldsymbol{\omega}_{\boldsymbol{P}}} \times \left(\boldsymbol{W}_{\boldsymbol{R_P}} \overline{\boldsymbol{P}_{\boldsymbol{P_G}}}\right) \tag{5.43}$$

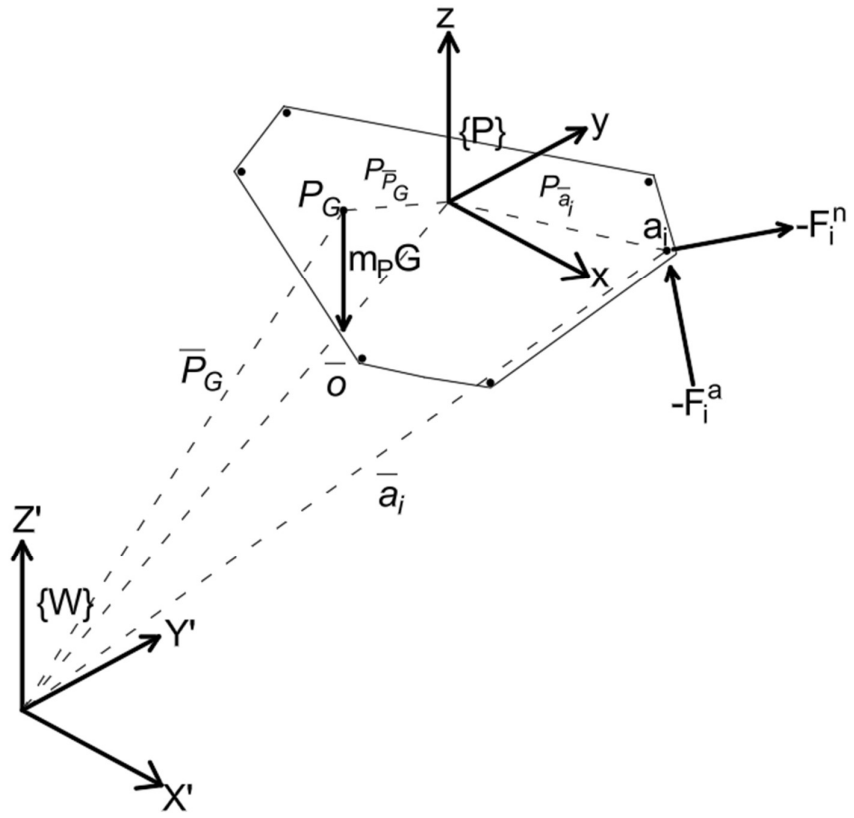

Figure 5. 7 – Forces and moments on the platform, in world frame

The acceleration $\overline{\boldsymbol{a}_{\boldsymbol{P_G}}}$ of the COM of platform is given by the time derivative of the velocity vector $\overline{\boldsymbol{v}_{\boldsymbol{P_G}}}$.

$$\overline{\boldsymbol{a}_{\boldsymbol{P_G}}} = \ddot{\boldsymbol{P}}_{\boldsymbol{G}} = \ddot{\boldsymbol{o}} + \overline{\boldsymbol{\alpha}_{\boldsymbol{P}}} \times \left(\boldsymbol{W}_{\boldsymbol{R_P}} \overline{\boldsymbol{P}_{\boldsymbol{P_G}}}\right) + \overline{\boldsymbol{\omega}_{\boldsymbol{P}}} \times \left[\overline{\boldsymbol{\omega}_{\boldsymbol{P}}} \times \left(\boldsymbol{W}_{\boldsymbol{R_P}} \overline{\boldsymbol{P}_{\boldsymbol{P_G}}}\right)\right] \tag{5.44}$$

The force balance equation for the base will be –

$$-\sum \boldsymbol{F}_{\boldsymbol{i}}^{\boldsymbol{a}} - \sum \boldsymbol{F}_{\boldsymbol{i}}^{\boldsymbol{n}} + \boldsymbol{m_P G} = \boldsymbol{m_P} \ddot{\boldsymbol{P}}_{\boldsymbol{G}} \tag{5.45}$$

The expression for the angular momentum of the base will be

$$\bar{L}_P = \bar{I}_P \overline{\omega_P} + m_P\left(\overline{P_G} \times \overline{v_{P_G}}\right) \tag{5.46}$$

Where, $\bar{I}_P$ is the inertia tensor of the platform in the world frame $\{W\}$ and is given by –

$$\bar{I}_P = W_{R_P} P_{\bar{I}_P} {W_{R_P}}^T \tag{5.47}$$

Where, $P_{\bar{I}_P}$ is the inertia tensor of the platform in the platform frame $\{P\}$.

The expression for the time rate of change of angular momentum of the platform will be

$$\dot{L}_P = \bar{I}_P \overline{\alpha_P} + \overline{\omega_P} \times (\bar{I}_P \overline{\omega_P}) + m_P\left(\overline{P_G} \times \overline{a_{P_G}}\right) \tag{5.48}$$

The moment balance equation for the platform will be –

$$\bar{P}_G \times m_P G - \sum \bar{a}_i \times F_i^a - \sum \bar{a}_i \times F_i^n = \dot{L}_P \tag{5.49}$$

$$\bar{P}_G \times m_P G - \sum \bar{a}_i \times F_i^a - \sum \bar{a}_i \times F_i^n = \bar{I}_P \overline{\alpha_P} + \overline{\omega_P} \times (\bar{I}_P \overline{\omega_P}) + m_P(\overline{P_G} \times \overline{a_{P_G}})$$

Therefore,

$$\sum \bar{a}_i \times F_i^a = \bar{P}_G \times m_P G - \bar{I}_P \overline{\alpha_P} - \overline{\omega_P} \times (\bar{I}_P \overline{\omega_P}) - m_P(\overline{P_G} \times \overline{a_{P_G}}) - \sum \bar{a}_i \times F_i^n$$

Let,

$$V_P = \bar{P}_G \times m_P G - \bar{I}_P \overline{\alpha_P} - \overline{\omega_P} \times (\bar{I}_P \overline{\omega_P}) - m_P\left(\overline{P_G} \times \overline{a_{P_G}}\right) \tag{5.50}$$

Therefore,

$$\sum \bar{a}_i \times F_i^a = V_P - \sum \bar{a}_i \times F_i^n \tag{5.51}$$

5.7.3 – Dynamics of the Leg.

Fig [5.8], shows the forces and moments acting on the $\boldsymbol{i^{th}}$ leg, and, also the position vectors of the points of application of these forces and moments. Similar terminology is applicable for each $\boldsymbol{i^{th}}$ leg, $(\boldsymbol{i = 1\ to\ 6})$.

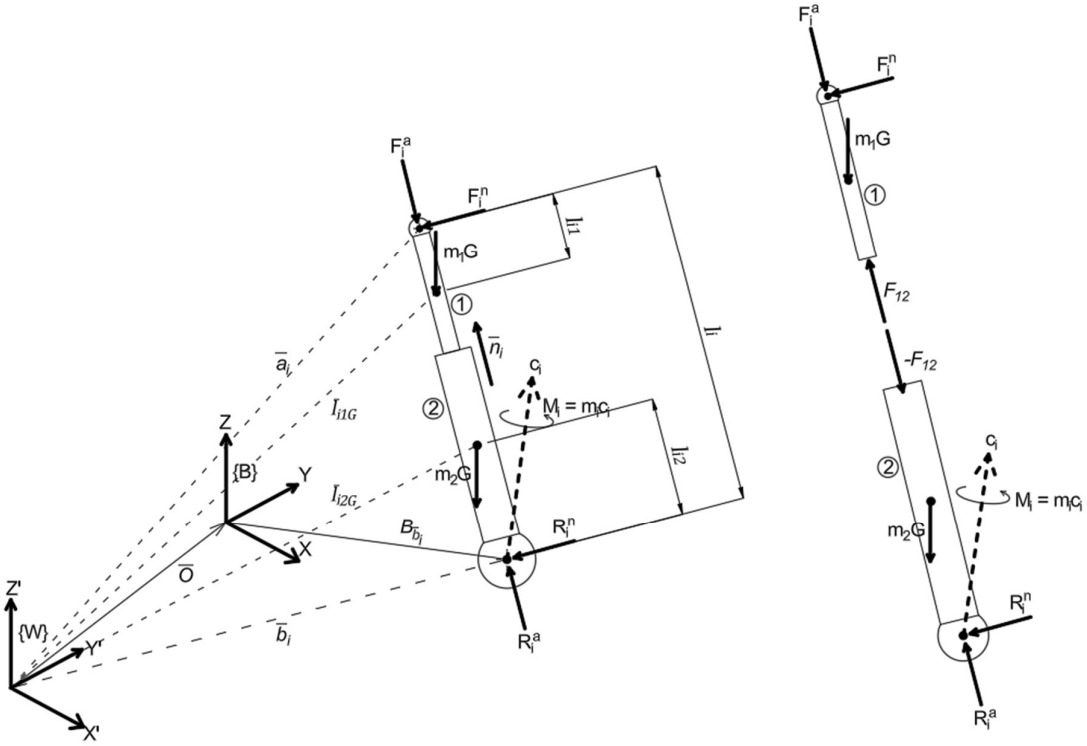

Figure 5. 8 – Forces and moments on the leg, in world frame

The position vector of the COM $\boldsymbol{l_{1G}}$ of the part 1 of the $\boldsymbol{i^{th}}$ leg, in the world frame $\{\boldsymbol{W}\}$ is given by

$$\overline{l_{i1G}} = \textbf{position vector of } l_{i1G} \textbf{ w.r.t } \{W\}$$

$$\overline{l_{i1G}} = \bar{b}_i + (l_i - l_{i1})\,\overline{n_i} \qquad (5.52)$$

The velocity $\overline{v_{l_{i1G}}}$ of the COM of part 1 of the leg is given by the time derivative of the position vector $\overline{l_{i1G}}$.

$$\overline{v_{l_{i1G}}} = \dot{l}_{i1G} = \dot{b}_i + \dot{l}_i \overline{n_i} + (l_i - l_{i1})(\overline{\omega_i} \times \overline{n_i}) \quad (5.53)$$

The acceleration $\overline{a_{l_{i1G}}}$ of the COM of part 1 of the leg is given by the time derivative of the velocity vector $\overline{v_{l_{i1G}}}$.

$$\overline{a_{l_{i1G}}} = \ddot{l}_{i1G} = \ddot{b}_i + \ddot{l}_i \overline{n_i} + \dot{l}_i (\overline{\omega_i} \times \overline{n_i}) + \dot{l}_i (\overline{\omega_i} \times \overline{n_i}) + (l_i - l_{i1})(\overline{\alpha_i} \times \overline{n_i}) + (l_i - l_{i1})[\overline{\omega_i} \times (\overline{\omega_i} \times \overline{n_i})] \quad (5.54)$$

Similarly, we find the velocity and acceleration of the part 2 of the leg.

The position vector of the COM l_{i2G} of the part 2 of the i^{th} leg, in the world frame $\{W\}$ is given by

$$\overline{l_{i2G}} = \textbf{position vector of } l_{i2G} \textbf{ w.r.t } \{W\}$$

$$\overline{l_{i2G}} = \overline{b_i} + l_{i2}\overline{n_i} \quad (5.55)$$

The velocity $\overline{v_{l_{i2G}}}$ of the COM of part 2 of the leg is given by the time derivative of the position vector $\overline{l_{i2G}}$.

$$\overline{v_{l_{i2G}}} = \dot{l}_{i2G} = \dot{b}_i + l_{i2}(\overline{\omega_i} \times \overline{n_i}) \quad (5.56)$$

The acceleration $\overline{a_{l_{i2G}}}$ of the COM of part 2 of the leg is given by the time derivative of the velocity vector $\overline{v_{l_{i2G}}}$.

$$\overline{a_{l_{i2G}}} = \ddot{l}_{i2G} = \ddot{b}_i + l_{i2}(\overline{\alpha_i} \times \overline{n_i}) + l_{i2}[\overline{\omega_i} \times (\overline{\omega_i} \times \overline{n_i})] \quad (5.57)$$

The force balance equation for the i^{th} leg will be –

$$F_i^a + F_i^n + R_i^a + R_i^n + m_1 G + m_2 G = m_1 \ddot{l}_{i1G} + m_2 \ddot{l}_{i2G} \quad (5.58)$$

$$\boldsymbol{F_i + R_i = m_1 \ddot{l}_{i1G} + m_2 \ddot{l}_{i2G} - m_1 G - m_2 G}$$

Let, $$\boldsymbol{N_i = m_1 \ddot{l}_{i1G} + m_2 \ddot{l}_{i2G} - m_1 G - m_2 G}$$

Therefore,

$$\boldsymbol{F_i + R_i = N_i} \tag{5.59}$$

The force balance equation for part 1 of the $\boldsymbol{i^{th}}$ leg will be –

$$\boldsymbol{F_i = m_1 \ddot{l}_{i1G} - m_1 G + F_{12}} \tag{5.60}$$

Where, $\boldsymbol{F_i = F_i^a + F_i^n}$ is the total reaction force, and $\boldsymbol{F_{12}}$ is the interaction force between parts 1 and 2.

The force balance equation for part 2 of the $\boldsymbol{i^{th}}$ leg will be –

$$\boldsymbol{R_i = m_2 \ddot{l}_{i2G} - m_2 G - F_{12}} \tag{5.61}$$

Where, $\boldsymbol{R_i = R_i^a + R_i^n}$ is the total reaction force, and $\boldsymbol{F_{12}}$ is the interaction force between parts 1 and 2.

The expression for the angular momentum of the $\boldsymbol{i^{th}}$ leg will be

$$\boldsymbol{\bar{L}_{li} = \bar{I}_1 \bar{\omega}_i + \bar{I}_2 \bar{\omega}_i + m_1\left(\overline{l_{i1G}} \times \overline{v_{l_{i1G}}}\right) + m_2\left(\overline{l_{i2G}} \times \overline{v_{l_{i2G}}}\right)} \tag{5.62}$$

Where, $\boldsymbol{\bar{I}_1}$ is the inertia tensor of the part 1 of the leg in the world frame $\{\boldsymbol{W}\}$ and is given by –

$$\boldsymbol{\bar{I}_1 = W_{R_{Li}} L_{i\bar{I}_{Li}} W_{R_{Li}}{}^T} \tag{5.63}$$

Where, $\boldsymbol{L_{i\bar{I}_{Li}}}$ is the inertia tensor of the part 1 of the leg in the leg frame $\{\boldsymbol{L_i}\}$**.** Similarly, we can find the inertia tensor $\boldsymbol{\bar{I}_2}$ of the part 2 of the frame.

The expression for the time rate of change of angular momentum of the platform will be

$$\dot{\boldsymbol{L}}_{\boldsymbol{li}} = (\bar{\boldsymbol{I}}_{\boldsymbol{1}} + \bar{\boldsymbol{I}}_{\boldsymbol{2}})\bar{\boldsymbol{\alpha}}_{\boldsymbol{i}} + \bar{\boldsymbol{\omega}}_{\boldsymbol{i}} \times [(\bar{\boldsymbol{I}}_{\boldsymbol{1}} + \bar{\boldsymbol{I}}_{\boldsymbol{2}})\bar{\boldsymbol{\omega}}_{\boldsymbol{i}}] + \boldsymbol{m}_{\boldsymbol{1}}\left(\overline{\boldsymbol{l}_{\boldsymbol{i1G}}} \times \overline{\boldsymbol{a}_{\boldsymbol{l_{i1G}}}}\right) + \boldsymbol{m}_{\boldsymbol{2}}\left(\overline{\boldsymbol{l}_{\boldsymbol{i2G}}} \times \overline{\boldsymbol{a}_{\boldsymbol{l_{i2G}}}}\right) \quad (\mathbf{5.64})$$

The moment balance equation for the $\boldsymbol{i^{th}}$ leg will be –

$$\dot{\boldsymbol{L}}_{\boldsymbol{li}} = (\bar{\boldsymbol{a}}_{\boldsymbol{i}} \times \boldsymbol{F}_{\boldsymbol{i}}^{\boldsymbol{a}}) + (\bar{\boldsymbol{a}}_{\boldsymbol{i}} \times \boldsymbol{F}_{\boldsymbol{i}}^{\boldsymbol{n}}) + (\bar{\boldsymbol{b}}_{\boldsymbol{i}} \times \boldsymbol{R}_{\boldsymbol{i}}^{\boldsymbol{a}}) + \left(\bar{\boldsymbol{b}}_{\boldsymbol{i}} \times \boldsymbol{R}_{\boldsymbol{i}}^{\boldsymbol{n}}\right) + \left(\overline{\boldsymbol{l}_{\boldsymbol{i1G}}} \times \boldsymbol{m}_{\boldsymbol{1}}\boldsymbol{G}\right) + \left(\overline{\boldsymbol{l}_{\boldsymbol{i2G}}} \times \boldsymbol{m}_{\boldsymbol{2}}\boldsymbol{G}\right) + \boldsymbol{M}_{\boldsymbol{i}} \quad (\mathbf{5.65})$$

Therefore,

$$(\bar{\boldsymbol{a}}_{\boldsymbol{i}} \times \boldsymbol{F}_{\boldsymbol{i}}) + \left(\bar{\boldsymbol{b}}_{\boldsymbol{i}} \times \boldsymbol{R}_{\boldsymbol{i}}\right) + \boldsymbol{M}_{\boldsymbol{i}} = \dot{\boldsymbol{L}}_{\boldsymbol{li}} - \left(\overline{\boldsymbol{l}_{\boldsymbol{i1G}}} \times \boldsymbol{m}_{\boldsymbol{1}}\boldsymbol{G}\right) - \left(\overline{\boldsymbol{l}_{\boldsymbol{i2G}}} \times \boldsymbol{m}_{\boldsymbol{2}}\boldsymbol{G}\right)$$

Let,

$$\boldsymbol{E}_{\boldsymbol{i}} = \dot{\boldsymbol{L}}_{\boldsymbol{li}} - \left(\overline{\boldsymbol{l}_{\boldsymbol{i1G}}} \times \boldsymbol{m}_{\boldsymbol{1}}\boldsymbol{G}\right) - \left(\overline{\boldsymbol{l}_{\boldsymbol{i2G}}} \times \boldsymbol{m}_{\boldsymbol{2}}\boldsymbol{G}\right) \quad (\mathbf{5.66})$$

Therefore,

$$(\bar{\boldsymbol{a}}_{\boldsymbol{i}} \times \boldsymbol{F}_{\boldsymbol{i}}) + \left(\bar{\boldsymbol{b}}_{\boldsymbol{i}} \times \boldsymbol{R}_{\boldsymbol{i}}\right) + \boldsymbol{M}_{\boldsymbol{i}} = \boldsymbol{E}_{\boldsymbol{i}} \quad (\mathbf{5.67})$$

5.7.4 – Expressions for the Reaction Forces and the Moments.

In this section we find the expressions for the $\boldsymbol{F}_{\boldsymbol{i}}^{\boldsymbol{a}}$, $\boldsymbol{F}_{\boldsymbol{i}}^{\boldsymbol{n}}$, $\boldsymbol{R}_{\boldsymbol{i}}^{\boldsymbol{a}}$, $\boldsymbol{R}_{\boldsymbol{i}}^{\boldsymbol{n}}$, $\boldsymbol{M}_{\boldsymbol{i}}$.

$$\boldsymbol{F}_{\boldsymbol{i}} = \boldsymbol{N}_{\boldsymbol{i}} - \boldsymbol{R}_{\boldsymbol{i}}$$

$$\left(\bar{\boldsymbol{a}}_{\boldsymbol{i}} \times (\boldsymbol{N}_{\boldsymbol{i}} - \boldsymbol{R}_{\boldsymbol{i}})\right) + \left(\bar{\boldsymbol{b}}_{\boldsymbol{i}} \times \boldsymbol{R}_{\boldsymbol{i}}\right) + \boldsymbol{M}_{\boldsymbol{i}} = \boldsymbol{E}_{\boldsymbol{i}}$$

$$(\bar{\boldsymbol{a}}_{\boldsymbol{i}} \times \boldsymbol{N}_{\boldsymbol{i}}) + \left(\left(\bar{\boldsymbol{b}}_{\boldsymbol{i}} - \bar{\boldsymbol{a}}_{\boldsymbol{i}}\right) \times \boldsymbol{R}_{\boldsymbol{i}}\right) + \boldsymbol{M}_{\boldsymbol{i}} = \boldsymbol{E}_{\boldsymbol{i}} \quad (\mathbf{5.68})$$

The moment $\boldsymbol{M}_{\boldsymbol{i}}$ is along the $\boldsymbol{c}_{\boldsymbol{i}}$ axis, and can therefore be written as $\boldsymbol{M}_{\boldsymbol{i}} = \boldsymbol{m}_{\boldsymbol{i}}\,\boldsymbol{c}_{\boldsymbol{i}}$

Dot product Eqn. [5.68] with $\left(\overline{\boldsymbol{b}}_{\boldsymbol{i}} - \overline{\boldsymbol{a}}_{\boldsymbol{i}}\right)$ and after certain simplifications, we get the expression for $\boldsymbol{m_i}$ as

$$\boldsymbol{m_i} = \frac{\boldsymbol{E_i} \,.\left(\overline{\boldsymbol{b}}_{\boldsymbol{i}} - \overline{\boldsymbol{a}}_{\boldsymbol{i}}\right) - \left(\overline{\boldsymbol{a}}_{\boldsymbol{i}} \times \boldsymbol{N_i}\right).\overline{\boldsymbol{b}}_{\boldsymbol{i}}}{\boldsymbol{c_i} \,.\left(\overline{\boldsymbol{b}}_{\boldsymbol{i}} - \overline{\boldsymbol{a}}_{\boldsymbol{i}}\right)} \tag{5.69}$$

Therefore,

$$\boldsymbol{M_i} = \frac{\boldsymbol{E_i} \,.\left(\overline{\boldsymbol{b}}_{\boldsymbol{i}} - \overline{\boldsymbol{a}}_{\boldsymbol{i}}\right) - \left(\overline{\boldsymbol{a}}_{\boldsymbol{i}} \times \boldsymbol{N_i}\right).\overline{\boldsymbol{b}}_{\boldsymbol{i}}}{\boldsymbol{c_i} \,.\left(\overline{\boldsymbol{b}}_{\boldsymbol{i}} - \overline{\boldsymbol{a}}_{\boldsymbol{i}}\right)} \;\; \boldsymbol{c_i} \tag{5.70}$$

Now,

$$\overline{\boldsymbol{b}}_{\boldsymbol{i}} - \overline{\boldsymbol{a}}_{\boldsymbol{i}} = -\boldsymbol{l_i} \; \overline{\boldsymbol{n}_{\boldsymbol{\iota}}}$$

$$\left(\overline{\boldsymbol{b}}_{\boldsymbol{i}} - \overline{\boldsymbol{a}}_{\boldsymbol{i}}\right) \times \boldsymbol{R_i} = \boldsymbol{E_i} - \boldsymbol{M_i} - \left(\overline{\boldsymbol{a}}_{\boldsymbol{i}} \times \boldsymbol{N_i}\right)$$

$$-\boldsymbol{l_i} \; \overline{\boldsymbol{n}_{\boldsymbol{\iota}}} \times \boldsymbol{R_i} = \boldsymbol{E_i} - \boldsymbol{M_i} - \left(\overline{\boldsymbol{a}}_{\boldsymbol{i}} \times \boldsymbol{N_i}\right) \tag{5.71}$$

Cross product Eqn. [5.71] with $\overline{\boldsymbol{n}_{\boldsymbol{\iota}}}$ and after certain simplifications, we get the expression for $\boldsymbol{R_i^n}$ as

$$\boldsymbol{R_i^n} = \frac{-\left(\boldsymbol{E_i} - \boldsymbol{M_i} - \left(\overline{\boldsymbol{a}}_{\boldsymbol{i}} \times \boldsymbol{N_i}\right)\right) \times \overline{\boldsymbol{n}_{\boldsymbol{\iota}}}}{\boldsymbol{l_i}} \tag{5.72}$$

Similarly, we find the expression for $\boldsymbol{F_i^n}$

$$\boldsymbol{R_i} = \boldsymbol{N_i} - \boldsymbol{F_i}$$

$$\left(\overline{\boldsymbol{a}}_{\boldsymbol{i}} \times \boldsymbol{F_i}\right) + \left(\overline{\boldsymbol{b}}_{\boldsymbol{i}} \times \left(\boldsymbol{N_i} - \boldsymbol{F_i}\right)\right) + \boldsymbol{M_i} = \boldsymbol{E_i}$$

$$\left(\overline{\boldsymbol{b}}_{\boldsymbol{i}} \times \boldsymbol{N_i}\right) + \left(\left(\overline{\boldsymbol{a}}_{\boldsymbol{i}} - \overline{\boldsymbol{b}}_{\boldsymbol{i}}\right) \times \boldsymbol{F_i}\right) + \boldsymbol{M_i} = \boldsymbol{E_i}$$

$$\left(\overline{\boldsymbol{a}}_{\boldsymbol{i}} - \overline{\boldsymbol{b}}_{\boldsymbol{i}}\right) \times \boldsymbol{F_i} = \boldsymbol{E_i} - \boldsymbol{M_i} - \left(\overline{\boldsymbol{b}}_{\boldsymbol{i}} \times \boldsymbol{N_i}\right)$$

$$\boldsymbol{l_i} \; \overline{\boldsymbol{n}_{\boldsymbol{\iota}}} \times \boldsymbol{F_i} = \boldsymbol{E_i} - \boldsymbol{M_i} - \left(\overline{\boldsymbol{b}}_{\boldsymbol{i}} \times \boldsymbol{N_i}\right) \tag{5.73}$$

Cross product Eqn. [5.73] with $\overline{\boldsymbol{n_i}}$ and after certain simplifications, we get the expression for $\boldsymbol{F_i^n}$ as

$$\boldsymbol{F_i^n = \frac{\left(E_i - M_i - \left(\bar{b}_i \times N_i\right)\right) \times \overline{n_i}}{l_i}} \quad (5.74)$$

To find the expression for $\boldsymbol{R_i^a}$ **.** From the force and moment balance equation of the base we have,

$$\sum \boldsymbol{R_i^a} = \boldsymbol{m_B G} - \boldsymbol{m_B \ddot{B}_G} - \sum \boldsymbol{R_i^n}$$

$$\sum \bar{\boldsymbol{b}}_i \times \boldsymbol{R_i^a} = \boldsymbol{V_B} - \sum \bar{\boldsymbol{b}}_i \times \boldsymbol{R_i^n} - \sum \boldsymbol{M_i}$$

The axial force $\boldsymbol{R_i^a}$ can be written as, $\boldsymbol{R_i^a = r_i^a \ \overline{n_i}}$ **,** where $\boldsymbol{r_i^a}$ is the magnitude of the axial force.

Substituting $\boldsymbol{R_i^a = r_i^a \ \overline{n_i}}$ in above equations and writing the summation terms in the LHS of the equations, as a matrix multiplication, we get

$$\begin{bmatrix} \left(\bar{b}_1 \times \overline{n_1}\right) & \left(\bar{b}_2 \times \overline{n_2}\right) & \dots & \left(\bar{b}_6 \times \overline{n_6}\right) \end{bmatrix} \begin{bmatrix} r_1^a \\ r_2^a \\ \vdots \\ r_6^a \end{bmatrix} = \left[V_B - \sum \bar{b}_i \times R_i^n - \sum M_i \right] \quad (5.75)$$

$$\begin{bmatrix} \overline{n_1} & \overline{n_2} & \dots & \overline{n_6} \end{bmatrix} \begin{bmatrix} r_1^a \\ r_2^a \\ \vdots \\ r_6^a \end{bmatrix} = \left[m_B G - m_B \ddot{B}_G - \sum R_i^n \right] \quad (5.76)$$

Combining the above two equations, we get the matrix of the values of $\boldsymbol{r_i^a}$ as,

$$\begin{bmatrix} r_1^a \\ r_2^a \\ \vdots \\ r_6^a \end{bmatrix} = \begin{bmatrix} \left(\bar{b}_1 \times \overline{n_1}\right) & \left(\bar{b}_2 \times \overline{n_2}\right) & \cdots & \left(\bar{b}_6 \times \overline{n_6}\right) \\ \overline{n_1} & \overline{n_2} & \cdots & \overline{n_6} \end{bmatrix}^{-1} \begin{bmatrix} V_B - \sum \bar{b}_i \times R_i^n - \sum M_i \\ m_B G - m_B \ddot{B}_G - \sum R_i^n \end{bmatrix} \quad (5.77)$$

The axial force $\boldsymbol{R_i^a}$ can be written as, $\boldsymbol{R_i^a = r_i^a \ \overline{n_i}}$ **,** for each $\boldsymbol{i^{th}}$ leg.

To find the expression for $\boldsymbol{F_i^a}$ **.** From the force and moment balance equation of the base we have,

$$\sum \boldsymbol{F_i^a} \;= \boldsymbol{m_P G} \;-\; \boldsymbol{m_P \ddot{P}_G} \;- \sum \boldsymbol{F_i^n}$$

$$\sum \boldsymbol{\bar{a}_i \times F_i^a} \;=\; \boldsymbol{V_P} \;- \sum \boldsymbol{\bar{a}_i \times F_i^n}$$

The axial force $\boldsymbol{F_i^a}$ can be written as, $\boldsymbol{F_i^a = f_i^a\ \overline{n_i}}$ **,** where $\boldsymbol{r_i^a}$ is the magnitude of the axial force.

Substituting $\boldsymbol{F_i^a = f_i^a\ \overline{n_i}}$ in above equations and writing the summation terms in the LHS of the equations, as a matrix multiplication, we get

$$\left[(\boldsymbol{\bar{a}_1 \times \overline{n_1}}) \quad (\boldsymbol{\bar{a}_2 \times \overline{n_2}}) \quad \ldots \quad (\boldsymbol{\bar{a}_6 \times \overline{n_6}})\right] \begin{bmatrix} \boldsymbol{f_1^a} \\ \boldsymbol{f_2^a} \\ \vdots \\ \boldsymbol{f_6^a} \end{bmatrix} = \left[\boldsymbol{V_P} - \sum \boldsymbol{\bar{a}_i \times F_i^n}\right] \qquad (\mathbf{5.77})$$

$$\left[\boldsymbol{\overline{n_1}} \quad \boldsymbol{\overline{n_2}} \quad \ldots \quad \boldsymbol{\overline{n_6}}\right] \begin{bmatrix} \boldsymbol{f_1^a} \\ \boldsymbol{f_2^a} \\ \vdots \\ \boldsymbol{f_6^a} \end{bmatrix} = \left[\boldsymbol{m_P G} - \boldsymbol{m_P \ddot{P}_G} - \sum \boldsymbol{F_i^n}\right] \qquad (\mathbf{5.78})$$

Combining the above two equations, we get the matrix of the values of $\boldsymbol{r_i^a}$ as,

$$\begin{bmatrix} \boldsymbol{f_1^a} \\ \boldsymbol{f_2^a} \\ \vdots \\ \boldsymbol{f_6^a} \end{bmatrix} = \begin{bmatrix} \underset{\boldsymbol{\overline{n_1}}}{(\boldsymbol{\bar{a}_1 \times \overline{n_1}})} & \underset{\boldsymbol{\overline{n_2}}}{(\boldsymbol{\bar{a}_2 \times \overline{n_2}})} & \cdots & \underset{\boldsymbol{\overline{n_6}}}{(\boldsymbol{\bar{a}_6 \times \overline{n_6}})} \end{bmatrix}^{-1} \begin{bmatrix} \boldsymbol{V_P} - \sum \boldsymbol{\bar{a}_i \times F_i^n} \\ \boldsymbol{m_P G} - \boldsymbol{m_P \ddot{P}_G} - \sum \boldsymbol{F_i^n} \end{bmatrix} \qquad (\mathbf{5.79})$$

The axial force $\boldsymbol{F_i^a}$ can be written as, $\boldsymbol{F_i^a = f_i^a\ \overline{n_i}}$ **,** for each $\boldsymbol{i^{th}}$ leg.

5.8 – Differential Equation of Motion to be solved to get platform position and orientation.

From the force balance equation for part 1 of the leg, we get

$$\boldsymbol{F_i = m_1\, \ddot{l}_{i1G} \; - \; m_1 G \; + \; F_{12}} \qquad \boldsymbol{(5.80)}$$

From the force balance equation for the platform, we have,

$$\boldsymbol{-m_P \ddot{P}_G + \; m_P G \;\; = \sum F_i \;\; = \sum \; \left[m_1\, \ddot{l}_{i1G} - \; m_1 G + F_{12}\right]} \qquad \boldsymbol{(5.81)}$$

Combining the above two equations, substituting the expression for $\boldsymbol{\ddot{l}_{i1G}}$, and performing certain simplifications we get the following equation

$$\boldsymbol{-m_P \ddot{P}_G + \; m_P G \; = \; m_1 \sum \left\{ \ddot{a}_i \; - \; \frac{l_{i1}}{l_i}(\dot{a}_i \; - \dot{b}_i)\left[1 \; - \; \frac{2\dot{l}_i}{l_i}\right] \; - \frac{l_{i1}}{l_i}\ddot{l}_i n_i \; - 2 l_{i1} \frac{\dot{l}_i^{\,2}}{l_i^{\,2}} n_i \right\} \; - \sum m_1 G + \; F_{12}} \qquad \boldsymbol{(5.82)}$$

In vibration isolation applications, the interaction force $\boldsymbol{F_{12}}$ is characterised by the stiffness and damping elements that are used inside the legs.

For example, suppose that a negative stiffness mechanism having Torsion Spring Configuration 1 is used as the stiffness element. Then the expression for $\boldsymbol{F_{12}}$ will be, (Refer Chapter 4, section 4.2.1)

$$\boldsymbol{F_{12} = K_v x \; - 3 \; . \; \frac{2k}{l} \; . \; \frac{\alpha \; - \; \mu \; - \; \left[\frac{R \; - \sqrt{R^2 \; - \; x^2}}{l \; \sin \alpha}\right]}{\sin\left[\alpha \; - \; \left(\frac{R \; - \sqrt{R^2 \; - \; x^2}}{l \; sin \, \alpha}\right)\right]} \; . \; \frac{x}{\sqrt{R^2 \; - \; x^2}}} \qquad \boldsymbol{(5.83)}$$

Where, the displacement $\boldsymbol{x}$ will be given by.

$$\boldsymbol{x = \; (l_i - \; l_o)} \qquad \boldsymbol{(5.84)}$$

Where, $\boldsymbol{l_i}$ is the instantaneous leg length and $\boldsymbol{l_o}$ is the initial leg length**.**

In Eqn. [5.82], the terms $\ddot{\boldsymbol{P}}_{\boldsymbol{G}}$, $\ddot{\boldsymbol{a}}_{\boldsymbol{i}}$, $\dot{\boldsymbol{a}}_{\boldsymbol{i}}$, $\ddot{\boldsymbol{l}}_{\boldsymbol{i}}$, $\dot{\boldsymbol{l}}_{\boldsymbol{i}}$, $\boldsymbol{l_i}$, $\boldsymbol{n_i}$ are all functions of the platform position and orientation. Hence the equation becomes an implicit differential equation and needs to be solved in the form

$$\boldsymbol{Eqn = 0} \qquad (\mathbf{5.85})$$

From the above force balance equation Eqn. [5.82], we will get three differential equations. Similarly, three more differential equations are obtained from the moment balance equation. These six differential equations are then solved to get the solution for the platform position and orientation, as a response of the platform of the GSP to the base excitations.

5.9 – Conclusion.

1) We have derived the analytical formulation of a 6-6 GSP, when its base is subjected to external excitations, or considering a moving base.
2) The expressions for the base velocity and acceleration, platform velocity and acceleration, leg extension rate, and the angular velocity and acceleration of the legs, have been discussed in the section on kinematics.
3) In dynamics section, we have applied newtons laws to formulate the equations of motion of the base, the platform, and the legs. These equations are used to derive the expressions for the reaction forces and moments.
4) Finally, we have seen the analytical formulation of the differential equation that needs to be solved to get the solution for the platform position and orientation.

Chapter 6 – Conclusion and Scope for Future Work.

6.1 – Conclusions

1) Negative Stiffness mechanisms can give us a system with low dynamic stiffness, without compromising the static stiffness of the system.
2) The oblique springs mechanism is a simple and effective mechanism to get NS in the system. However, it has only one unknown control parameter to control the behaviour of the system.
3) The response of the oblique springs system can be studied for small values of the normalized displacement, by approximating the oblique springs mechanism to standard duffing's oscillator.
4) The response obtained from the duffing's approximation shows that the system exhibits the jump phenomenon at certain frequency. This sudden change in the mass displacement can cause system failure, and need to be handled appropriately.
5) Three different configurations for generating negative stiffness in a simple spring mass system are discussed and their force and stiffness formulation is done.
6) Torsion springs are used in two different configurations as the negative stiffness element.
7) Torsion spring Configuration 1 has four control parameters, which provide higher level of control over the stiffness behaviour. However, higher number of control parameters may lead to higher deviation from QZS condition.
8) Torsion spring Configuration 2 and Negative Helical Spring Configuration has only one control parameter. It is theoretically possible to get zero dynamic stiffness in the system under certain mathematical condition on this control parameter.
9) We have derived the analytical formulation of a 6-6 GSP, when its base is subjected to external excitations, or considering a moving base.
10) The expressions for the base velocity and acceleration, platform velocity and acceleration, leg extension rate, and the angular velocity and acceleration of the legs, have been discussed in the section on kinematics.

11) In dynamics section, we have applied newtons laws to formulate the equations of motion of the base, the platform, and the legs. These equations are used to derive the expressions for the reaction forces and moments.
12) Finally, we have seen the analytical formulation of the differential equation that needs to be solved to get the solution for the platform position and orientation.

6.2 – Scope for Future Work.

1) Experimental and software validation of the stiffness behavior of the newly introduced NS configurations.
2) To find the deviation in the stiffness values of the system, if the values of the control parameters deviate from their ideal values, as required to satisfy the QZS condition. The effect of the deviation of each control parameter, on the error in the stiffness of the system.
3) To find the dynamic response of a vibration isolation system, consisting these NS configurations, as the stiffness elements, when excited in a single degree of freedom.
4) To study the dynamic response of the GSP for six degree of freedom vibration isolation.
5) To analytically find the response of the platform of the GSP, when the base is excited in six degrees of freedom, for both conventional GSP and MGSP, when the prismatic joints in the legs have the NS configurations discussed in chapter 4.
6) To perform experimental and software validation of the response of the GSP.
7) To invent newer configurations for NS characteristics, to get the dynamic stiffness and natural frequency of the vibration isolation system as low as possible.

Appendix A

A.1 – Derivation of Eqn. [4.2]

In this section we derive the following equation.

$$\boldsymbol{F_n = \frac{2k\gamma}{\cos\theta . \sin(\mu + \gamma) . l}}$$

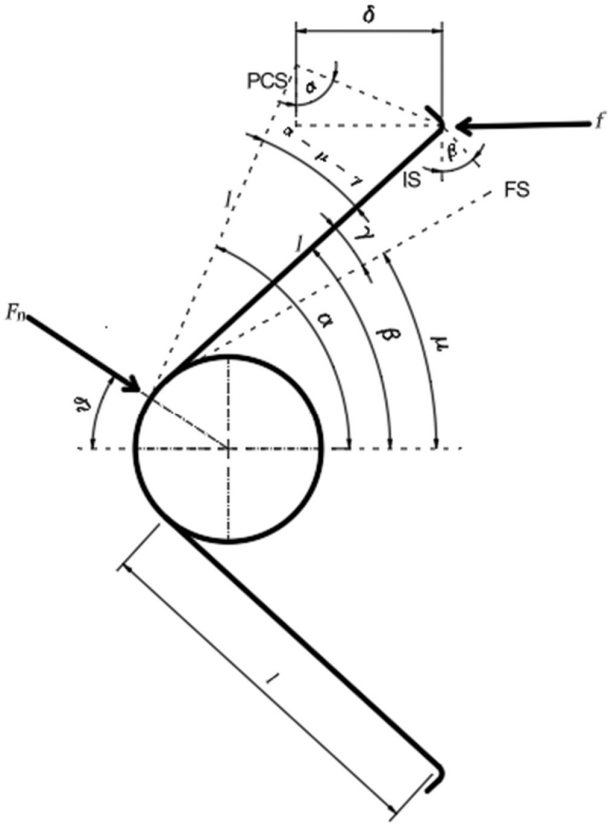

Refer Fig [4.2],

$$\boldsymbol{F_n \cos\theta = 2f \quad ; \quad f = \frac{F_n \cos\theta}{2}} \qquad (\boldsymbol{A.1})$$

$$\boldsymbol{M = f \sin\beta \ . \ l} \qquad (\boldsymbol{A.2})$$

Where, $\boldsymbol{M}$ is the moment about the center of the torsion spring, due to the force $\boldsymbol{f}$ on its legs.

$$\frac{F_n \cos\theta}{2} \sin\beta \; . \; l \; = \; k\gamma$$

$$F_n = \frac{2k\gamma}{\cos\theta \sin\beta \; . \; l} \qquad (A.3)$$

From the figure,

$$\beta = \mu + \gamma$$

Therefore,

$$F_n = \frac{2k\gamma}{\cos\theta . \sin(\mu + \gamma) . l} \qquad (A.4)$$

A.2 – Derivation of Eqn. [4.4]

In this section we derive the following equation.

$$\gamma = \alpha - \mu - \left\{\frac{R - \sqrt{R^2 - x^2}}{l \sin\alpha}\right\}$$

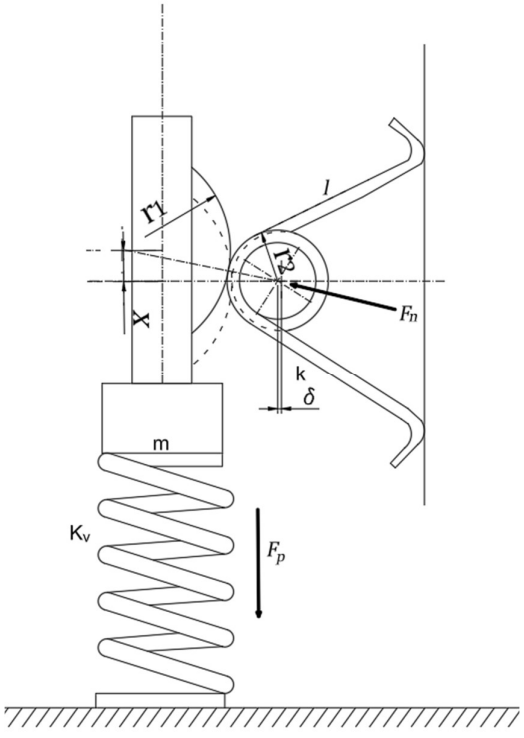

Refer Fig [4.2], and Fig [4.3].

$$\sin\alpha = \frac{\delta}{l\,.\,(\alpha-\mu-\gamma)}$$

$$(\alpha-\mu-\gamma) = \frac{\delta}{l\,\sin\alpha}$$

$$\gamma = \alpha-\mu-\frac{\delta}{l\,\sin\alpha} \qquad (A.5)$$

From Fig [4.2], and Fig [4.3], we see that the δ is the horizontal displacement of the ends of the legs of the torsion springs, which is same as the horizontal displacement of the center of the torsion springs.

Therefore,

$$\delta = (r_1 + r_2) - \sqrt{(r_1 + r_2)^2 - x^2} \qquad (A.6)$$

$$\gamma = \alpha-\mu-\left[\frac{(r_1 + r_2) - \sqrt{(r_1 + r_2)^2 - x^2}}{l\,\sin\alpha}\right] \qquad (A.7)$$

Let, $(r_1 + r_2) = R$

Therefore,

$$\gamma = \alpha-\mu-\left[\frac{R - \sqrt{R^2 - x^2}}{l\,\sin\alpha}\right] \qquad (A.8a)$$

$$\sin(\mu+\gamma) = \sin\left\{\alpha-\left[\frac{R - \sqrt{R^2 - x^2}}{l\,\sin\alpha}\right]\right\} \qquad (A.8b)$$

A.3 – Derivation of Eqn. [4.15]

In this section we derive the following equation.

$$F_n = k \frac{\left\{\alpha - \left(2\sin^{-1} B + \frac{(r_1 + r_2)}{l}\left[1 - \sqrt{1 - \bar{x}^2}\right]\right)\right\}}{l\,.\,\left(C\,.\,\sqrt{1 - B^2}\right)\left(\sqrt{1 - \bar{x}^2}\right)}$$

Refer Fig [4.9], and Fig [4.10].

$$M = F_n \cos\theta \;.\; h \qquad (A.9)$$

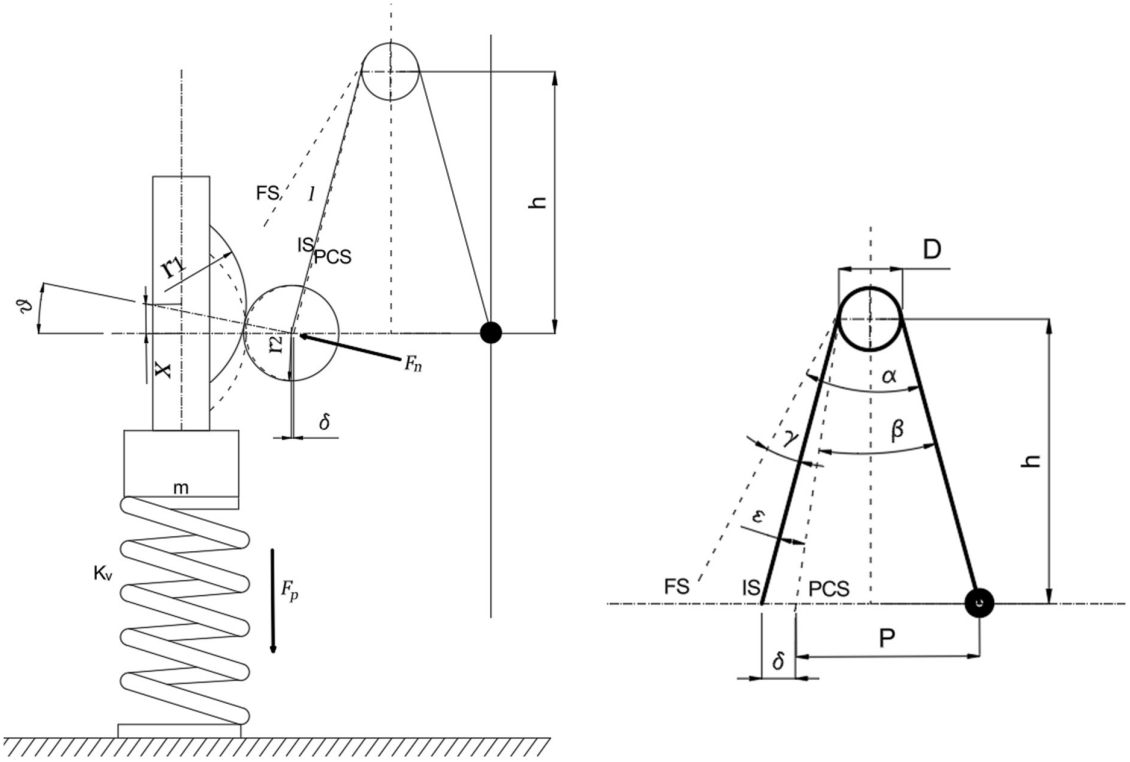

For very small ε , $\quad h = l\,\cos\left(\beta/2\right)$

$$h = \sqrt{l^2 - \left(\frac{P - D}{2}\right)^2} \qquad (A.10)$$

$$M = F_n \cos\theta \;.\; \sqrt{l^2 - \left(\frac{P - D}{2}\right)^2} \;=\; k\theta_t \qquad (A.11)$$

$$\theta_t = \gamma + \theta_e$$

$$\boldsymbol{\theta_t = \alpha - (\beta + \varepsilon) + \frac{64ML}{3\pi d^4 E}} \qquad (\boldsymbol{A.12})$$

For, the expressions of $\boldsymbol{\theta_t}$ **and** $\boldsymbol{\theta_e}$ **,** refer the chapter on torsion springs from the book Shigley's Mechanical Design.

$$\boldsymbol{\sin\left(\frac{\beta}{2}\right) = \frac{P-D}{2l}}$$

$$\boldsymbol{\beta = 2\ \sin^{-1}\left(\frac{P-D}{2l}\right)} \qquad (\boldsymbol{A.13})$$

$$\boldsymbol{\delta = l\,\varepsilon \quad \overset{yields}{\Longrightarrow} \quad \varepsilon = \frac{\delta}{l}} \qquad (\boldsymbol{A.14})$$

$$\boldsymbol{\theta_t = \alpha - \left\{2\ \sin^{-1}\left(\frac{P-D}{2l}\right) + \frac{\delta}{l}\right\} + \frac{64ML}{3\pi d^4 E}} \qquad (\boldsymbol{A.15})$$

$$\boldsymbol{(r_1 + r_2)^2 = (r_1 + r_2 - \delta)^2 + x^2}$$

$$\boldsymbol{\delta = (r_1 + r_2) - \sqrt{(r_1 + r_2)^2 - x^2}}$$

$$\boldsymbol{\frac{\delta}{(r_1 + r_2)} = 1 - \sqrt{1 - \left(\frac{x}{r_1 + r_2}\right)^2}} \qquad (\boldsymbol{A.16})$$

$$\boldsymbol{M = k\theta_t = k\left\{\alpha - \left\{2\ \sin^{-1}\left(\frac{P-D}{2l}\right) + \frac{\delta}{l}\right\} + \frac{64ML}{3\pi d^4 E}\right\}}$$

Therefore,

$$\boldsymbol{M = \frac{k\left\{\alpha - \left\{2\ \sin^{-1}\left(\frac{P-D}{2l}\right) + \frac{\delta}{l}\right\}\right\}}{\left\{1 - \frac{64kL}{3\pi d^4 E}\right\}}} \qquad (\boldsymbol{A.17})$$

Therefore,

$$F_n \cos\theta \cdot \sqrt{l^2 - \left(\frac{P-D}{2}\right)^2} = \frac{k\left\{\alpha - \left\{2\ \sin^{-1}\left(\frac{P-D}{2l}\right) + \frac{\delta}{l}\right\}\right\}}{\left\{1 - \frac{64kL}{3\pi d^4 E}\right\}}$$

$$\cos\theta = 1 - \frac{\delta}{r_1 + r_2} = \sqrt{1 - \left(\frac{x}{r_1 + r_2}\right)^2} \qquad (A.18)$$

$$F_n = \frac{k\left\{\alpha - \left\{2\ \sin^{-1}\left(\frac{P-D}{2l}\right) + \frac{\delta}{l}\right\}\right\}}{\left\{1 - \frac{64kL}{3\pi d^4 E}\right\}\left\{\sqrt{l^2 - \left(\frac{P-D}{2}\right)^2}\right\}\left\{\sqrt{1 - \left(\frac{x}{r_1 + r_2}\right)^2}\right\}} \qquad (A.19)$$

Substitute the expression for k for torsion springs in the term $\left\{1 - \frac{64kL}{3\pi d^4 E}\right\}$

$$\left\{1 - \frac{64kL}{3\pi d^4 E}\right\} = 1 - \frac{l}{3\pi N_a D}$$

Therefore,

$$F_n = \frac{k\left\{\alpha - \left\{2\ \sin^{-1}\left(\frac{P-D}{2l}\right) + \frac{\delta}{l}\right\}\right\}}{\left\{1 - \frac{l}{3\pi N_a D}\right\}\left\{\sqrt{l^2 - \left(\frac{P-D}{2}\right)^2}\right\}\left\{\sqrt{1 - \left(\frac{x}{r_1 + r_2}\right)^2}\right\}} \qquad (A.20)$$

Substituting the expression for δ

$$F_n = \frac{k\left\{\alpha - \left\{2\ \sin^{-1}\left(\frac{P-D}{2l}\right) + \frac{(r_1 + r_2)}{l}\left(1 - \sqrt{1 - \left(\frac{x}{r_1 + r_2}\right)^2}\right)\right\}\right\}}{\left\{1 - \frac{l}{3\pi N_a D}\right\}\left\{l\sqrt{1 - \left(\frac{P-D}{2l}\right)^2}\right\}\left\{\sqrt{1 - \left(\frac{x}{r_1 + r_2}\right)^2}\right\}} \qquad (A.21)$$

For,

$$\bar{x} = \frac{x}{r_1 + r_2} \quad , \quad B = \frac{P - D}{2l} \quad , \quad C = 1 - \frac{l}{3\pi N_a D}$$

$$F_n = k \frac{\left\{\alpha - \left(2\sin^{-1} B + \frac{(r_1 + r_2)}{l}\left[1 - \sqrt{1 - \bar{x}^2}\right]\right)\right\}}{l \,.\, \left(C \,.\, \sqrt{1 - B^2}\right)\left(\sqrt{1 - \bar{x}^2}\right)} \qquad (A.22)$$

A.4 – Derivation of Eqn. [4.23]

In this section we derive the following equation.

$$F_n = \frac{\frac{A_1}{A_2} k \left\{d - \frac{A_1}{A_2}\left[(r_1 + r_2) - \sqrt{(r_1 + r_2)^2 - x^2}\right]\right\}}{\frac{\sqrt{(r_1 + r_2)^2 - x^2}}{(r_1 + r_2)}}$$

Refer Fig [4.12].

$$\frac{F_n \cos\theta}{A_1} = \frac{F}{A_2} = \frac{k\,(d - y)}{A_2} \qquad (A.23)$$

Also, by volume conservation for the hydraulic fluid in the cylinder and tube assembly,

$$A_1 \delta = A_1 y$$

$$y = \frac{A_1}{A_2} \delta \qquad (A.24)$$

Therefore,

$$F_n \cos\theta = \frac{A_1}{A_2} k \left(d - \frac{A_1}{A_2} \delta\right) \qquad (A.25)$$

$$\cos\theta = \frac{(r_1 + r_2 - \delta)}{(r_1 + r_2)} \qquad (A.26)$$

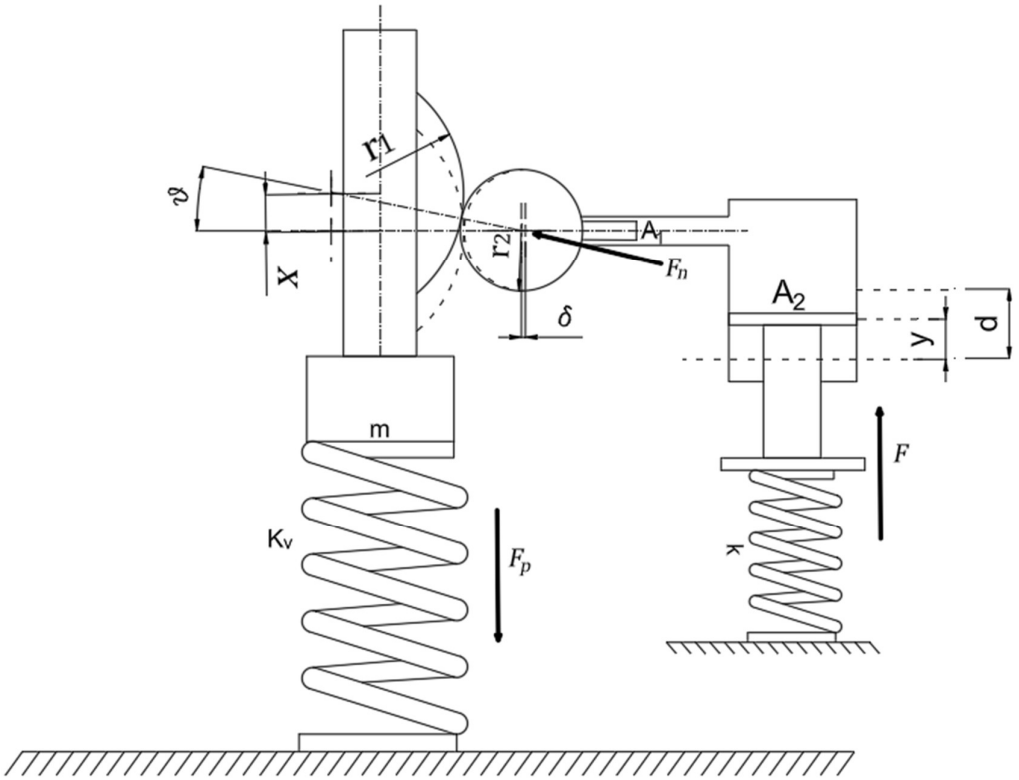

$$(r_1 + r_2)^2 = (r_1 + r_2 - \delta)^2 + x^2$$

$$\delta = (r_1 + r_2) - \sqrt{(r_1 + r_2)^2 - x^2}$$

$$\frac{\delta}{(r_1 + r_2)} = 1 - \sqrt{1 - \left(\frac{x}{r_1 + r_2}\right)^2} \qquad (A.27)$$

$$\cos\theta = \frac{\sqrt{(r_1 + r_2)^2 - x^2}}{(r_1 + r_2)} \qquad (A.28)$$

Therefore,

$$F_n \frac{\sqrt{(r_1 + r_2)^2 - x^2}}{(r_1 + r_2)} = \frac{A_1}{A_2} k \left(d - \frac{A_1}{A_2} \delta\right) \qquad (A.29)$$

Therefore,

$$F_n = \frac{\frac{A_1}{A_2} k \left\{d - \frac{A_1}{A_2}\left[(r_1 + r_2) - \sqrt{(r_1 + r_2)^2 - x^2}\right]\right\}}{\frac{\sqrt{(r_1 + r_2)^2 - x^2}}{(r_1 + r_2)}} \qquad (A.30)$$

References

1) Harib, K., & Srinivasan, K. (2003). Kinematic and dynamic analysis of Stewart platform-based machine tool structures. *Robotica*, *21*(5), 541-554.

2) Singh, Y. P., Ahmad, N., & Ghosal, A. (2024). Dynamically isotropic Gough–Stewart platform for micro-vibration isolation in spacecrafts. *Mechanism and Machine Theory*, *201*, 105735.

3) Zhang, Y., Guo, Z., He, H., Zhang, J., Liu, M., & Zhou, Z. (2014). A novel vibration isolation system for reaction wheel on space telescopes. *Acta Astronautica*, *102*, 1-13.

4) Carrella, A., Brennan, M. J., & Waters, T. P. (2007). Static analysis of a passive vibration isolator with quasi-zero-stiffness characteristic. *Journal of sound and vibration*, *301*(3-5), 678-689.

5) Josephs, H., & Huston, R. (2002). *Dynamics of mechanical systems*. CRC Press.

6) Han, Q., Gao, S., & Chu, F. (2024). Micro-Vibration Analysis, Suppression, and Isolation of Spacecraft Flywheel Rotor Systems: A Review. *Vibration*, *7*(1), 229-263.